University of Colorado, Boulder
CU Scholar

Chemistry & Biochemistry Graduate Theses & Dissertations

Chemistry & Biochemistry

Spring 1-1-2012

Hydrating Aldehydes in the Gas Phase: Atmospheric Consequences

Jessica Lynne Axson
University of Colorado at Boulder, jessica.axson@colorado.edu

Follow this and additional works at: http://scholar.colorado.edu/chem_gradetds

 Part of the Atmospheric Sciences Commons, and the Chemistry Commons

Recommended Citation
Axson, Jessica Lynne, "Hydrating Aldehydes in the Gas Phase: Atmospheric Consequences" (2012). *Chemistry & Biochemistry Graduate Theses & Dissertations.* Paper 56.

This Dissertation is brought to you for free and open access by Chemistry & Biochemistry at CU Scholar. It has been accepted for inclusion in Chemistry & Biochemistry Graduate Theses & Dissertations by an authorized administrator of CU Scholar. For more information, please contact cuscholaradmin@colorado.edu.

HYDRATING ALDEHYDES IN THE GAS PHASE: ATMOSPHERIC CONSEQUENCES

by

JESSICA LYNNE AXSON

B.S., Randolph Macon College, 2007

A thesis submitted to the

Faculty of the Graduate School of the

University of Colorado in partial fulfillment

of the requirements for the degree of

Doctor of Philosophy

Department of Chemistry and Biochemistry

2012

This thesis entitled:

Hydrating Aldehydes in the Gas Phase: Atmospheric Consequences

Written by Jessica Lynne Axson

has been approved for the department of Chemistry and Biochemistry program by

_____

Veronica Vaida

_____

Barbara Ervens

Date: _____

The final copy of this thesis has been examined by both the signatories, and we find that both the content and the form meet acceptable presentation standards of scholarly work in the above mentioned discipline.

Axson, Jessica Lynne (Ph.D., Chemistry and Biochemistry)

Hydrating Aldehydes in the Gas Phase: Atmospheric Consequences

Thesis directed by Professor Veronica Vaida

Atmospheric organics originate from biogenic and anthropogenic sources including volatile organic compounds (VOCs) and oxidation products of these VOCs. In the atmosphere, the organics can be processed and become important components of atmospheric aerosols. Methylglyoxal (CH_3COCHO) is a known oxidation product of VOCs and has been observed in field studies and incorporated into atmospheric models. While the gas-phase chemistry of methylglyoxal is fairly well understood, its modeled concentration and role in the formation of secondary organic aerosols (SOA) remains controversial. In this thesis, I investigate aqueous chemistry of methylglyoxal to better understand the link between VOCs and the formation of SOA.

The gas-phase hydration is a process not previously considered to occur in water-restricted environments, such as the atmosphere, but could have important consequences for the atmospheric processing of organics. Methylglyoxal is an interesting molecule for studying gas-phase hydration of because it contains both a ketone and an aldehyde group. This allows for the simultaneous analysis of the effect of gas-phase hydration on both carbonyl groups. I examine the gas-phase hydration of methylglyoxal leading to diol and hydrates (water clusters), and examine their water and photon mediated chemistry.

The gas-phase hydration of methylglyoxal has important consequences to its atmospheric processing. Methylglyoxal diol and its hydrates have a lower vapor pressure than the parent

aldehyde and a tendency to form intermolecular hydrogen bonds. The ability to more readily form hydrogen bonds can increase the diol and diol hydrate contributions to aerosol growth by partitioning more readily into the aqueous phase. This would increase methylglyoxal content in aerosols and affect the organic content of aqueous-phase aerosols and cloud droplets. Additionally, hydration of methylglyoxal to form the diol can alter the electronic state of the parent aldehyde. Formation of methylglyoxal diol will eliminate the $n \rightarrow \pi^*$ transition of the aldehyde carbonyl, which undergoes near-ultraviolet (UV) photochemistry. This allows for methylglyoxal diol to form new products via UV photochemistry through its remaining ketone carbonyl and opens the way for other photochemistry through excitation of the OH vibrational overtone in the near-infrared (IR).

To examine the hydration of methylglyoxal and the formation of methylglyoxal diol I employed a variety of spectroscopic techniques including, Fourier transform IR spectroscopy (FTIR), cavity ringdown spectroscopy (CRDS), incoherent broad band cavity enhanced absorption spectroscopy (IBBCEAS), UV-visible spectroscopy, and nuclear magnetic resonance (NMR) spectroscopy. The FTIR and CRD are used to observe and characterize the formation of methylglyoxal diol and its hydrates. The IBBCEAS was used to investigate the changes in the UV absorption cross section of methylglyoxal with increasing relative humidity. UV-visible and NMR spectroscopy was used to analyze the aqueous-phase hydration of methylglyoxal and its photolysis products.

These results may impact the understanding of the atmospheric fate and processing of methylglyoxal and the role of organics in atmospheric chemistry. Hydration of aldehydes such as methylglyoxal has implications for modification of atmospheric radical production and provides important degradation pathways of potential SOA precursors.

This thesis is dedicated to my family and friends for their support through this journey

Acknowledgements

There are so many people I should thank for contributing to my education and inspiring me to a life of science. First and foremost, I would like to thank my advisor, Prof. Veronica Vaida. She has been an outstanding advisor and has gone above and beyond to educate me in both the laboratory and in life. I want to thank her for nurturing my confidence and creativity. I would also like to thank my undergraduate advisor, Prof. Rebecca Michelsen, and my NASA advisor, Dr. Laura Iraci, for all of their advice and support during my undergraduate and graduate years.

I would like to thank past and present Vaida group members, with special thanks to Katy Plath, Nabilah Rontu Carlon, Jessica Gilman, Molly Larsen, and Elizabeth Griffith. I would like to add a big thanks to Katy Plath for taking me under her wing when I first entered the Vaida lab and supporting me long after she graduated. I would like to thank all of my friends at CU, with special thanks to Danielle Buckley, Rob Hall, Erik Heath and Nate Campbell.

While at CU I had the privilege to work with many wonderful people in and outside of the institution. I would like to thank Zeb Kramer and Kaito Takahashi for their beautiful theoretical work, without it I might still be wondering who all those peaks belong to. I would like to thank Dr. Geoff Tyndall for his encouraging words and spectroscopic knowhow. I thank Dr. Rebecca Washenfelder for teaching me how to build and IBBCEAS. I am grateful to everyone at NCAR and NOAA that I have collaborated with and those who have encouraged and supported me. To Don David, Dennis Steffey, Yehor Novikov, and Rich Shoemaker who have helped me with projects.

I would like to acknowledge my funding sources including a National Science Foundation (NSF) grant, a NASA Earth and Space Science fellowship and a CIRES Graduate student fellowship.

Last, but certainly not least, I would like to thank my family members for supporting and encouraging me throughout my graduate studies. I am grateful of my mom and dad, for always believing in me and supporting my education. I would like to thank my great Uncle Jim for being a major inspiration for pursing my career in chemistry. Big thanks to my older brother, Daniel, for the long phone calls and encouragement to stay focused and work hard.

Table of Contents

Table of Tables

Table of Figures

1. Introduction

Atmospheric aerosols are a major topic of current studies, given the important role they play in the Earth's radiative balance[1]. Atmospheric aerosols can affect the global radiative forcing directly by absorbing or scattering radiation and indirectly by enhancing cloud albedo[1-3]. Aerosol optical and physiochemical properties vary because of their diverse and changing chemical compositions. This variation greatly complicates the quantification of atmospheric aerosol global radiative forcing. Efforts at modeling aerosol effects on climate are primarily based on sulfate aerosol studies, as assessed by the International Panel on Climate Change (IPCC)[1], though there is growing evidence that organic aerosols play an important role in climate change[4-6].

Organic molecules have been identified as important components of atmospheric aerosols[4,7]. Atmospheric organic molecules originate from biogenic and anthropogenic primary emissions. The primary emissions can be photolyzed in the atmosphere to form secondary species, which can contribute to or form aerosols[2-4]. Recent studies have shown that 20 – 90% of aerosols contain organics[7,8]. Several of these aerosols can contain a significant amount of organics, up to 90% of the particle[2,4,9].

The chemical processing of organics in the atmosphere is complex and much remains unknown. Organics can be chemically processed in a number of ways in the atmosphere to form secondary organic products, including gas-phase oxidation and photolysis and aqueous phase cloud processing (photo-oxidation)[10-12]. The secondary organics can then form or grow secondary organic aerosols (SOA). The formation pathways of SOA remain highly speculative,

leading to uncertainties in predictions of atmospheric models which generate discrepancies when compared with results from atmospheric measurements[13-15]. Currently, a large SOA source is missing from models as illustrated by simultaneous field measurements of volatile organic compounds (VOCs) and aerosol particles[13,14,16,17]. Recent studies show there is a correlation between water and SOA formation[10,18-21]. This thesis reports on the effect of water on the transition between VOCs leading to atmospheric aerosol with the example of methylglyoxal.

Methylglyoxal is a small α–dicarbonyl that is ubiquitous in the atmosphere, having been measured in urban, rural, and remote environments[22-24]. It is produced from several biogenic and anthropogenic VOCs including isoprene and aromatic hydrocarbons[24-27]. Recent modeling and experimental studies suggest that methylglyoxal can contribute to SOA[11,12,28-33]. Methylglyoxal was seen to increase organic acid formation (i.e. oxalic and pyruvic acid) particularly in cloud water, by the oxidation with hydroxyl radicals and other aqueous radical species[11,30,34]. It was also theoretically and experimentally observed to produce oligomers in the aqueous phase and through the evaporation of droplets[11,28,29,31,33]. These studies suggest that methylglyoxal's water-mediated chemistry may have important consequences to the formation of SOA[35-37].

The focus of this body of work was to examine the gas-phase formation of methylglyoxal diol from methylglyoxal and water vapor and assess the consequences of the diol formation in the atmosphere. Methylglyoxal is an interesting model for studying gas-phase hydration of because it contains both a ketone and an aldehyde group. This allows for the simultaneous analysis of the effect of gas-phase hydration on both carbonyl groups. This work was motivated by two questions: (1) can methylglyoxal diol form and exist in the gas phase and (2) how does gas phase diol formation contribute to atmospheric chemistry (Fig. 1.1). While the aqueous phase hydration of small aldehydes is well known[38-41], their gas-phase hydration has not yet been

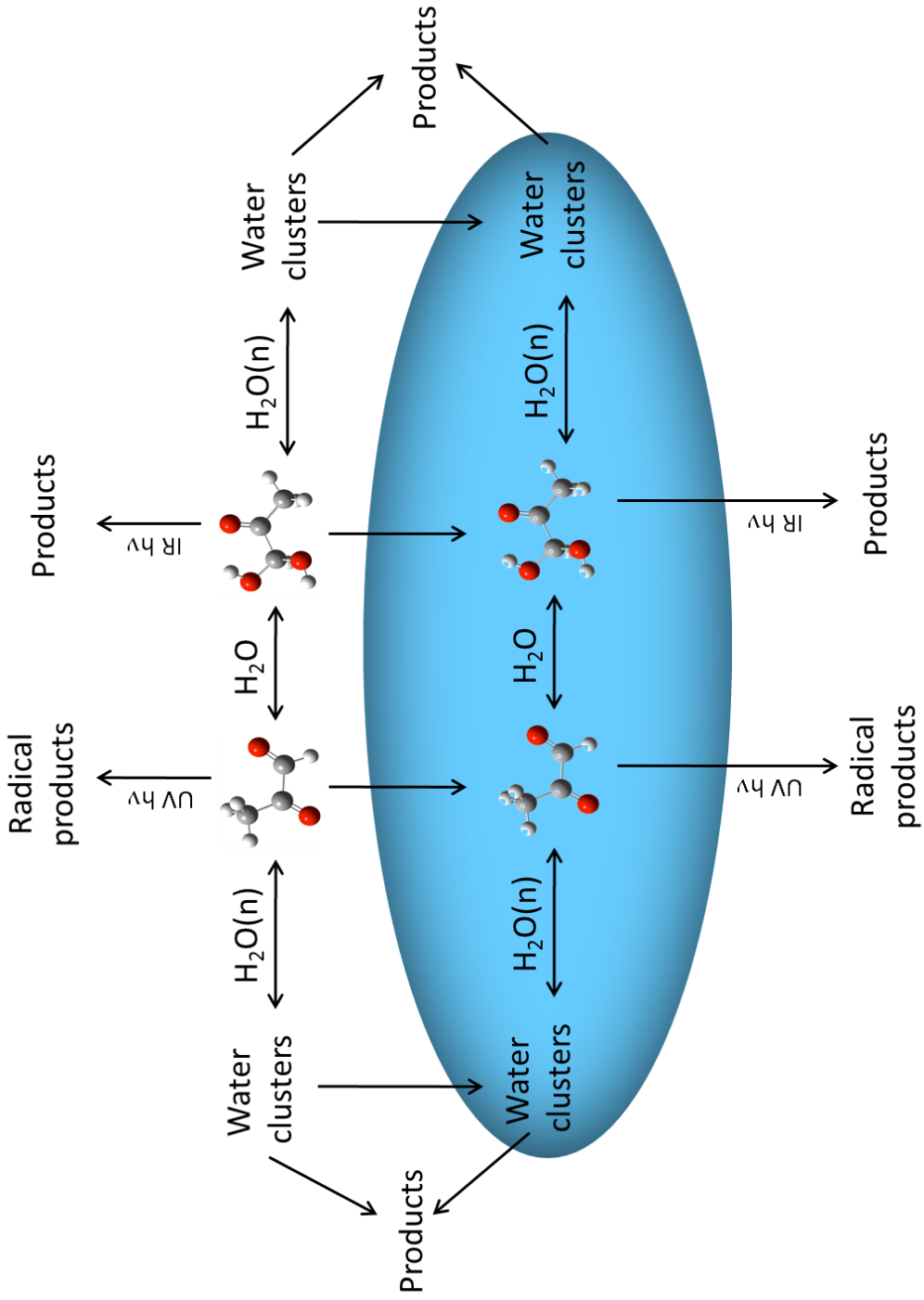

Figure 1.1 Depiction of the gas phase formation of methylglyoxal diol and the possible methylglyoxal diol atmospheric chemistry

considered or included in atmospheric models. This exclusion is mainly due to the belief that there is not enough water present in the gas phase to make such hydration reactions favorable. However, it has been seen more recently that aldehydes can, in fact, hydrate in gas phase or in water restricted environments to form diols[35,36,42].

The gas-phase hydration of methylglyoxal has important consequences to its atmospheric chemistry. Methylglyoxal diol and its hydrates have a lower vapor pressure than the parent aldehyde and a tendency to form intermolecular hydrogen bonds. The ability to more readily form hydrogen bonds can increase the diol and diol hydrate contributions to aerosol growth by partitioning more readily into the aqueous phase. This would increase methylglyoxal content in aerosols and affect the organic content of aqueous-phase aerosols and cloud droplets. Methylglyoxal diol and its hydrates would also have different ultraviolet (UV) spectroscopy than aldehydes and ketones because of its OH chromophore. While aldehydes and ketones can undergo UV photochemistry through $n \rightarrow \pi^*$ transition of the carbonyl, the diol OH chromophore is too high in energy to undergo UV photochemistry. Recent experimental and theoretical studies have focused on excited ground electronic vibrational state photochemistry of the OH chromophore that can occur by absorption of red solar photons ($\lambda > 400$ nm)[43-45]. By pumping the ground electronic state vibrational overtones with near-IR and visible radiation, a concerted, photochemical reaction initiates and there is eventual bond dissociation[43-49]. This sunlight driven photochemical pathway may be relevant to methylglyoxal diol, given the OH stretching overtones available for overtone pumping.

The gas-phase mid- and near-infrared (IR) spectrum of methylglyoxal diol is examined in Chapter 3 and 4. In Chapter 3, I identified and assigned the first gas-phase vibrational spectra of methylglyoxal diol from 1000 – 4000 cm^{-1} using Fourier transform infrared spectroscopy (FTIR)

and characterized the water-mediated gas-phase equilibrium between methylglyoxal and methylglyoxal diol[35]. I used a combination of FTIR and cavity ringdown spectroscopy (CRD) to further confirm the spectroscopic signatures of methylglyoxal diol and investigate its chemistry Chapter 4. The FTIR was used to extend the spectroscopic study to the fingerprint region in the mid-IR down to 600 cm^{-1}. The CRD was used to observe and characterize the third ($4\nu_{OH}$) and fourth ($5\nu_{OH}$) OH stretching vibrational overtones of methylglyoxal diol in the near-IR. The consequences of forming methylglyoxal diol in the gas phase include opening the way for new water and photon mediated atmospheric chemistry. The addition of the two alcohol (OH) groups on methylglyoxal changes its ability to hydrogen bond and its near-UV photochemistry. For example, methylglyoxal diol can more readily form hydrogen bonds with water molecules than the parent aldehyde, leading to a greater gas-to-particle phase partitioning. The OH groups on methylglyoxal diol alter the photochemical processing of methylglyoxal by removing the aldehyde carbonyl $n\rightarrow\pi^*$ transition. This chemistry was examined further in Chapter 6.

Chapter 5 discusses the development and characterization of the incoherent broadband cavity enhanced absorption spectroscopy (IBBCEAS) instrument used to observe UV cross sections from 350 – 470 nm[50]. The increased sensitivity of this instrument compared to single-pass or multi-pass cells allows for the measurement of weak absorption cross sections with higher signal-to-noise and higher accuracy. The instrument was designed with three channels centered at 365, 405, and 455 nm channels and characterized to measure absolute O_3 UV absorption cross section in the region from 350 – 470 nm. Ozone has well characterized cross sections[51-55] with the exception of the large discrepancy in current literature cross sections in this region from 350 – 470 nm between the Huggins and Chappuis bands. The measurement of O_3 in this region addresses this discrepancy and provides new measurements of the O_3 absorption cross

sections which is useful for applications such as satellite retrievals, ground-based O_3 monitoring, and atmospheric radiative transfer models.

In Chapter 6, the IBBCEAS instrument was used to measure the methylglyoxal near-UV cross section from 440 – 470 nm and examine changes in the UV cross section with relative humidity (%RH). Methylglyoxal, like other aldehydes and ketones, has carbonyl $n \rightarrow \pi^*$ UV transitions that are available for photochemistry. The hydration of the aldehyde or ketone can suppress one or both $n \rightarrow \pi^*$ transition as observed in the aqueous phase for α-dicarbonyls, altering the electronic state of the molecule and its photochemistry. The aqueous phase UV photochemistry of methylglyoxal was also examined to help understand the possible photochemical pathways that methylglyoxal diol can undergo in the atmosphere.

Chapter Three - Gas-phase water-mediated equilibrium between methylglyoxal and its geminal diol.

Published in: *Proc Natl Acad Sci US.,* **107**, 6687-6692, 2010.

Author list – Jessica L. Axson, Kaito Takahashi, David O. De Haan, and Veronica Vaida

Contributions - Preparation of sample, experiments, and spectral analysis were performed by Jessica Axson. Theoretical calculations were performed by Kaito Takahashi. The manuscript was prepared by Jessica Axson with contributions from all authors. Valuable insight was provided by Geoff Tyndall (NCAR), John Orlando (NCAR), Jim Burkholder (NOAA), Ranajit Talukdar (NOAA), and Barbara Ervens (NOAA).

Chapter Four - Spectroscopic analysis and reanalysis of methylglyoxal diol in the mid- and near-infrared

Published in: Manuscript in preparation

Author list – Jessica L. Axson, Zeb Kramer, Rex T. Sodje, and Veronica Vaida

Contributions – Preparation of gas and aqueous phase sample, experiments, and spectral analysis were performed by Jessica Axson. The theoretical calculations were performed by Zeb Kramer. The nuclear magnetic resonance (NMR) spectra were taken by Richard Shoemaker and analysis of the NMR spectra was performed by Jessica Axson and Richard Shoemaker. Valuable spectroscopic insight was provided by Geoff Tyndall (NCAR), John Orlando (NCAR), and Jim Burkholder (NOAA).

Chapter Five - The Absolute Ozone Absorption Cross Section in the Huggins Chappuis Minimum (350 – 470 nm) at 296 K

Published in: *Atmos. Chem. Phys.*, **11**, 1-10, 2011.

Author List - Jessica L. Axson, Rebecca A. Washenfelder, Cora J. Young, Tara F. Kahan, Veronica Vaida, and Steve S. Brown

Contributions - The IBBCEAS instrument was a designed and constructed by Jessica Axson and Rebecca Washenfelder. Custom parts were created by Rich McLaughlin and Steve Ciciora. Ozone cross section experiments and analysis were performed by Jessica Axson with contributions from Rebecca Washenfelder. Ozone water cluster experiments were performed by Jessica Axson and Tara Kahan. Ozone water cluster analysis was performed by Tara Kahan. The manuscript was prepared by Jessica Axson with contributions from all authors.

Chapter Six - Ultraviolet cross section changes in methylglyoxal as a factor of relative humidity: Photochemical implications

Published in: Manuscript in preparation

Author list – Jessica L. Axson and Veronica Vaida

Contributions – Preparation of gas and aqueous phase sample, experiments and spectral analysis were performed by Jessica Axson. The nuclear magnetic resonance (NMR) spectra were taken by Richard Shoemaker and analysis of the NMR spectra was performed by Jessica Axson and Richard Shoemaker. Valuable insight was provided by Rebecca Washenfelder, Cora Young, and Steve Brown from NOAA.

Appendix A - Gas-phase vibrational spectra of glyoxylic acid and its geminal diol monohydrate: Implications for atmospheric chemistry

Published in: *React. Kinet. Catal. Lett.*, **96**, 209-224 (2009).

Author list – Kathryn L. Plath, Jessica L. Axson, Galen C. Nelson, Kaito Takahashi, Rex T. Sodje, and Veronica Vaida

Contributions - Preparation of sample and experiments was done by Jessica Axson. Spectral analysis was performed by Kathryn Plath. Theoretical calculations were provided by Kaito Takahashi and Galen Nelson. The manuscript was prepared by Kathryn Plath with contributions from all authors.

1.1 References

1. Solomon, S., Qin, D., Manning, M., Chen, Z., Marquis, M., Averyt, K. B., Tignor, M.,Miller, H. L. e. *IPCC, 2007: Climate Change 2007: The Physical Science Basis. Contribution of Working Group I to the Fourth Assessment Report of the Intergovernmental Panel on Climate Change* Cambridge University Press: Cambridge, United Kingdom and New York, NY, USA, 2007.
2. Seinfeld, J. S.,Pandis, S. N. *Atmospheric Chemistry and Physics: From Air Pollution to Climate Change*, Second ed.; John Wiley & Sons, Inc., 2006.
3. Finlayson-Pitts, B. J.,Pitts, J. N. *Chemistry of the Upper and Lower Atmosphere: Theory, Experiments, and Applications*; Academic Press, 2000.
4. Kanakidou, M., Seinfeld, J. H., Pandis, S. N., Barnes, I., Dentener, F. J., Facchini, M. C., Van Dingenen, R., Ervens, B., Nenes, A., Nielsen, C. J., Swietlicki, E., Putaud, J. P., Balkanski, Y., Fuzzi, S., Horth, J., Moortgat, G. K., Winterhalter, R., Myhre, C. E. L., Tsigaridis, K., Vignati, E., Stephanou, E. G.,Wilson, J. Organic aerosol and global climate modelling: a review. *Atmos. Chem. Phys.*, (2005), **5**, 1053-1123.
5. De Gouw, J.,Jimenez, J. L. Organic aerosols in the Earth's atmosphere. *Environ. Sci. Technol.*, (2009), **43**, 7614-7618.
6. Rincon, A. G., Guzman, M. I., Hoffmann, M. R.,Colussi, A. J. Optical absorptivity versus molecular composition of model organic aerosol matter. *J. Phys. Chem. A*, (2009), **113**, 10512-10520.
7. Zhang, Q., Jimenez, J. L., Canagaratna, M. R., Allan, J. D., Coe, H., Ulbrich, I., Alfarra, M. R., Takami, A., Middlebrook, A. M., Sun, Y. L., Dzepina, K., Dunlea, E., Docherty, K., DeCarlo, P. F., Salcedo, D., Onasch, T., Jayne, J. T., Miyoshi, T., Shimono, A., Hatakeyama, S., Takegawa, N., Kondo, Y., Schneider, J., Drewnick, F., Borrmann, S., Weimer, S., Demerjian, K., Williams, P., Bower, K., Bahreini, R., Cottrell, L., Griffin, R. J., Rautiainen, J., Sun, J. Y., Zhang, Y. M.,Worsnop, D. R. Ubiquity and dominance of oxygenated species in organic aerosols in anthropogenically-influenced Northern Hemisphere midlatitudes. *Geophys. Res. Lett.*, (2007), **34**, L13801.
8. Murphy, D. M., Cziczo, D. J., Froyd, K. D., Hudson, P. K., Matthew, B. M., Middlebrook, A. M., Peltier, R. E., Sullivan, A., Thomson, D. S.,Weber, R. J. Single-particle mass spectrometry of tropospheric aerosol particles. *J. Geophys. Res.-Atmos.*, (2006), **111**, 15.
9. Jimenez, J. L., Canagaratna, M. R., Donahue, N. M., Prevot, A. S. H., Zhang, Q., Kroll, J. H., DeCarlo, P. F., Allan, J. D., Coe, H., Ng, N. L., Aiken, A. C., Docherty, K. S., Ulbrich, I. M., Grieshop, A. P., Robinson, A. L., Duplissy, J., Smith, J. D., Wilson, K. R., Lanz, V. A., Hueglin, C., Sun, Y. L., Tian, J., Laaksonen, A., Raatikainen, T., Rautiainen, J., Vaattovaara, P., Ehn, M., Kulmala, M., Tomlinson, J. M., Collins, D. R., Cubison, M. J., Dunlea, E. J., Huffman, J. A., Onasch, T. B., Alfarra, M. R., Williams, P. I., Bower, K., Kondo, Y., Schneider, J., Drewnick, F., Borrmann, S., Weimer, S., Demerjian, K., Salcedo, D., Cottrell, L., Griffin, R., Takami, A., Miyoshi, T., Hatakeyama, S., Shimono, A., Sun, J. Y., Zhang, Y. M., Dzepina, K., Kimmel, J. R., Sueper, D., Jayne, J. T., Herndon, S. C., Trimborn, A. M., Williams, L. R., Wood, E. C., Middlebrook, A. M., Kolb, C. E., Baltensperger, U.,Worsnop, D. R. Evolution of Organic Aerosols in the Atmosphere. *Science*, (2009), **326**, 1525-1529.

10. Carlton, A. G., Turpin, B. J., Altieri, K. E., Seitzinger, S., Reff, A., Lim, H. J.,Ervens, B. Atmospheric oxalic acid and SOA production from glyoxal: Results of aqueous photooxidation experiments. *Atmos. Environ.,* (2007), **41**, 7588-7602.
11. Altieri, K. E., Seitzinger, S. P., Carlton, A. G., Turpin, B. J., Klein, G. C.,Marshall, A. G. Oligomers formed through in-cloud methylglyoxal reactions: Chemical composition, properties, and mechanisms investigated by ultra-high resolution FT-ICR mass spectrometry. *Atmos. Environ.,* (2008), **42**, 1476-1490.
12. Ervens, B., Feingold, G., Frost, G. J.,Kreidenweis, S. M. A modeling study of aqueous production of dicarboxylic acids: 1. Chemical pathways and speciated organic mass production. *J. Geophys. Res.-Atmos.,* (2004), **109**, 20.
13. Heald, C. L., Jacob, D. J., Park, R. J., Russell, L. M., Huebert, B. J., Seinfeld, J. H., Liao, H.,Weber, R. J. A large organic aerosol source in the free troposphere missing from current models. *Geophys. Res. Lett.,* (2005), **32**, L18809.
14. Volkamer, R., Jimenez, J. L., San Martini, F., Dzepina, K., Zhang, Q., Salcedo, D., Molina, L. T., Worsnop, D. R.,Molina, M. J. Secondary organic aerosol formation from anthropogenic air pollution: Rapid and higher than expected. *Geophys. Res. Lett.,* (2006), **33**, 4.
15. Finlayson-Pitts, B. J. Reactions at surfaces in the atmosphere: integration of experiments and theory as necessary (but not necessarily sufficient) for predicting the physical chemistry of aerosols. *Phys. Chem. Chem. Phys.,* (2009), **11**, 7760-7779.
16. Fast, J., Aiken, A. C., Allan, J., Alexander, L., Campos, T., Canagaratna, M. R., Chapman, E., DeCarlo, P. F., de Foy, B., Gaffney, J., de Gouw, J., Doran, J. C., Emmons, L., Hodzic, A., Herndon, S. C., Huey, G., Jayne, J. T., Jimenez, J. L., Kleinman, L., Kuster, W., Marley, N., Russell, L., Ochoa, C., Onasch, T. B., Pekour, M., Song, C., Ulbrich, I. M., Warneke, C., Welsh-Bon, D., Wiedinmyer, C., Worsnop, D. R., Yu, X. Y.,Zaveri, R. Evaluating simulated primary anthropogenic and biomass burning organic aerosols during MILAGRO: Implications for assessing treatments of secondary organic aerosols. *Atmos. Chem. Phys.,* (2009), **9**, 6191-6215.
17. De Gouw, J. A., Middlebrook, A. M., Warneke, C., Goldan, P. D., Kuster, W. C., Roberts, J. M., Fehsenfeld, F. C., Worsnop, D. R., Canagaratna, M. R., Pszenny, A. A. P., Keene, W. C., Marchewka, M., Bertman, S. B.,Bates, T. S. Budget of organic carbon in a polluted atmosphere: Results from the New England Air Quality Study in 2002. *J. Geophys. Res.-Atmos.,* (2005), **110**, 22.
18. Hallquist, M., Wenger, J. C., Baltensperger, U., Rudich, Y., Simpson, D., Claeys, M., Dommen, J., Donahue, N. M., George, C., Goldstein, A. H., Hamilton, J. F., Herrmann, H., Hoffmann, T., Iinuma, Y., Jang, M., Jenkin, M. E., Jimenez, J. L., Kiendler-Scharr, A., Maenhaut, W., McFiggans, G., Mentel, T. F., Monod, A., Prevot, A. S. H., Seinfeld, J. H., Surratt, J. D., Szmigielski, R.,Wildt, J. The formation, properties and impact of secondary organic aerosol: current and emerging issues. *Atmos. Chem. Phys.,* (2009), **9**, 5155-5236.
19. Ervens, B., Turpin, B. J.,Weber, R. J. Secondary organic aerosol formation in cloud droplets and aqueous particles (aqSOA): a review of laboratory, field and model studies. *Atmos. Chem. Phys.,* (2011), **11**, 11069-11102.
20. Tan, Y., Carlton, A. G., Seitzinger, S. P.,Turpin, B. J. SOA from methylglyoxal in clouds and wet aerosols: Measurement and prediction of key products. *Atmos. Environ.,* (2010), **44**, 5218-5226.

21. Volkamer, R., Ziemann, P. J.,Molina, M. J. Secondary organic aerosol formation from acetylene (C_2H_2): seed effect on SOA yields due to organic photochemistry in the aerosol aqueous phase. *Atmos. Chem. Phys.,* (2009), **9**, 1907-1928.
22. Kawamura, K., Kasukabe, H.,Barrie, L. A. Source and reaction pathways of dicarboxylic acids, ketoacids and dicarbonyls in arctic aerosols: One year of observations. *Atmos. Environ.,* (1996), **30**, 1709-1722.
23. Kawamura, K.,Yasui, O. Diurnal changes in the distribution of dicarboxylic acids, ketocarboxylic acids and dicarbonyls in the urban Tokyo atmosphere. *Atmos. Environ.,* (2005), **39**, 1945-1960.
24. Fu, T. M., Jacob, D. J., Wittrock, F., Burrows, J. P., Vrekoussis, M.,Henze, D. K. Global budgets of atmospheric glyoxal and methylglyoxal, and implications for formation of secondary organic aerosols. *J. Geophys. Res.-Atmos.,* (2008), **113**, 17.
25. Jang, M. S.,Kamens, R. M. Characterization of secondary aerosol from the photooxidation of toluene in the presence of NO_x and 1-propene. *Environ. Sci. Technol.,* (2001), **35**, 3626-3639.
26. Tuazon, E. C., Macleod, H., Atkinson, R.,Carter, W. P. L. Alpha-dicarbonyl yields from the NO_X-air photooxidations of a aeries of aromatic-hydrocarbons in air. *Environ. Sci. Technol.,* (1986), **20**, 383-387.
27. Grosjean, D., Williams, E. L.,Grosjean, E. Atmospheric chemistry of isoprene and of its carbonyl products. *Environ. Sci. Technol.,* (1993), **27**, 830-840.
28. De Haan, D. O., Corrigan, A. L., Tolbert, M. A., Jimenez, J. L., Wood, S. E.,Turley, J. J. Secondary Organic Aerosol Formation by Self-Reactions of Methylglyoxal and Glyoxal in Evaporating Droplets. *Environ. Sci. Technol.,* (2009), **43**, 8184-8190.
29. Krizner, H. E., De Haan, D. O.,Kua, J. Thermodynamics and kinetics of methylglyoxal dimer formation: A computational study. *J. Phys. Chem. A,* (2009), **113**, 6994-7001.
30. Warneck, P. In-cloud chemistry opens pathway to the formation of oxalic acid in the marine atmosphere. *Atmos. Environ.,* (2003), **37**, 2423-2427.
31. Loeffler, K. W., Koehler, C. A., Paul, N. M.,De Haan, D. O. Oligomer formation in evaporating aqueous glyoxal and methylglyoxal solutions. *Environ. Sci. Technol.,* (2006), **40**, 6318-6323.
32. Sareen, N., Schwier, A. N., Shapiro, E. L., Mitroo, D.,McNeill, V. F. Secondary organic material formed by methylglyoxal in aqueous aerosol mimics. *Atmos. Chem. Phys.,* (2010), **10**, 997-1016.
33. Yasmeen, F., Sauret, N., Gal, J. F., Maria, P. C., Massi, L., Maenhaut, W.,Claeys, M. Characterization of oligomers from methylglyoxal under dark conditions: a pathway to produce secondary organic aerosol through cloud processing during nighttime. *Atmos. Chem. Phys.,* (2010), **10**, 3803-3812.
34. Ervens, B., Carlton, A. G., Turpin, B. J., Altieri, K. E., Kreidenweis, S. M.,Feingold, G. Secondary organic aerosol yields from cloud-processing of isoprene oxidation products. *Geophys. Res. Lett.,* (2008), **35**, 5.
35. Axson, J. L., Takahashi, K., De Haan, D. O.,Vaida, V. Gas-phase water-mediated equilibrium between methylglyoxal and its geminal diol. *Proc Natl Acad Sci USA,* (2010), **107**, 6687-6692.
36. Plath, K. L., Axson, J. L., Nelson, G. C., Takahashi, K., Skodje, R. T.,Vaida, V. Gas-phase vibrational spectra of glyoxylic acid and its gem diol monohydrate. Implications for atmospheric chemistry. *React. Kinet. Catal. Lett.,* (2009), **96**, 209-224.

37. Takahashi, K., Plath, K. L., Axson, J. L., Nelson, G. C., Skodje, R. T.,Vaida, V. Dynamics and spectroscopy of vibrational overtone excited glyoxylic acid and 2,2-dihydroxyacetic acid in the gas-phase. *J. Chem. Phys.*, (2010), **132**, 1-10.
38. Wolfe, S., Kim, C. K., Yang, K., Weinberg, N.,Shi, Z. Hydration of the carbonyl group - A theoretical-study of the cooperative mechanism. *J. Am. Chem. Soc.*, (1995), **117**, 4240-4260.
39. Betterton, E. A.,Hoffmann, M. R. Kinetics, mechanism, and thermodynamics of the reversable-reaction of methylglyoxal (CH_3COCHO) with S(IV). *J. Phys. Chem.*, (1987), **91**, 3011-3020.
40. Nemet, I., Vikic-Topic, D.,Varga-Defterdarovic, L. Spectroscopic studies of methylglyoxal in water and dimethylsulfoxide. *Bioorganic Chem.*, (2004), **32**, 560-570.
41. Faust, B. C., Powell, K., Rao, C. J.,Anastasio, C. Aqueous-phase photolysis of biacetyl (an alpha-dicarbonyl compound): A sink for biacetyl, and a source of acetic acid, peroxyacetic acid, hydrogen peroxide, and the highly oxidizing acetylperoxyl radical in aqueous aerosols, fogs, and clouds. *Atmos. Environ.*, (1997), **31**, 497-510.
42. Maron, M. K., Takahashi, K., Shoemaker, R. K.,Vaida, V. Hydration of pyruvic acid to its geminal-diol, 2,2-dihydroxypropanoic acid, in a water-restricted environment. *Chem. Phys. Lett.*, (2011), **513**, 184-190.
43. Vaida, V. Spectroscopy of photoreactive systems: Implications for atmospheric chemistry. *J. Phys. Chem. A*, (2009), **113**, 5-18.
44. Donaldson, D. J., Tuck, A. F.,Vaida, V. Atmospheric photochemistry via vibrational overtone absorption. *Chem. Rev.*, (2003), **103**, 4717-4729.
45. Vaida, V., Feierabend, K. J., Rontu, N.,Takahashi, K. Sunlight-initiated photochemistry: Excited vibrational states of atmospheric chromophores. *Int. J. Photoenergy*, (2008, 1-13.
46. Havey, D. K., Feierabend, K. J.,Vaida, V. Vapor-phase vibrational spectrum of glycolic acid, $CH_2OHCOOH$, in the region 2000-8500 cm^{-1}. *J. Phys. Chem. A*, (2004), **108**, 9069-9073.
47. Takahashi, K., Plath, K. L., Skodje, R. T.,Vaida, V. Dynamics of vibrational overtone excited pyruvic acid in the gas phase: Line broadening through hydrogen-atom chattering. *J. Phys. Chem. A*, (2008), **112**, 7321-7331.
48. Mills, M. J., Toon, O. B., Vaida, V., Hintze, P. E., Kjaergaard, H. G., Schofield, D. P.,Robinson, T. W. Photolysis of sulfuric acid vapor by visible light as a source of the polar stratospheric CN layer. *J. Geophys. Res.-Atmos.*, (2005), **110**, 7.
49. Vaida, V., Kjaergaard, H. G., Hintze, P. E.,Donaldson, D. J. Photolysis of sulfuric acid vapor by visible solar radiation. *Science*, (2003), **299**, 1566-1568.
50. Axson, J. L., Washenfelder, R. A., Young, C. J., Kahan, T. F., Vaida, V.,Brown, S. S. Absolute ozone absorption cross section in the Huggins and Chappuis minimum (350-450 nm) at 296 K. *Atmos. Chem. Phys.*, (2011), **11**, 1-10.
51. Burkholder, J. B. and Talukdar, R. K. Temperature-dependence of the ozone absorption-spectrum over the wavelength range 410 to 760 nm. *Geophys. Res. Lett.*, (1994), **21**, 581-584.
52. Brion, J., Chakir, A., Charbonnier, J., Daumont, D., Parisse, C.,Malicet, J. Absorption spectra measurements for the ozone molecule in the 350-830 nm region. *J. Atmos. Chem.*, (1998), **30**, 291-299.
53. Burrows, J. P., Richter, A., Dehn, A., Deters, B., Himmelmann, S.,Orphal, J. Atmospheric remote-sensing reference data from GOME - Part 2. Temperature-

dependent absorption cross sections of O_3 in the 231-794 nm range. *J. Quant. Spectrosc. Radiat. Transf.,* (1999), **61**, 509-517.

54. Voigt, S., Orphal, J., Bogumil, K.,Burrows, J. P. The temperature dependence (203-293 K) of the absorption cross sections of O_3 in the 230-850 nm region measured by Fourier-transform spectroscopy. *J. Photochem. Photobiol. A-Chem.,* (2001), **143**, 1-9.
55. Bogumil, K., Orphal, J., Homann, T., Voigt, S., Spietz, P., Fleischmann, O. C., Vogel, A., Hartmann, M., Kromminga, H., Bovensmann, H., Frerick, J.,Burrows, J. P. Measurements of molecular absorption spectra with the SCIAMACHY pre-flight model: Instrument characterization and reference data for atmospheric remote-sensing in the 230-2380 nm region. *J. Photochem. Photobiol. A-Chem.,* (2003), **157**, 167-184.

2. Experimental Techniques and Instruments

2.1 Introduction

The gas-phase spectroscopic experiments conducted in this work span the spectral regions from the mid-infrared (IR) to the ultraviolet (UV). To identify and analyze gas-phase methylglyoxal, methylglyoxal diol, and products resulting from their reaction (organic acids) in these spectral regions several spectroscopic techniques were utilized, including Fourier transform infrared spectroscopy (FTIR), cavity ringdown spectroscopy (CRD) and incoherent broadband cavity enhanced absorption spectroscopy (IBBCEAS). The spectroscopic techniques each presented advantages for measuring these gas-phase species, but were limited in spectral range. Aqueous-phase methylglyoxal spectroscopic and photochemical studies were performed using UV-visible spectroscopy and nuclear magnetic resonance (NMR) spectroscopy. Below is a summary of each technique and description of the instruments used in this work.

2.2 Fourier transform infrared spectroscopy

Fourier transform infrared spectroscopy is a widely used spectroscopic technique for characterizing molecules using their vibrational spectra. A commercial Bruker IFSv 66 Fourier transform spectrometer equipped with a Michelson interferometer was used to acquire gas-phase fundamental vibrational spectra (Fig. 2.1a). The Michelson interferometer consists of a light source, a fixed and moving mirror, a beam splitter, and a detector. The light source is directed

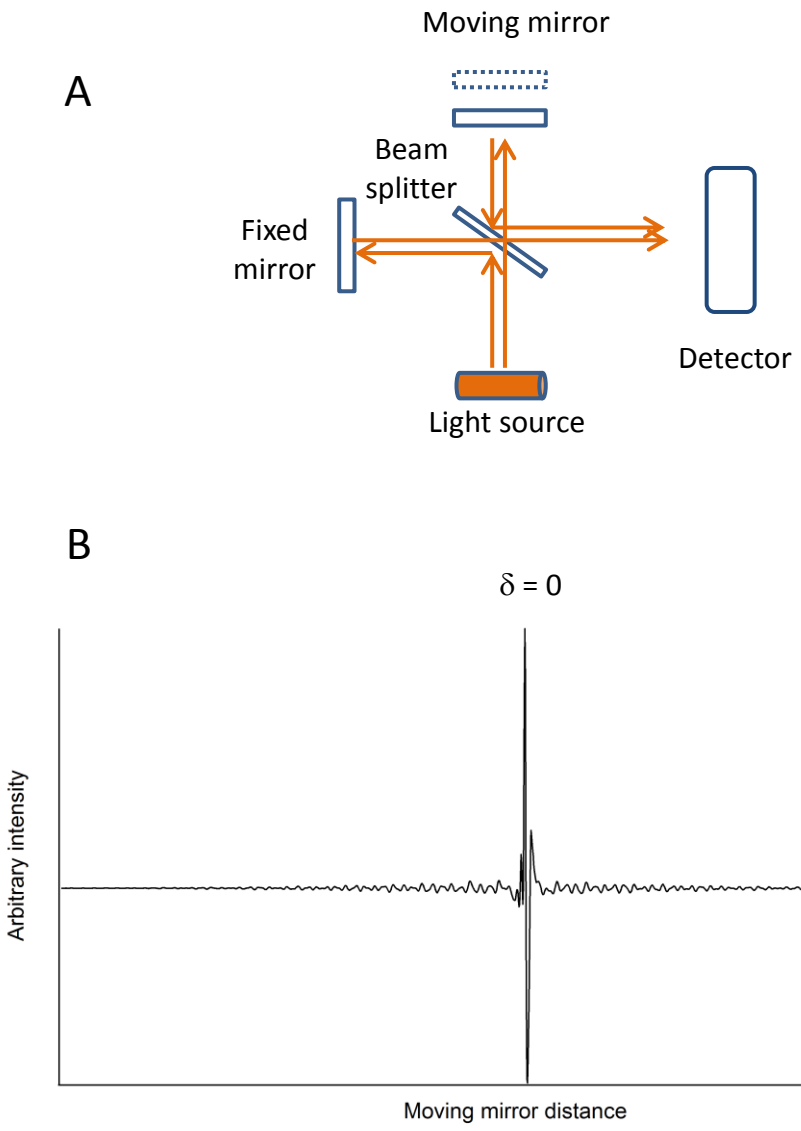

Figure 2.1 The (a) schematic of a Michelson interferometer and (b) a typical interferogram for a broadband light source.

onto the beam splitter, where half of the light is reflected to the fixed mirror and half is transmitted to the moving mirror. The fixed mirror is a certain distance, d, from the beam splitter and the reflected light will travel a total distance of 2d. The light transmitted to the moving mirror will travel a total distance of 2(d + δ), where δ is the optical retardation or the additional distance the mirror can be moved from its original position. As the light from these mirrors recombine, there will be constructive interference ($\frac{n}{2}\lambda$) or destructive interference ($\frac{n+\frac{1}{2}}{2}\lambda$), where n is an integer. The intensity from the interferometer as a factor of mirror distance is measured by the detector. This intensity measurement is given by the following equation where I(δ) is the intensity of the light signal and S(υ) is the intensity of the monochromatic line at a certain wavenumber (cm^{-1})[1,2].

$$I(\delta) = S(\nu)\cos(2\pi\nu\delta) \qquad (2.1)$$

When the fixed and moving mirrors are the same distance from the beam splitter (δ = 0) there is no optical retardation and only constructive interference occurs, as seen by the large intensity peak in the interferogram (Fig. 2.1b). As the mirror moves, there is increasing optical retardation and consequently destructive interference, which causes the intensity of the interferogram to decrease.

In order to get a spectrum of intensity of the absorption (B($\bar{\upsilon}$)) versus wavenumber (υ), the interferogram is Fourier transformed. In the Fourier transform, the x-axis of mirror distance (cm) is inverted to wavenumbers (cm^{-1}), an energy domain, using the following equations where B($\bar{\upsilon}$) is the intensity as a factor of wavenumber.

$$B(\bar{\upsilon}) = \int_{-\infty}^{+\infty} I(\delta) \cos 2\pi \bar{\upsilon}\delta \, d\delta \tag{2.2}$$

This technique has several advantages over traditional spectroscopic techniques such as grating spectrometers. The Michelson interferometer uses an aperture instead of a slit to allow for a greater portion of light to reach the detector; this is known as the throughput or Jacquinot advantage[1,2]. The most important advantage of the Michelson interferometer is its ability to measure all wavelengths simultaneously instead of having to step through each wavelength. This is known as the multiplex or Fellget advantage. These two advantages allow for the acquisition of the spectrum in a shorter amount of time and with a higher signal to noise.

The Bruker IFSv 66 has with several components including light sources, beam splitters, and detectors, in order to optimize for a specific spectral region of interest. For my gas-phase FTIR experiments, I was interested in the mid-IR region, from 600 – 4000 cm^{-1}. To optimize the instrument for this region, I used a globar light source, KBr or CaF2 beamsplitter, and a mercury cadmium telluride (MCT) detector. The globar light source operated at temperatures of 1400 K, produced infrared radiation from 200 – 10,000 cm^{-1}. This was then paired with either a KBr beamsplitter which transmitted from 450 – 4000 cm^{-1} or a CaF_2 beamsplitter which transmitted from 1200 – 8500 cm^{-1} or 4000 – 25,000 cm^{-1}. The MCT detector had a range of 400 – 5000 cm^{-1}. The MCT detector outputs signal in voltage, which is turned into intensity, and therefore is cooled with liquid nitrogen before use to minimize dark signal. The instrument has a maximum resolution of 0.25 cm^{-1} and was operated at a resolution of 0.5 cm^{-1} for all experiments.

The schematic of the apparatus for the mid-IR gas-phase studies described in Chapter 3 and 4 is shown in Fig. 2.2. A static cell was optimal for these experiments to allow time for the

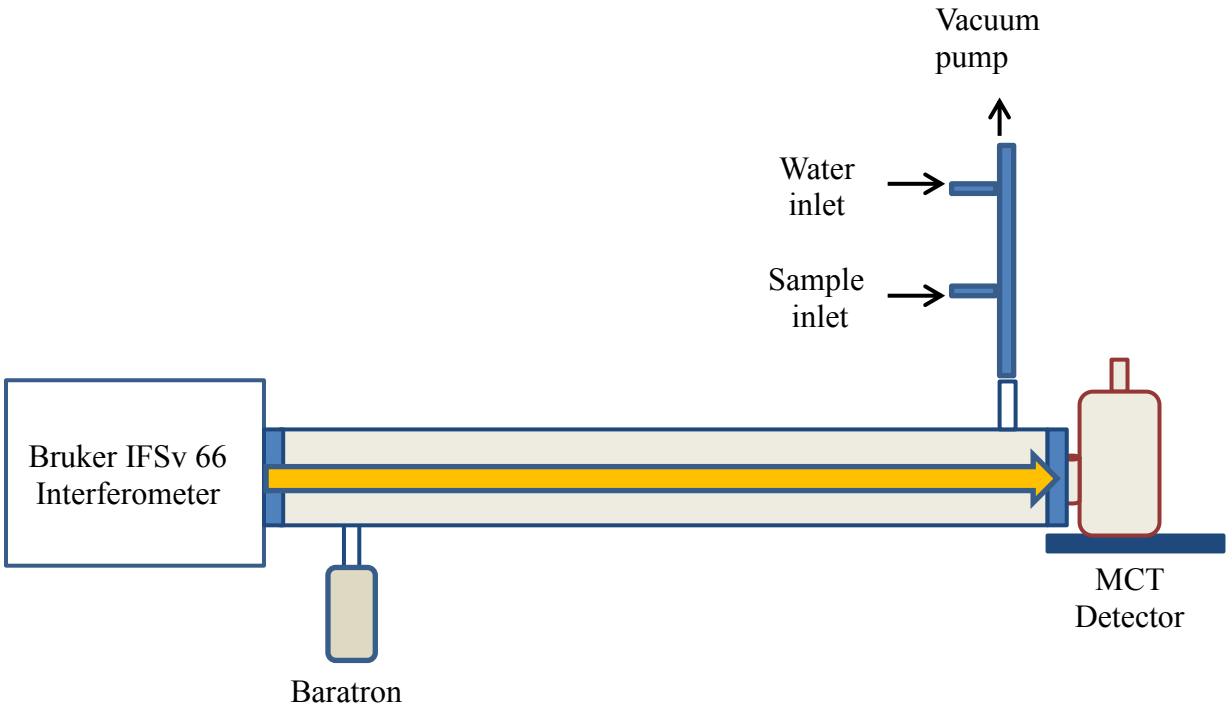

Figure 2.2 Schematic of the apparatus for gas-phase mid-IR methylglyoxal diol studies

hydration reaction to occur. The cell pressure was monitored using a baratron manometer (MKS, Type PDR 2000) which had a range of 0.02 – 10,000 Torr. Initial experiments were performed using CaF_2 windows on the static cell because they transmit light in the mid-IR from 1000 – 4000 $cm^{-1}$and are insoluble in water, a major component in these studies. The windows were switched to KBr (400 – 4000 cm^{-1}) to observe in the fingerprint region of the spectrum. During the experiment, the gas-phase sample was introduced to the evacuated static cell to get an initial spectrum and water was subsequently added for hydration.

2.3 Cavity ringdown spectroscopy

Cavity ringdown spectroscopy (CRD) is a highly sensitive spectroscopic technique that can be used to measure trace gases and weak absorption cross sections[3-7]. Its sensitivity arises from the long effective path lengths that the instruments cavity can achieve. For the CRD instrument constructed in the Vaida lab, the pathlength can be up to 51 km[8-15].

A typical CRD system consists of a laser system, optics, cavity, and detector. The optical cavity is made of two highly reflective mirrors and the total cavity loss is given by the quantity (1 – R) where R is the mirror reflectivity (i.e. 99.9%). As the light enters the cavity, it is reflected between the mirrors of the cavity. The time it takes for the light pulse to make a round trip is given by t (ns), which depends on twice the cavity length, d (cm), and the speed of light, c (3×10^{10} cm s^{-1}). Therefore, the decay of light in an empty cell is from the transmittance of light from the mirrors and is given by the following equation[16].

$$I = I_0 e^{\left(\frac{-(1-R)\,tc}{d}\right)} \quad (2.3)$$

For CRD, the intensity of the signal is measured as a time constant, τ (μs). The time constant for an empty cell, $\tau_{0,}$ is determined by the following equation[4,16]:

$$\tau_0 = \frac{d}{c(1-R)} \quad (2.4)$$

When an absorber is present in the cavity then the decay of light is from the cavity transmittance and optical extinction, α (cm^{-1}), of the absorber and is given by Eqn. 2.5, which is also measured in terms of a time constant, τ, for an absorber present as in Eqn. 2.6[4,16].

$$I = I_0 e^{\left(\frac{-[(1-R)+\alpha d]\tau c}{d}\right)} \quad (2.5)$$

$$\tau = \frac{d}{c[(1-R)+\alpha d]} \quad (2.6)$$

The optical extinction of the absorber, a product of the number density (N/v molecules cm^{-3}) and the cross section (σ cm^2), is calculated using the measured τ_0 and τ. An effective path length (R_d) is used in place of the total cavity length when the length of the sampling area is not the same as the length of the cavity. This happens when the cavity mirrors are being purged. The R_d is defined as the ratio of the sample length of the cavity length[4,16].

$$\alpha = \frac{N}{v}\sigma = \left(\frac{R_d}{c}\right)\left(\frac{1}{\tau} - \frac{1}{\tau_0}\right) \quad (2.7)$$

A schematic of the CRD system constructed in the Vaida laboratory is shown in Fig. 2.3. The two laser system consists of a pulsed neodymium-doped yttrium aluminum garnet (Nd:YAG) laser (Big Sky) that pumps a tunable dye laser (Northern Lights, NL-5-2-MF6)). The Nd:YAG is frequency doubled to produce 532 nm light and has 6.4 ns pulses with approximately 40 mJ per pulse. The beam from the Nd:YAG is turned by a mirror set at a 45° angle and to directed to a cylindrical lens that makes the beam optimal size and shape for the dye laser prism. The dye laser has a manual control box which is used to move a grating and select for various wavelength outputs. The dye can be changed according to the desired wavelength range and energy (~3 mJ pulses) of the dye laser depends on the dye used. The light from the dye laser is then directed to a polarizer which acts to direct any light not vertically polarized away from the dye laser. Following the polarizer is a ¼″ waveplate, which changes the vertical to circularly polarized light. Both the polarizer and wave plate act as an optical isolator, preventing any back reflection from the beam to the dye laser. After the optical isolator is a 50 cm focal length lens which focuses the light at approximately the center of the cavity. The beam is then directed by a sires of turning mirrors into a cavity that is made up of two highly reflective mirrors (R = 99.997 %). The cavity is purged with helium (He), a gas with small Rayleigh scattering cross sections, to ensure cleanliness of the mirrors. Once the beam reflects, the resulting light is then sent to a photomultiplier tube (PMT) detector. The α_{min} or sensitivity of our CRD apparatus is approximately 10^{-10} cm^{-1}.

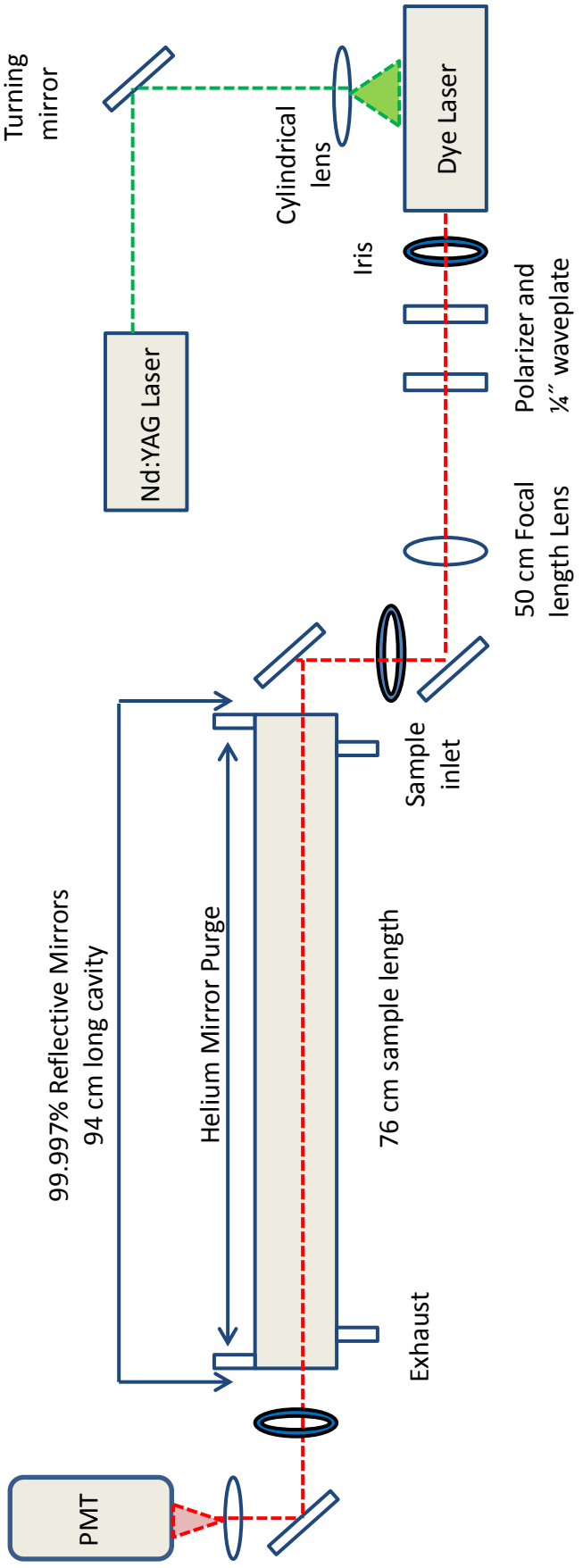

Figure 2.3 Schematic of the Vaida laboratory CRD instrument.

2.4 Incoherent broadband cavity enhanced absorption spectroscopy

Incoherent broadband cavity enhanced absorption spectroscopy (IBBCEAS) is a recently developed, highly sensitive method to measure trace gases and weak absorption cross sections[17]. IBBCEAS instrument consists of an intense broadband light source, such as an arc lamp or light emitting diode (LED), high-finesse optical cavity, and multichannel detector. Like the CRD, the pathlength generated by the optical cavity can be several kilometers, making IBBCEAS more sensitive than traditional spectroscopic techniques. This increased optical path length is balanced by a reduction in intensity throughput, such that the greatest sensitivity increase is realized for bright input light sources. This technique was first described in the literature by Fiedler et al., and has subsequently been used for spectroscopic measurements of O_3, NO_2, NO_3, CHOCHO, HONO, and other trace gasses[17-25].

Absolute measurement of optical extinction by IBBCEAS requires calibration of the mirror reflectivity, or alternatively, total cavity loss. For my apparatus, this calibration was based on Rayleigh scattering cross sections (α_{Ray}) of pure gases such as He (I_{He}) and N_2 (I_{N2}) using Eqn. 2.8[23].

$$\frac{1 - \mathrm{R}\,(\lambda)}{\mathrm{d}} = \frac{\left(\frac{I_{\mathrm{N2}}}{I_{\mathrm{He}}}\right)\alpha_{\mathrm{Ray}}^{\mathrm{N2}} - \alpha_{\mathrm{Ray}}^{\mathrm{He}}}{1 - \frac{I_{\mathrm{N2}}}{I_{\mathrm{He}}}} \tag{2.8}$$

Example spectra and calculated reflectivities are shown in Fig. 2.4. The factor (1– R (λ))/d, where d is the cavity length, is used directly from this calibration to derive concentrations rather than the mirror reflectivity itself. Following calibration of mirror reflectivity, spectra of sample

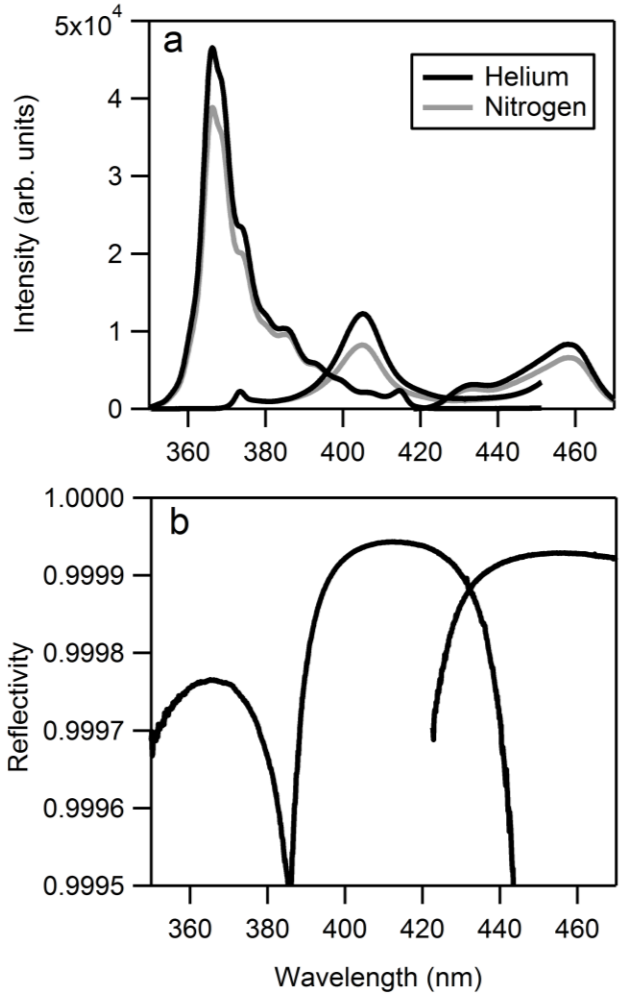

Figure 2.4 (a) Example spectra of the transmitted intensity of He and N_2 through the 365 nm, 405 nm, and 455 nm IBBCEAS cavities. The structure observed for the 365 nm channel is due to the etalon structures from the 365 nm LED. (b) The derived reflectivity curves of the 365 nm, 405 nm, and 455 nm centered mirrors from Eqn. (2)[29].

gas (O_3 for example) in He ($I(\lambda)$) are acquired alternately with zeros, or spectra of pure He ($I_0(\lambda)$). Optical extinction due to the sample is then determined as follows.

$$\alpha_{abs}(\lambda) = [O_3]\sigma_{O_3} = \left(\frac{1 - R(\lambda)}{d} + \alpha_{Ray}(\lambda)\right)\left(\frac{I_0(\lambda) - I(\lambda)}{I(\lambda)}\right) \quad (2.9)$$

From this you can derive an absolute cross section of the sample using the number density (molecule cm^{-3}) of the sample and the $\alpha_{abs}(\lambda)$.

The σ_{Ray} were taken from Bodhaine et al. and the σ_{Ray} calibrations are accurate to within 3%[26]. This accuracy is based on the ±3% accuracy of the Rayleigh N_2 cross sections compared to the measured values and the 3% repeatability of successive reflectivity measurements[21,22,27,28]. The uncertainty of the Rayleigh scattering cross section for He is similar, but makes a minor contribution to the total uncertainty.

For my studies, I designed and constructed an IBBCEAS instrument to measure O_3 absorption cross sections from 350 to 470 nm (Fig. 2.5)[29]. Each channel consists of an LED, lenses, a cavity composed of high-reflectivity mirrors, and an optical filter. An optical fiber connects the spectral output to a grating spectrometer with a CCD array detector. Three cavities were required to span from 350 to 470 nm. The spectral bandwidth for any single cavity is defined both by the emission spectrum of the LED light source, the useful bandwidth of the high reflectivity mirrors, and any optical filtering requirements, as described below. The broadband radiation was supplied by LEDs centered at 365 nm (Nichia NCSU033A(T) UV LED), 405 nm (LedEngin, Inc., LZ1-00UA05) and 455 nm (LedEngin, Inc., LZ1-00DB05) powered by custom-built, constant current DC power supplies controlled at 0.5, 0.7, and 1.0 A respectively. Each LED was mounted on a temperature-controlled block with a servoed thermoelectric cooler

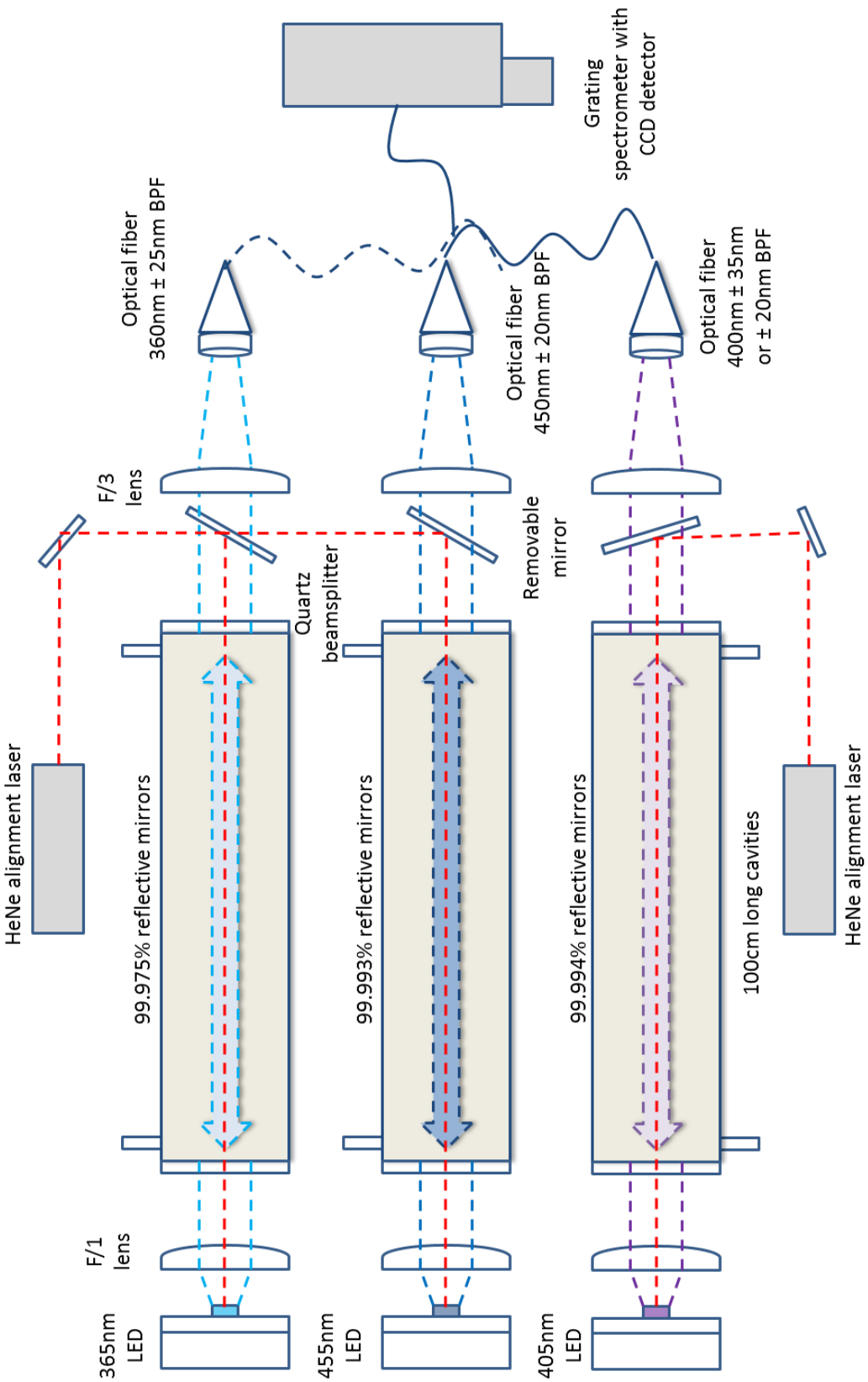

Figure 2.5 Schematic of the three channel IBBCEAS consisting of LED light sources, optical cavities, and a CCD detector.

(Watlow, EZ-ZONE® PM) and maintained at 293 K. Radiation was collimated and coupled into each of the 100 cm long cavities using a 2″ diameter F/1.2 lens. The cavities were formed using highly reflective mirrors (Advanced Thin Films) with 1 m radius of curvature. The center wavelengths and maximum reflectivities were 362 nm (R = 0.99975), 405 nm (R = 0.99994), and 455 nm (R = 0.99993). In cavity enhanced absorption spectroscopy, the effective path length can be defined as equal to an e^{-1} decay of light from the cavity. From this definition, the effective path lengths were 4.0 km, 17 km, and 14 km respectively, when the three cavities contained pure helium (He). Apertures of 1.5 cm diameter were used at the entrance and exit of each cavity to prevent light transmission at the uncoated edges of the 2.5 cm cavity mirrors.

Upon exiting the cavity, the light passed through a quartz beam splitter that was used to turn the beam of a HeNe laser through the cavity for alignment purposes. A 1″ F/3 lens collimated the exiting radiation onto an optical fiber. Bandpass filters on each of the optical fibers prevented stray light from entering the spectrometer. The center wavelength and full width at half maximum (FWHM) for the bandpass filters were 360 nm with FWHM of 50 nm (Omega Optical 360WB50); 400 nm with FWHM of 70 nm (Andover Corp. 400FS70-25) or 40 nm (ThorLabs, FB400-40); and 450 nm with FWHM of 40 nm (Thorlabs, FB450-40). The optical fibers were coupled to a fiber bundle that was input to a Czerny-Turner grating spectrometer with CCD detector (Acton InSpectrum 150), as described in detail by Washenfelder et al.[23]. The fiber bundle illuminated two separate regions of the CCD, allowing spectra from two independent channels to be measured simultaneously. The spectrometer was configured with a 20 μm slit width and 1200 groove/mm grating (500 nm blaze), giving a spectral range of ~117 nm. Spectra of the three channels covering the 350 – 470 nm spectral region were acquired in two separate experiments. The grating was rotated to give a useful spectral range from 331 to

451 nm while measuring the 365 nm and 405 nm channels, and a spectral range from 380 to 484 nm while measuring the 405 nm and 455 nm channels.

The wavelength calibration of the spectrometer was determined using an Hg/Ar calibration lamp with vacuum wavelengths of 334.24, 404.77, 407.90, and 435.96 nm, and is accurate within 0.5 nm[30]. The fixed slit width of 20 μm was found to give a nearly Gaussian lineshape. Because the experiment used an imaging spectrometer to image the input light onto the CCD, the FWHM increased linearly with wavelength (but was constant in frequency space) for the two wavelength determinations. For the 365 nm and 405 nm cavity experiment, the FWHM was 0.27 nm at 350 nm and 0.51 nm at 430 nm. For the 405 nm and 455 nm cavity experiment, the FWHM was 0.29 nm at 380 nm and 0.50 nm at 470 nm.

The sample cells were cylindrical aluminum cells of 2.2 cm inner diameter centered on the optical cavities with ports for the introduction and exhaust of the sample gas. The O_3 concentration entering and exiting the cells was measured and it was determined that there was no loss to the walls. The ports were immediately adjacent to the end mirrors, such that there was no purge volume used between the mirrors and the sample, as has often been employed in previous field and laboratory IBBCEAS and CRDS experiments[31,32]. Mounts with 2.0 cm diameter graphite rods were used to stabilize the cavities. Temperature and pressure in the cavities were measured at the connection between the two IBBCEAS cavities. A thermocouple monitored the temperature, which ranged from 295.1 – 295.8 K, and a transducer (Honeywell, PPT0015AXN5V) monitored pressure, which ranged from 820.7 – 830.8 hPa.

2.5 Ultraviolet-visible spectroscopy

Analysis of the electronic transitions of aqueous phase methylglyoxal was performed using a UV-visible spectrometer from the physical chemistry laboratory at the University of Colorado. Using Beer's law, I was able to extract a molar absorptivity (ε) which describes the inherent strength of the absorption transition from a known methylglyoxal concentration (c) and measured absorbance (A).

$$A = \log (I/I_0) = \varepsilon c l \quad (2.9)$$

The aqueous phase methylglyoxal UV cross section was obtained using an Ocean Optics ISS-UV-Vis spectrometer (CHEM2000, Ocean Optics Inc.). Prior to use the instrument lamp, consisting of a deuterium and tungsten bulb, was turned on and allowed to warm up 15 minutes to ensure stability. To avoid saturation the parameters for the experiment were 50 scans with an integration time of 100 ms. Sample was placed in a quartz 1 cm pathlength cell.

2.6 Nuclear Magnetic Resonance spectroscopy

Nuclear magnetic resonance (NMR) spectroscopy is a useful analytical technique used to identify the structure of a molecule and follow its dynamics. It utilizes electromagnetic radiation associated with radio frequencies, usually ranging from 200-800 Hz, to probe the magnetic properties of atomic nuclei in a molecule. A charged particle, such as a proton, has a magnetic moment arising from its spin angular momentum. A proton (^{1}H) has a nuclear spin angular momentum that can only be values of +½ or -½, which refer to the orientation of the magnetic

moment vectors. This spin angular momentum can change, or split, in the presence of an external magnetic field and used to follow molecular structure[33,34].

In this study, NMR was used to identify methylglyoxal diol aqueous phase solutions and analyze methylglyoxal aqueous phase UV photolysis products. The University of Colorado has an NMR facility (NMR Spectroscopy Facility) that is under the direction of Dr. Richard Shoemaker. The facility has three different spectrometers operating in the 300, 400, and 500 MHz range. These instruments can be used to elucidate structures containing ^{1}H, ^{13}C, ^{19}F, or ^{31}P, obtain high-resolution spectra, and apply multidimensional NMR techniques such as H,C-COSY. In this work, the Varian INOVA 400 MHz NMR was used to perform proton (^{1}H) and carbon (^{13}C) NMR. The NMR studies performed in this work were done in collaboration with Dr. Richard Shoemaker.

2.7 References

1. Smith, B. C. *Fundamentals of Fourier Transform Infrared Spectroscopy*; CRC Press: New York, 1996.
2. Griffiths, P. R.,J.A., D. *Fourier Transform Infrared Spectroscopy*, 2nd ed.; John Wiley and Sons, Inc: New Jersey, 2007.
3. Brown, S. S., Stark, H.,Ravishankara, A. R. Cavity ring-down spectroscopy for atmopheric trace gas detection: application to the nitrate radical (NO_3). *Applied Physics B: Lasers and Optics*, (2002), **75**, 173-182.
4. Brown, S. S. Absorption spectroscopy in high-finesse cavities for atmospheric studies. *Chem. Rev.*, (2003), **103**, 5219-5238.
5. Wheeler, M. D., Newman, S. M., Orr-Ewing, A. J.,Ashfold, M. N. R. Cavity ring-down spectroscopy. *J. Chem. Soc.-Faraday Trans.*, (1998), **94**, 337-351.
6. Zalicki, P.,Zare, R. N. Cavity ring-down spectroscopy for quantitative absorption measurements. *J. Chem. Phys.*, (1994), **102 (7)**, 2708-2717.
7. Scherer, J. J., Paul, J. B., Okeefe, A.,Saykally, R. J. Cavity ringdown laser absorption spectroscopy: History, development, and application to pulsed molecular beams. *Chem. Rev.*, (1997), **97**, 25-51.
8. Dunn, M. E., Shields, G. C., Takahashi, K., Skodje, R. T.,Vaida, V. Experimental and theoretical study of the OH vibrational spectra and overtone chemistry of gas-phase vinylacetic acid. *J. Phys. Chem. A*, (2008), **112**, 10226-10235.
9. Havey, D. K., Feierabend, K. J., Takahashi, K., Skodje, R. T.,Vaida, V. Experimental and theoretical investigation of vibrational overtones of glycolic acid and its hydrogen bonding interactions with water. *J. Phys. Chem. A*, (2006), **110**, 6439-6446.
10. Feierabend, K. J., Havey, D. K., Brown, S. S.,Vaida, V. Experimental absolute intensities of the 4v(9) and 5v(9) O-H stretching overtones of H_2SO_4. *Chem. Phys. Lett.*, (2006), **420**, 438-442.
11. Lane, J. R., Kjaergaard, H. G., Plath, K. L.,Vaida, V. Overtone spectroscopy of sulfonic acid derivatives. *J. Phys. Chem. A*, (2007), **111**, 5434-5440.
12. Rontu, N.,Vaida, V. Vibrational spectroscopy of perfluorocarboxylic acids from the infrared to the visible regions. *J. Phys. Chem. B*, (2008), **112**, 276-282.
13. Takahashi, K., Plath, K. L., Skodje, R. T.,Vaida, V. Dynamics of vibrational overtone excited pyruvic acid in the gas phase: Line broadening through hydrogen-atom chattering. *J. Phys. Chem. A*, (2008), **112**, 7321-7331.
14. Takahashi, K., Plath, K. L., Axson, J. L., Nelson, G. C., Skodje, R. T.,Vaida, V. Dynamics and spectroscopy of vibrational overtone excited glyoxylic acid and 2,2-dihydroxyacetic acid in the gas-phase. *J. Chem. Phys.*, (2010), **132**.
15. Plath, K. L., Takahashi, K., Skodje, R. T.,Vaida, V. Fundamental and overtone vibrational spectra of gas-phase pyruvic acid. *J. Phys. Chem. A*, (2009), **113**, 7294-7303.
16. Busch, K. W.,Busch, M. A. *Cavity-Ringdown Spectroscopy: An Ultratrace-Absorption Measurement Technique*; American Chemical Society: Washington D.C., 1999.
17. Fiedler, S. E., Hese, A.,Ruth, A. A. Incoherent broad-band cavity-enhanced absorption spectroscopy. *Chem. Phys. Lett.*, (2003), **371**, 284-294.

18. Gherman, T., Venables, D. S., Vaughan, S., Orphal, J.,Ruth, A. A. Incoherent broadband cavity-enhanced absorption spectroscopy in the near-ultraviolet: Application to HONO and NO_2. *Environ. Sci. Technol.,* (2008), **42**, 890-895.
19. Langridge, J. M., Ball, S. M., Shillings, A. J. L.,Jones, R. L. A broadband absorption spectrometer using light emitting diodes for ultrasensitive, in situ trace gas detection. *Rev. Sci. Instrum.,* (2008), **79**, 123110.
20. Vaughan, S., Gherman, T., Ruth, A. A.,Orphal, J. Incoherent broad-band cavity-enhanced absorption spectroscopy of the marine boundary layer species I_2, IO and OIO. *Phys. Chem. Chem. Phys.,* (2008), **10**, 4471-4477.
21. Venables, D. S., Gherman, T., Orphal, J., Wenger, J. C.,Ruth, A. A. High sensitivity in situ monitoring of NO_3 in an atmospheric simulation chamber using incoherent broadband cavity-enhanced absorption spectroscopy. *Environ. Sci. Technol.,* (2006), **40**, 6758-6763.
22. Langridge, J. M., Ball, S. M.,Jones, R. L. A compact broadband cavity enhanced absorption spectrometer for detection of atmospheric NO_2 using light emitting diodes. *Analyst,* (2006), **131**, 916-922.
23. Washenfelder, R. A., Langford, A. O., Fuchs, H.,Brown, S. S. Measurement of glyoxal using an incoherent broadband cavity enhanced absorption spectrometer. *Atmos. Chem. Phys.,* (2008), **8**, 7779-7793.
24. Thalman, R.,Volkamer, R. Inherent calibration of a blue LED-CE-DOAS instrument to measure iodine oxide, glyoxal, methyl glyoxal, nitrogen dioxide, water vapour and aerosol extinction in open cavity mode. *Atmos. Meas. Tech.,* (2010), **3**, 1797-1814.
25. Chen, J.,Venables, D. S. A broadband optical cavity spectrometer for measureing weak near-ultraviolet absorption spectra of gases. *Atmos. Meas. Tech. ,* (2011), **4**, 425-436.
26. Bodhaine, B. A., Wood, N. B., Dutton, E. G.,Slusser, J. R. On Rayleigh optical depth calculations. *J. Atmos. Ocean. Technol.,* (1999), **16**, 1854-1861.
27. Sneep, M.,Ubachs, W. Direct measurement of the Rayleigh scattering cross section in various gases. *J. Quant. Spectrosc. Radiat. Transf.,* (2005), **92**, 293-310.
28. Naus, H.,Ubachs, W. Experimental verification of Rayleigh scattering cross sections. *Opt. Lett.,* (2000), **25**, 347-349.
29. Axson, J. L., Washenfelder, R. A., Young, C. J., Kahan, T. F., Vaida, V.,Brown, S. S. Absolute ozone absorption cross section in the Huggins and Chappuis minimum (350-450 nm) at 296 K. *Atmos. Chem. Phys.,* (2011), **11**, 1-10.
30. Sansonetti, C. J., Salit, M. L.,Reader, J. Wavelengths of spectral lines in mercury pencil lamps. *Applied Optics,* (1996), **35**, 74-77.
31. Brown, S. S., Wilson, R. W.,Ravishankara, A. R. Absolute intensities for third and fourth overtone absorptions in HNO_3 and H_2O_2 measured by cavity ring down spectroscopy. *J. Phys. Chem. A,* (2000), **104**, 4976-4983.
32. Dube, W. P., Brown, S. S., Osthoff, H. D., Nunley, M. R., Ciciora, S. J., Paris, M. W., McLaughlin, R. J.,Ravishankara, A. R. Aircraft instrument for simultaneous, in situ measurement of NO_3 and N_2O_5 via pulsed cavity ring-down spectroscopy. *Rev. Sci. Instrum.,* (2006), **77**.
33. Macomber, R. S. *A Complete Introduction to Modern NMR Spectroscopy*; John Wiley & Sons, Inc.: New York, 1998.
34. Balci, M. *Basic ^{1}H and ^{13}C-NMR Spectroscopy*; Elsevier, Inc.: Amsterdam, Netherlands, 2005.

3. Gas-Phase Water Mediated Equilibrium between Methylglyoxal and its Geminal Diol

3.1 Introduction

Atmospheric aerosols are a major topic of current atmospheric studies, given the important, but not fully understood, role that aerosols play in the Earth's radiative balance[1]. Aerosols affect global radiative forcing directly by absorbing or scattering radiation and indirectly by enhancing cloud albedo[1]. Because of their changing chemical composition, aerosol optical and physiochemical properties vary, which greatly complicates the quantification of their global radiative forcing. Efforts at modeling aerosol effects on climate, as assessed by the International Panel on Climate Change (IPCC)[1], are primarily based on sulfate aerosol studies, though there is growing evidence that organic aerosols play an important role in climate change[2-4]. Organic molecules formed by the oxidation of biogenic and anthropogenic organic emissions have been identified as important components of atmospheric aerosols[2,5]. The formation pathways of these secondary organic aerosols (SOA) remain highly speculative, leading to uncertainties in predictions of atmospheric models[6-8]. A large SOA source is missing from models as illustrated by simultaneous field measurements of volatile organic compounds (VOCs) and aerosol particles[6,7,9,10].

Organic acids, especially oxalic and pyruvic acid, are found in SOA, though the origin of these acids is not predicted correctly by the gas-phase chemistry considered in models[11-14]. Recent studies suggest that these acids are made in the aqueous phase, particularly in cloud

water, by the oxidation of aldehydes (e.g. glyoxal and methylglyoxal) with hydroxyl radicals and other aqueous radical species[14-17]. Methylglyoxal is one of the most abundant α–dicarbonyls present in the atmosphere and is produced from VOCs of both biogenic and anthropogenic origin[14,18-20].

Water-mediated aldehyde chemistry is expected to have important consequences to the formation of SOA. For example, laboratory studies of methylglyoxal hydration performed using theoretical[21] and spectroscopic techniques[14,22-24] suggest that in aqueous environments methylglyoxal can become hydrated to form methylglyoxal diol via R3.1 and undergo further reactions to form oligomers[14,21,24]. Like other aldehydes and ketones in aqueous solution, methylglyoxal hydrates through proton addition to the aldehyde carbonyl (C=O) and reaction to form methylglyoxal diol[21-23,25-27]. Methylglyoxal has both an aldehydic and ketonic C=O and it was determined computationally that the aldehydic C=O is more favorably hydrated in solution (ΔG = -1.4 kcal mol^{-1}) than the ketonic C=O (ΔG = +2.5 kcal mol^{-1})[21]. In solution, methylglyoxal is present primarily as methylglyoxal diol (60% diol to 40% tetrol) with the aldehydic group forming a geminal diol[21,23]. Methylglyoxal diol has a lower vapor pressure than methylglyoxal, which allows the molecule to partition more easily into the particle phase, lending to the formation of SOA.

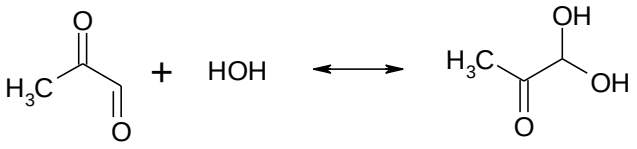

(R3.1)

Although the hydration of small aldehydes in aqueous solutions is known to be extensive, gas-phase hydration of carbonyls has not yet been considered in atmospheric models because it is

commonly believed that there is not enough water present to make such reactions favorable. Gas-phase studies of glyoxylic acid performed in our laboratory observed hydration of glyoxylic acid and allowed for the identification of the gem diol through mid- and near-IR spectroscopy, suggesting this chemistry can occur in water restricted environments[28]. In a CCl_4 matrix with restricted water present, similar results were obtained for the hydration of pyruvic acid[29].

In this infrared (IR) spectroscopic study, we identify and assign the vibrational features of the first gas-phase vibrational spectra of methylglyoxal diol and characterize the water-mediated gas-phase equilibrium between methylglyoxal and methylglyoxal diol. The equilibrium constant, K_P, is calculated using spectroscopically determined concentrations of methylglyoxal, methylglyoxal diol, and water. This study shows gas-phase hydration to be significant even under relatively dry environmental conditions. This affects the gas-phase/aqueous particle partitioning of methylglyoxal and could provide insight into the discrepancy between measured and modeled amounts of SOA[30,31].

3.2 Experimental

3.2.1 Sample preparation

Methylglyoxal (CH_3COCHO) in aqueous solution (40wt%, Sigma-Aldrich) was dried and distilled before use. A 20 mL sample of methylglyoxal solution was attached to a vacuum line at around 15 mTorr and gently heated and stirred at 313 K for 12 – 15 hours. Under these conditions the solution became increasingly viscous. An equal amount of P_2O_5 was added to the sample, which was heated to 393 K and put under vacuum. Two condensers were employed in

the distillation, each cooled with cold water, similar to Gurnick et al[32]. A liquid nitrogen bath was used to trap the purified methylglyoxal. The methylglyoxal solution was orange-brown in color in contrast to the pure methylglyoxal which is bright yellow-green and methylglyoxal diol which is colorless. The methylglyoxal was put under nitrogen and kept frozen so it would remain in its aldehydic form until the experiment. The methylglyoxal diol was prepared in situ, by introducing small amounts of water to the sample in the spectroscopic cell, and allowing methylglyoxal and water vapor to equilibrate over a period of about 10 – 30 minutes.

3.2.2 Fourier transformation infrared spectra

The mid-IR absorption spectra of methylglyoxal and methylglyoxal diol were measured between 1000 cm^{-1} and 8000 cm^{-1} using FTIR spectroscopy at 0.5 cm^{-1} resolution in a static cell. A Bruker IFSv 66 spectrometer equipped with a globar source, KBr beamsplitter, and MCT detector was used for optimal mid-IR absorption spectroscopy. This set up has been described previously[33,34]. The spectroscopic cell was both pressure- and temperature-controlled and was pumped down to approximately 15 mTorr and then closed off to the pump. Methylglyoxal sample was introduced to the cell and water vapor was subsequently added and allowed to equilibrate. All experiments were performed at 298 K.

3.2.3 Theoretical calculations

The structures and fundamental vibrational mode frequencies of methylglyoxal and methylglyoxal diol were calculated by Kaito Takahashi using the hybrid density functional

theory method of B3LYP[35,36] with the 6-31+G(d,p) basis set[37-41] using the Gaussian 03 program[39]. The anharmonic frequencies using the perturbation theory developed by Barone et al.[42] using the B3LYP method is reported along with the intensity calculated by the double harmonic approximation. The optimized structures indicate that *trans*-methylglyoxal is the most stable structure of methylglyoxal, with the *cis*-methylglyoxal structure being 4.9 kcal mol^{-1} higher in energy. Calculations also confirmed that methylglyoxal would hydrate at the aldehydic group. The theoretical frequencies and intensities along with the experimental frequencies are presented in Table 3.1.

3.3 Results and Discussion

3.3.1 Fundamental gas-phase spectra methylglyoxal and methylglyoxal diol

The fundamental gas-phase IR spectrum of methylglyoxal has been previously observed and provides the basis for determining the presence of methylglyoxal diol in this study (Fig. 3.1)[43]. In the lower energy region of the methylglyoxal spectrum (Fig. 3.1a), from 1050 cm^{-1} to 1500 cm^{-1}, there are three distinguishable bands which are assigned to the C-C-C asymmetric stretch at 1240 cm^{-1} (ν_4), the C-H bend (ν_6) at 1373 cm^{-1}, and the CH_3 bends (ν_7) in the 1415 cm^{-1} to 1440 cm^{-1} region (Table 3.1). Methylglyoxal contains a ketonic and aldehydic C=O, which are present in the methylglyoxal spectrum at 1723 cm^{-1} (ν_8) and 1741 cm^{-1} (ν_9) respectively (Fig. 3.1a).

Table 3.1 The theoretical and observed experimental frequencies for methylglyoxal and methylglyoxal diol with vibrational modes assignments. The δ denotes a methylglyoxal diol vibration, Hb denotes hydrogen bonding, and Fr denotes free OH. B3LYP/6-31+G(d,p) theoretical frequencies were scaled using wavenumber linear scaling method.

Theoretical Frequency (cm^{-1})	Theoretical Intensity (km mol^{-1})	Experimental Frequency (cm^{-1})	Mode Assignments	
1099	182	1088	ν^{δ}_1	Hb C-O stretch
1185	73	1173	ν^{δ}_2	C-O-H wag
1180	18	1199	ν^{δ}_3	C-C-C stretch
1207	22	1240	ν_4	C-C-C stretch
1275	48	1292	ν^{δ}_5	Hb C-O-H bend
1335	2	1373	ν_6	C-H bend
1366-1415	-	1415-1440	ν_7	CH_3 bend
1754	132	1723	ν_8	C=O stretch
1774	114	1741	ν_9	HC=O stretch
-	-	1780	ν^{δ}_{10}	Diol feature
2811	72	2835	ν_{11}	C-H stretch
2838	43	2895	ν^{δ}_{12}	C-H stretch
3497	-	3443	$2\nu_8$	C=O overtone
3530	-	3458	$2\nu_9$	C=O overtone
3478	86	3505	ν^{δ}_{13}	Hb OH stretch
3623	55	3585	ν^{δ}_{14}	Fr OH stretch

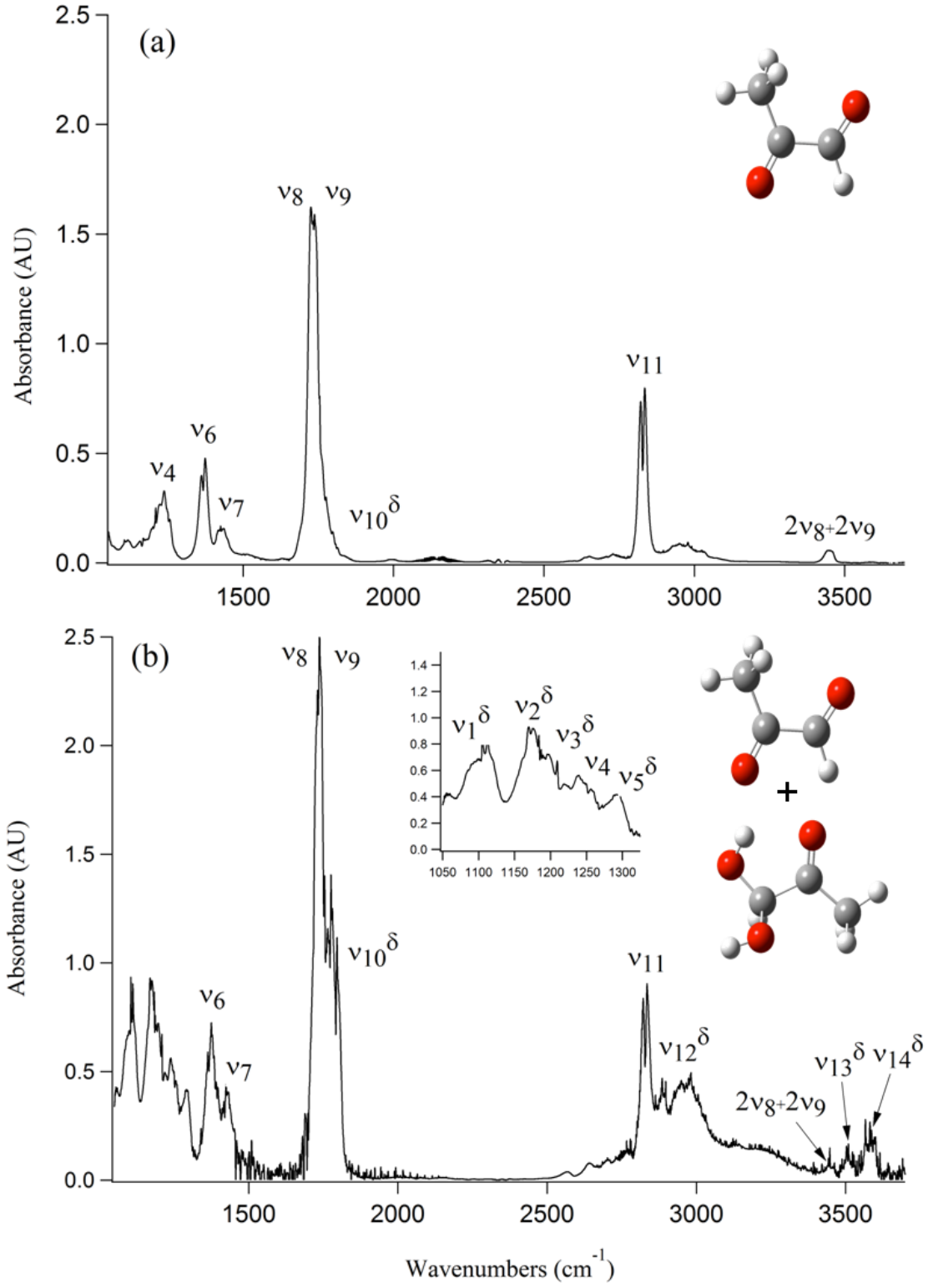

Figure 3.1 The fundamental gas-phase spectra from 1050 cm^{-1} to 3600 cm^{-1} of (a) methylglyoxal and (b) methylglyoxal and methylglyoxal diol. The methylglyoxal diol frequencies are labeled with δ.

The C-H stretching vibration of methylglyoxal has been previously assigned and occurs at 2835 cm^{-1} (ν_{11})[43]. The methylglyoxal C-H stretch is very prominent and was used to compare the methylglyoxal and methylglyoxal diol spectra and to identify methylglyoxal diol. The peak at 3450 cm^{-1}, which normally corresponds to the OH stretching region, I assign to the first overtone, $2\nu_8$ and $2\nu_9$, of the ν_8 and ν_9 C=O stretches as seen in Fig. 3.1a. This peak has been previously observed, but not assigned[43].

The addition of water to the methylglyoxal sample hydrates methylglyoxal to form methylglyoxal diol (Fig. 3.1b). The spectrum in Fig. 3.1b shows both methylglyoxal and methylglyoxal diol features under very low relative humidity (RH% <5%). In the absence of literature assignments, theoretical frequency and intensity calculations aided in assigning methylglyoxal diol vibrational modes (Table 3.1). The formation of methylglyoxal diol can be observed by the coincidence of the distinct methylglyoxal diol vibrational modes that appear in the lower energy region from 1050 cm^{-1} to 1500 cm^{-1} (Fig. 3.1b inset), the decrease in the ν_9 intensity relative to ν_8 intensity, and the appearance of OH stretching vibrations at 3505 cm^{-1} (ν^{δ}_{13}) and 3585 cm^{-1} (ν^{δ}_{14}) (Fig. 3.1b) with the addition of water vapor. In addition to this, the C-H stretching mode of methylglyoxal diol is observed at 2895 cm^{-1} (ν^{δ}_{12}). Since the lower energy region from 1050 cm^{-1} to 1500 cm^{-1} becomes increasingly complex due to overlapping bands from the addition of water, the intensities of the ν_8, ν_9, ν^{δ}_{13}, and ν^{δ}_{14} stretches were used to quantify and follow the formation of methylglyoxal diol.

3.3.2 C=O fundamental and overtone stretching region

With the addition of trace amounts of water, the C=O stretching region is altered by the decrease in intensity of ν_9 relative to the ν_8, presumably due to the formation of methylglyoxal diol. To better understand these changes in the fundamental C=O stretching region, the intensity and peak width (FWHM) of the fundamental and overtone C=O stretches for methylglyoxal and methylglyoxal diol were modeled by two Lorenzian curves. The fundamental methylglyoxal C=O stretching region shows ν_8 and ν_9 with roughly the same intensity (Fig. 3.2a). As methylglyoxal is hydrated to form methylglyoxal diol, the aldehydic C=O is hydrated to form the gem diol, which can be observed spectroscopically by the decrease in the relative intensity of ν_9 in Fig. 3.2b, intensity $\nu_8 : \nu_9 = 1.0 : 0.75$. In addition to the methylglyoxal and methylglyoxal diol fundamental C=O stretches near 1730 cm^{-1}, there is a third peak around 1780 cm^{-1} (ν^{δ}_{10}), which is attributed to the diol because of its intensity increase mirroring the increase in partial pressure of water. The methylglyoxal and methylglyoxal diol C=O first overtone region near 3450 cm^{-1} has the ketonic C=O overtone at 3443 cm^{-1} ($2\nu_8$) and the aldehydic C=O overtone at 3458 cm^{-1} ($2\nu_9$). In both methylglyoxal and methylglyoxal diol spectra, the intensity of the first overtone C=O stretches drops by at least a factor of 10 from the intensity of the fundamental C=O stretches. In the methylglyoxal C=O first overtone spectrum in Fig. 3.2c, the relative intensity of $2\nu_8 : 2\nu_9 = 1.00 : 0.23$, while in Fig. 3.2d it is 1.00 : 0.17. This relative intensity decrease seen for ν_9 in Fig. 3.2d is consistent with the decrease in the fundamental C=O, reinforcing the suggestion that the fundamental aldehydic C=O intensity is decreasing because of hydration of the carbonyl to generate diol.

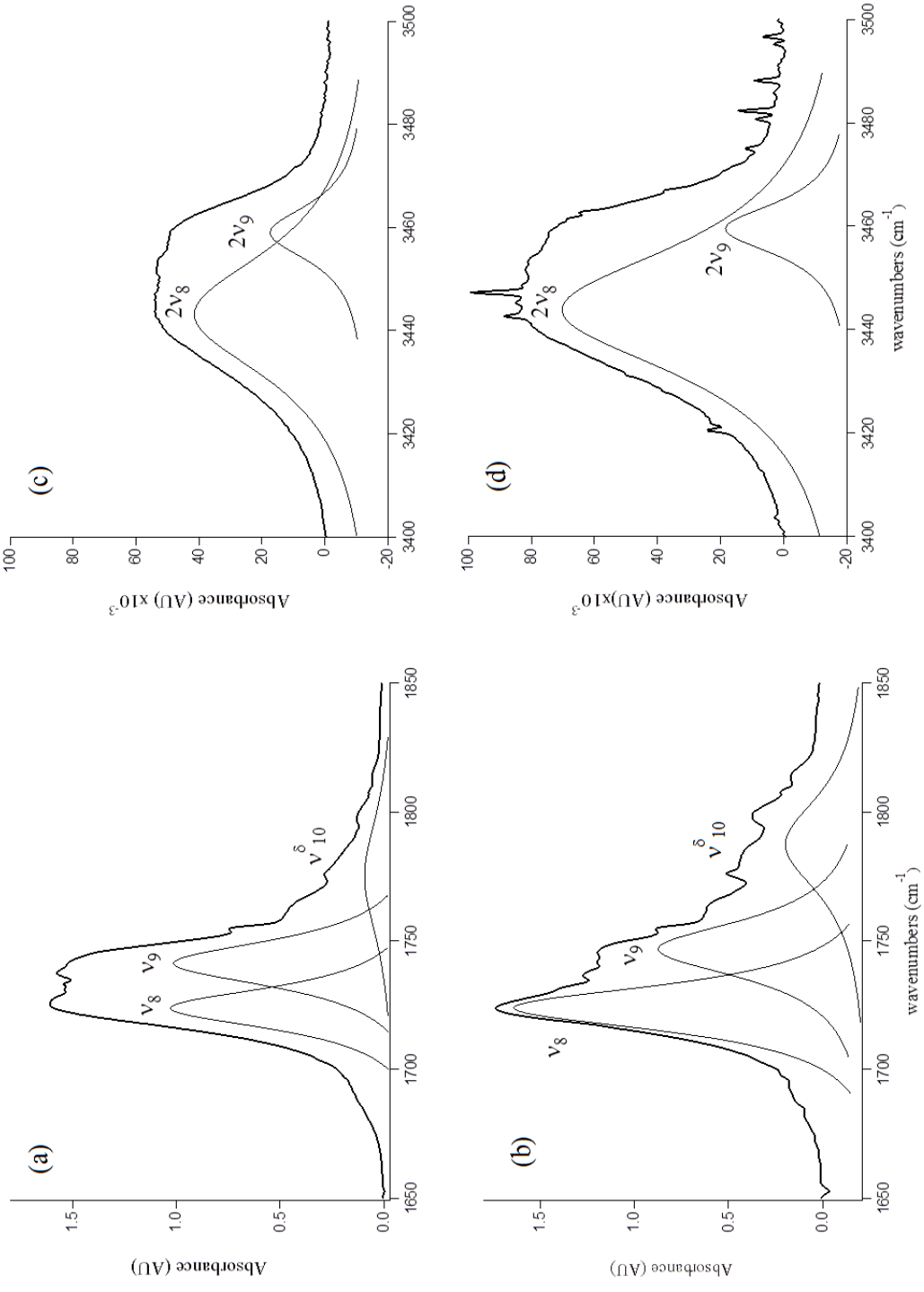

Figure 3.2 The fundamental C=O stretching region of (a) methylglyoxal and (b) methylglyoxal diol and the first overtone, $2\nu_8$ and $2\nu_9$, of (c) methylglyoxal and (d) methylglyoxal diol showing a decrease in the relative intensity of ν_9 in (b) when compared to (a) and a decrease in the $2\nu_8$ and $2\nu_9$ aldehydic peak in (d) when compared to (c).

3.3.3 OH stretching region of methylglyoxal diol

In the methylglyoxal diol spectrum (Fig. 3.3), there are two OH vibrational stretching modes, with the δ denoting methylglyoxal diol vibration, located at 3505 cm^{-1} (ν^{δ}_{13}) and 3585 cm^{-1} (ν^{δ}_{14}), in addition to the 3450 cm^{-1} peak assigned to $2\nu_8$ and $2\nu_9$. The first OH vibrational stretch at ν^{δ}_{13} is attributed to the hydrogen-bonded OH of methylglyoxal diol and the ν^{δ}_{14} is attributed to the free OH of methylglyoxal diol. Our theoretical frequency puts the ν^{δ}_{13} at 3478 cm^{-1}, which is slightly red shifted compared to the experimental value of 3505 cm^{-1}. This discrepancy between the theoretically and experimentally derived frequencies is consistent with results from other studies[28,44-47]. The ν^{δ}_{13} and ν^{δ}_{14} could also have a contribution from tetrol OH stretching vibrations which all fall near to those of methylglyoxal diol, making it difficult to distinguish or model them. In solution, the ratio of diol to tetrol is approximately 60/40[23]. While this ratio has not been measured for the gas-phase, at much lower water concentration in our gas-phase experiments we expect methylglyoxal diol to be favored over the tetrol. The ν^{δ}_{14} stretch is present in very small amounts even in our lowest relative humidity methylglyoxal spectrum. The ν^{δ}_{14} stretch increases in intensity in response to increasing the partial pressure of water in the experiments.

The region from 3100 cm^{-1} to 3350 cm^{-1} contains water clusters and hydrated complexes of methylglyoxal and methylglyoxal diol. The long red shift relative to computations and very broad appearance of these features are consistent with observations and predictions of hydrogen bonded water clusters[28,44-46,48,49]. The broad and overlapping features in this region make it difficult to qualitatively and quantitatively identify these clusters.

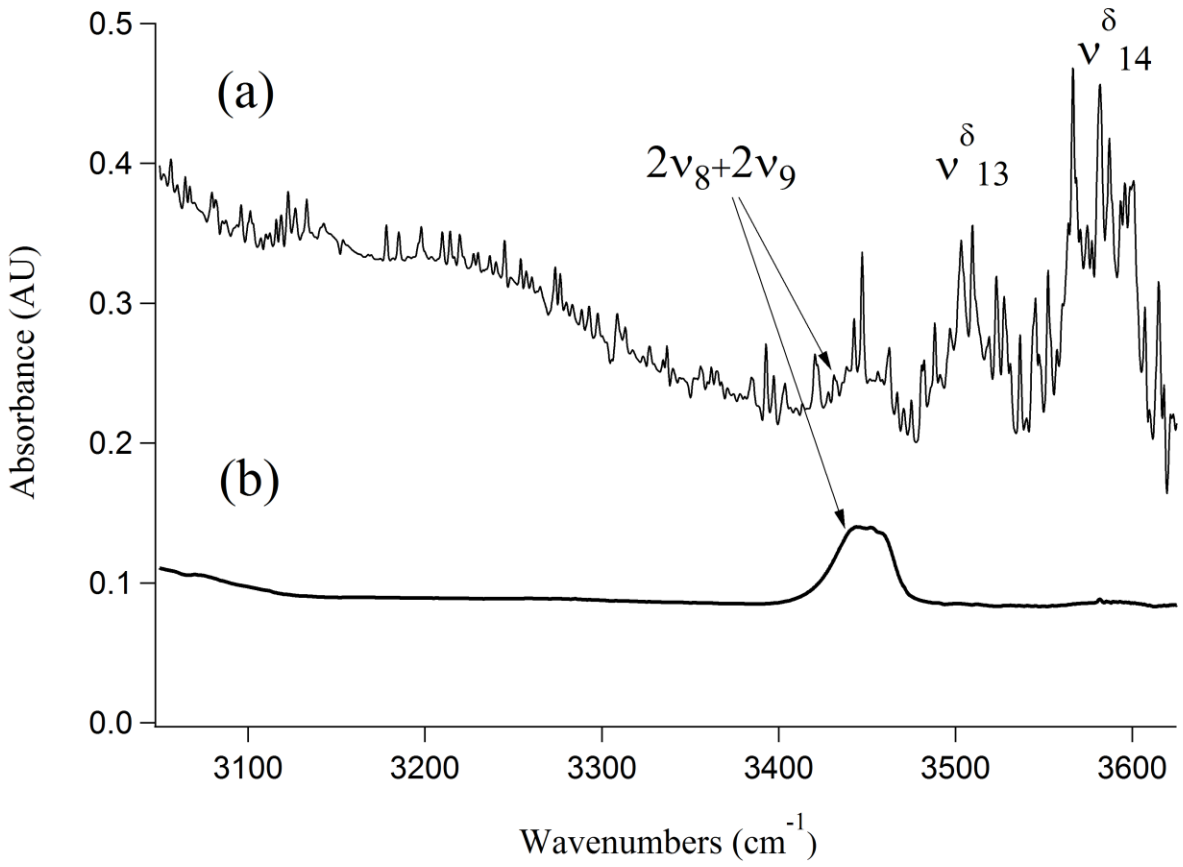

Figure 3.3 The 3000 cm^{-1} to 3650 cm^{-1} region of (a) methylglyoxal diol and (b) methylglyoxal, showing the appearance of water clusters (3100 cm^{-1} to 3350 cm^{-1}), the $2\nu_8$ and $2\nu_9$ of C=O, and the ν^{δ}_{13} and ν^{δ}_{14} of methylglyoxal diol.

3.3.4 Determination of methylglyoxal, methylglyoxal diol, and water partial pressures

Based on the spectroscopic identification of methylglyoxal diol, we quantified the amount of methylglyoxal, methylglyoxal diol, and water present in each spectrum as outlined below. Spectra that were saturated were not used in the calculation of partial pressures, but were useful in making methylglyoxal and methylglyoxal diol mode assignments. Experimentally observed spectroscopic water lines were compared with HITRAN water lines and cross sections to determine the partial pressure of water (Table 3.2), P_{H2O}, and percent relative humidity, RH%, in each experiment[50]. Three water lines at 1550, 1918, and 3920 cm^{-1} were isolated and analyzed. Each observed water line was integrated and the H_2O number density (N/v) was determined via Eqn. 3.1:

$$\frac{N}{v} = \frac{\text{Integrated Absorbance}}{L \times \sigma_{H2O}} \qquad (3.1)$$

The path length of the cell, L, was 71 cm and σ_{H2O} (cm $molecule^{-1}$) is the HITRAN cross section for each waterline. The P_{H2O} was determined using the average N/v from the three water lines and converted to RH% using the ideal gas law and the vapor pressure of water.

The partial pressure of methylglyoxal, P_{mgly}, was determined spectroscopically using the integrated absorbance of the methylglyoxal CH stretch at 2835 cm^{-1} (Table 3.3) and a theoretically calculated methylglyoxal cross section, σ_{mgly}, of 1.19×10^{-17} cm $molecule^{-1}$ (Table 3.1). The theoretical and literature value for σ_{mgly} were compared: there is a discrepancy, with the literature value being higher[43]. In this work, I chose to use the theoretically calculated σ_{mgly} because of the agreement of the calculated and experimental frequencies and intensities (Table

Table 3.2 The partial pressures, $P_{H2O,}$ of water determined from experimental spectra and HITRAN. The integrated absorbance (Int Abs) for each experimental water line was taken. The water lines at 1550, 1918, and 3920 cm^{-1}, had the following cross sections 2.88×10^{-20} cm $molecule^{-1}$, 2.93×10^{-20} cm $molecule^{-1}$, 2.61×10^{-20} cm $molecule^{-1}$.[50]

Experiment	Int Abs (1550 cm^{-1})	Int Abs (1918 cm^{-1})	Int Abs (3920 cm^{-1})	Avg. N/v (molecule cm^{-3})	P_{H2O} (atm)
1	0.003	0.003	0.002	1.33×10^{15}	5.40×10^{-5}
2	0.003	0.003	0.002	1.33×10^{15}	5.40×10^{-5}
3	0.003	0.003	0.002	1.33×10^{15}	5.40×10^{-5}
4	0.008	0.006	0.005	3.17×10^{15}	1.29×10^{-4}

Table 3.3 Partial pressures of methylglyoxal, P_{mgly}, determined from experimental spectra. The integrated absorbance (Int Abs) for the methylglyoxal CH stretch at 2835 cm^{-1} was taken. The theoretical calculated σ_{mgly} of 1.19×10^{-17} cm $molecule^{-1}$ is used.

Experiment	Int Abs (cm^{-1})	N/v (molecule cm^{-3})	P_{mgly} (atm)
1	26.05	3.08×10^{16}	1.25×10^{-3}
2	25.93	3.07×10^{16}	1.24×10^{-3}
3	25.66	3.04×10^{16}	1.23×10^{-3}
4	33.15	3.92×10^{16}	1.59×10^{-3}

3.1). For consistency, the theoretical σ_{mgly} was used to determine the K_P from these experiments. The methylglyoxal N/v was determined for each experiment using Eqn. 3.1 and the P_{mgly} was then determined using the ideal gas law.

The partial pressure of methylglyoxal diol (P_{diol}) was determined spectroscopically using the methylglyoxal diol OH stretching vibration at 3585 cm^{-1} (Table 3.4). This peak was used because of its presence in each of the spectra containing methylglyoxal diol and its response to water. It is assumed that this peak contains only methylglyoxal diol (although it may also contain a small acid contribution) and this feature was integrated to obtain an integrated absorbance. The integrated absorbance along with the theoretically determined cross section, σ_{OH}, of 9.14×10^{-18} cm $molecule^{-1}$, which is in agreement with a typical alcohol cross section, was used in Eqn. 1 to determine methylglyoxal diol N/v[46,51,52]. The P_{diol} was then determined using Eqn. 3.1 and ideal gas law. The experimentally obtained partial pressures are shown in Table 3.5.

3.3.5 Water-mediated gas-phase equilibrium constant

Previous methylglyoxal hydration studies have been primarily performed in the solution phase[21,22]. There have been few thermodynamic studies of the hydration of methylglyoxal and none performed in the gas-phase. As shown in Table 3.5, under very dry conditions like those used in this study (RH% <5%), easily detectable quantities of methylglyoxal diol are formed. Assuming that this reaction involves equilibrium R3.1, and that the tetrol formation is inefficient under conditions like those in our investigation, the equilibrium constant K_P can be derived from the partial pressures extracted from our spectra using Eqn 3.2.

Table 3.4 Partial pressures of methylglyoxal diol, P_{diol}, determined from experimental spectra. The integrated absorbance (Int Abs) for the methylglyoxal diol Fr OH stretch at 3585 cm^{-1} was taken. The theoretically calculated σ_{OH} of 9.14×10^{-18} cm $molecule^{-1}$ is used.

Experiment	Int Abs (cm^{-1})	N/v (molecule cm^{-3})	P_{diol} (atm)
1	0.172	2.65×10^{14}	1.08×10^{-5}
2	0.169	2.60×10^{14}	1.06×10^{-5}
3	0.171	2.63×10^{14}	1.07×10^{-5}
4	0.505	7.78×10^{14}	3.16×10^{-5}

Table 3.5 The experimentally determined gas-phase water mediated equilibrium constant, K_P, calculated using Eqn. 2 for R1 between methylglyoxal and methylglyoxal diol, and the experimentally determined Gibbs free energy, $\Delta G°$, values calculated using Eqn. 3. Temperature was 298 K. K_P values have an error of ±13.0 and $\Delta G°$ values of ±0.05 kcal mol^{-1}.

Experiment	P_{diol} (atm)	P_{mgly} (atm)	P_{H2O} (atm)	K_P	$\Delta G°$ (kcal mol^{-1})
1	1.08×10^{-5}	1.25×10^{-3}	5.40×10^{-5}	159	-3.13
2	1.06×10^{-5}	1.24×10^{-3}	5.40×10^{-5}	157	-3.12
3	1.07×10^{-5}	1.23×10^{-3}	5.40×10^{-5}	161	-3.13
4	3.16×10^{-5}	1.59×10^{-3}	1.29×10^{-4}	154	-2.98

$$K_P = \frac{P_{diol}}{P_{mgly} \times P_{H2O}} \quad (3.2)$$

The K_P values for the four experiments (Table 3.5) fall within the range of 154 to 161 (±13.0) and are favorable to methylglyoxal diol production. The low relative humidity conditions of the experiments (RH% <5%) did not allow for the water concentration to be varied over a large range and there was little clustering observed by FTS. As noted previously, there was a discrepancy between the theoretical and literature σ_{mgly}, which leads to ~11% discrepancy in the K_P values determined using the same spectra; with the theoretical values being slightly higher than the literature K_P values.

The Gibbs free energy ($\Delta G°$) was calculated from K_P using Eqn. (3.3):

$$\Delta G° = -RT (\ln K_P) \quad (3.3)$$

Our experimentally determined $\Delta G°$ values, which range from -2.98 kcal mol^{-1} to -3.1 kcal mol^{-1} (±0.051) (Table 3.5) show that the production of methylglyoxal diol is favorable in the gas-phase.

3.4 Conclusion

Methylglyoxal is a known product of VOC oxidation and is prevalent in the atmosphere. In this work we assign the first gas-phase IR spectrum of methylglyoxal diol and find that the gas-phase hydration of methylglyoxal is favorable at low relative humidity (RH%<5%). One of

the consequences of this gas-phase water-mediated chemistry is a change in the electronic state of the molecule, eliminating the n→π* transition of the aldehyde carbonyl which is well known to undergo near-UV photochemistry[53-55]. Instead, the OH vibrational chromophore of the diol may react (through excitation of the OH vibrational overtone in the near-IR) to form new products by dehydration, decarboxylation, and decarbonylation, as suggested recently for a number of alcohols and acids[44,56-59]. Using methylglyoxal and methylglyoxal diol spectral features we determine the gas-phase water-mediated equilibrium K_P. This K_P suggests that the gas-phase formation of the diol in the atmosphere is possible and could be expected to affect gas-particle partitioning of methylglyoxal and its potential to form SOA.

3.5 References

1. Solomon, S., Qin, D., Manning, M., Chen, Z., Marquis, M., Averyt, K. B., Tignor, M.,Miller, H. L. e. *IPCC, 2007: Climate Change 2007: The Physical Science Basis. Contribution of Working Group I to the Fourth Assessment Report of the Intergovernmental Panel on Climate Change* Cambridge University Press: Cambridge, United Kingdom and New York, NY, USA, 2007.
2. Kanakidou, M., Seinfeld, J. H., Pandis, S. N., Barnes, I., Dentener, F. J., Facchini, M. C., Van Dingenen, R., Ervens, B., Nenes, A., Nielsen, C. J., Swietlicki, E., Putaud, J. P., Balkanski, Y., Fuzzi, S., Horth, J., Moortgat, G. K., Winterhalter, R., Myhre, C. E. L., Tsigaridis, K., Vignati, E., Stephanou, E. G.,Wilson, J. Organic aerosol and global climate modelling: a review. *Atmos. Chem. Phys.,* (2005), **5**, 1053-1123.
3. De Gouw, J.,Jimenez, J. L. Organic aerosols in the Earth's atmosphere. *Environ. Sci. Technol.,* (2009), **43**, 7614-7618.
4. Rincon, A. G., Guzman, M. I., Hoffmann, M. R.,Colussi, A. J. Optical absorptivity versus molecular composition of model organic aerosol matter. *J. Phys. Chem. A,* (2009), **113**, 10512-10520.
5. Zhang, Q., Jimenez, J. L., Canagaratna, M. R., Allan, J. D., Coe, H., Ulbrich, I., Alfarra, M. R., Takami, A., Middlebrook, A. M., Sun, Y. L., Dzepina, K., Dunlea, E., Docherty, K., DeCarlo, P. F., Salcedo, D., Onasch, T., Jayne, J. T., Miyoshi, T., Shimono, A., Hatakeyama, S., Takegawa, N., Kondo, Y., Schneider, J., Drewnick, F., Borrmann, S., Weimer, S., Demerjian, K., Williams, P., Bower, K., Bahreini, R., Cottrell, L., Griffin, R. J., Rautiainen, J., Sun, J. Y., Zhang, Y. M.,Worsnop, D. R. Ubiquity and dominance of oxygenated species in organic aerosols in anthropogenically-influenced Northern Hemisphere midlatitudes. *Geophys. Res. Lett.,* (2007), **34**, L13801.
6. Heald, C. L., Jacob, D. J., Park, R. J., Russell, L. M., Huebert, B. J., Seinfeld, J. H., Liao, H.,Weber, R. J. A large organic aerosol source in the free troposphere missing from current models. *Geophys. Res. Lett.,* (2005), **32**, L18809.
7. Volkamer, R., Jimenez, J. L., San Martini, F., Dzepina, K., Zhang, Q., Salcedo, D., Molina, L. T., Worsnop, D. R.,Molina, M. J. Secondary organic aerosol formation from anthropogenic air pollution: Rapid and higher than expected. *Geophys. Res. Lett.,* (2006), **33**, 4.
8. Finlayson-Pitts, B. J. Reactions at surfaces in the atmosphere: integration of experiments and theory as necessary (but not necessarily sufficient) for predicting the physical chemistry of aerosols. *Phys. Chem. Chem. Phys.,* (2009), **11**, 7760-7779.
9. Fast, J., Aiken, A. C., Allan, J., Alexander, L., Campos, T., Canagaratna, M. R., Chapman, E., DeCarlo, P. F., de Foy, B., Gaffney, J., de Gouw, J., Doran, J. C., Emmons, L., Hodzic, A., Herndon, S. C., Huey, G., Jayne, J. T., Jimenez, J. L., Kleinman, L., Kuster, W., Marley, N., Russell, L., Ochoa, C., Onasch, T. B., Pekour, M., Song, C., Ulbrich, I. M., Warneke, C., Welsh-Bon, D., Wiedinmyer, C., Worsnop, D. R., Yu, X. Y.,Zaveri, R. Evaluating simulated primary anthropogenic and biomass burning organic aerosols during MILAGRO: Implications for assessing treatments of secondary organic aerosols. *Atmos. Chem. Phys.,* (2009), **9**, 6191-6215.
10. De Gouw, J. A., Middlebrook, A. M., Warneke, C., Goldan, P. D., Kuster, W. C., Roberts, J. M., Fehsenfeld, F. C., Worsnop, D. R., Canagaratna, M. R., Pszenny, A. A. P.,

Keene, W. C., Marchewka, M., Bertman, S. B.,Bates, T. S. Budget of organic carbon in a polluted atmosphere: Results from the New England Air Quality Study in 2002. *J. Geophys. Res.-Atmos.*, (2005), **110**, 22.

11. Ervens, B., Feingold, G., Frost, G. J.,Kreidenweis, S. M. A modeling study of aqueous production of dicarboxylic acids: 1. Chemical pathways and speciated organic mass production. *J. Geophys. Res.-Atmos.*, (2004), **109**, 20.
12. Tervahattu, H., Juhanoja, J.,Kupiainen, K. Identification of an organic coating on marine aerosol particles by TOF-SIMS. *J. Geophys. Res.-Atmos.*, (2002), **107**, 7.
13. Veres, P., Roberts, J. M., Warneke, C., Welsh-Bon, D., Zahniser, M., Herndon, S., Fall, R.,de Gouw, J. Development of negative-ion proton-transfer chemical-ionization mass spectrometry (NI-PT-CIMS) for the measurement of gas-phase organic acids in the atmosphere. *Int. J. Mass Spectrom.*, (2008), **274**, 48-55.
14. Altieri, K. E., Seitzinger, S. P., Carlton, A. G., Turpin, B. J., Klein, G. C.,Marshall, A. G. Oligomers formed through in-cloud methylglyoxal reactions: Chemical composition, properties, and mechanisms investigated by ultra-high resolution FT-ICR mass spectrometry. *Atmos. Environ.*, (2008), **42**, 1476-1490.
15. Ervens, B., Carlton, A. G., Turpin, B. J., Altieri, K. E., Kreidenweis, S. M.,Feingold, G. Secondary organic aerosol yields from cloud-processing of isoprene oxidation products. *Geophys. Res. Lett.*, (2008), **35**, 5.
16. Carlton, A. G., Turpin, B. J., Altieri, K. E., Seitzinger, S., Reff, A., Lim, H. J.,Ervens, B. Atmospheric oxalic acid and SOA production from glyoxal: Results of aqueous photooxidation experiments. *Atmos. Environ.*, (2007), **41**, 7588-7602.
17. Warneck, P. In-cloud chemistry opens pathway to the formation of oxalic acid in the marine atmosphere. *Atmos. Environ.*, (2003), **37**, 2423-2427.
18. Fu, T. M., Jacob, D. J., Wittrock, F., Burrows, J. P., Vrekoussis, M.,Henze, D. K. Global budgets of atmospheric glyoxal and methylglyoxal, and implications for formation of secondary organic aerosols. *J. Geophys. Res.-Atmos.*, (2008), **113**, 17.
19. Jang, M. S.,Kamens, R. M. Characterization of secondary aerosol from the photooxidation of toluene in the presence of NO_x and 1-propene. *Environ. Sci. Technol.*, (2001), **35**, 3626-3639.
20. Tuazon, E. C., Macleod, H., Atkinson, R.,Carter, W. P. L. Alpha-dicarbonyl yields from the NO_X-air photooxidations of a aeries of aromatic-hydrocarbons in air. *Environ. Sci. Technol.*, (1986), **20**, 383-387.
21. Krizner, H. E., De Haan, D. O.,Kua, J. Thermodynamics and kinetics of methylglyoxal dimer formation: A computational study. *J. Phys. Chem. A*, (2009), **113**, 6994-7001.
22. Betterton, E. A.,Hoffmann, M. R. Kinetics, mechanism, and thermodynamics of the reversable-reaction of methylglyoxal (CH_3COCHO) with S(IV). *J. Phys. Chem.*, (1987), **91**, 3011-3020.
23. Nemet, I., Vikic-Topic, D.,Varga-Defterdarovic, L. Spectroscopic studies of methylglyoxal in water and dimethylsulfoxide. *Bioorganic Chem.*, (2004), **32**, 560-570.
24. Loeffler, K. W., Koehler, C. A., Paul, N. M.,De Haan, D. O. Oligomer formation in evaporating aqueous glyoxal and methylglyoxal solutions. *Environ. Sci. Technol.*, (2006), **40**, 6318-6323.
25. Bell, R. P., Rand, M. H.,Wynnejones, K. M. A. Kinetics of the hydration of acetaldehyde. *Transactions of the Faraday Society*, (1956), **52**, 1093-1102.

26. Buschmann, H. J., Dutkiewicz, E.,Knoche, W. The reversable hydration of carbonyl-compounds in aqueous-solution.2. The kinetics of the keto gem-diol transition. *Ber. Bunsen-Ges. Phys. Chem. Chem. Phys.,* (1982), **86**, 129-134.
27. Wolfe, S., Kim, C. K., Yang, K., Weinberg, N.,Shi, Z. Hydration of the carbonyl group - A theoretical-study of the cooperative mechanism. *J. Am. Chem. Soc.,* (1995), **117**, 4240-4260.
28. Plath, K. L., Axson, J. L., Nelson, G. C., Takahashi, K., Skodje, R. T.,Vaida, V. Gas-phase vibrational spectra of glyoxylic acid and its gem diol monohydrate. Implications for atmospheric chemistry. *React. Kinet. Catal. Lett.,* (2009), **96**, 209-224.
29. Maron, M. K., Takahashi, K., Shoemaker, R. K.,Vaida, V. Hydration of pyruvic acid to its geminal-diol, 2,2-dihydroxypropanoic acid, in a water-restricted environment. *Chem. Phys. Lett.,* (2011), **513**, 184-190.
30. Bao, L., Matsumoto, M., Kubota, T., Kazuhiko, S., Wang, Q.,Sakamoto, K. Gas/particle partioning of low-molecular-weight diacarboxylic acids at the suburban site in Saitama, Japan. *Atmos. Environ.,* (2009.
31. Matsunaga, S., Mochida, M.,Kawamura, K. Variation on the atmospheric concentrations of biogenic carbonyl compounds and their removal processes in the northern forest at Moshiri, Hokkaido Island in Japan. *J. Geophys. Res.-Atmos.,* (2004), **109**, 9.
32. Gurnick, M., Chaiken, J., Benson, T.,McDonald, J. D. Vibrational and rotational spectroscopy of the 1st electronically allowed transition of alpha-dicarbonyls. *J. Chem. Phys.,* (1981), **74**, 99-105.
33. Rontu, N.,Vaida, V. Vibrational spectroscopy of perfluoroproplonic acid in the region between 1000 and 11000 cm^{-1}. *J. Mol. Spectrosc.,* (2006), **237**, 19-26.
34. Dunn, M. E., Shields, G. C., Takahashi, K., Skodje, R. T.,Vaida, V. Experimental and theoretical study of the OH vibrational spectra and overtone chemistry of gas-phase vinylacetic acid. *J. Phys. Chem. A,* (2008), **112**, 10226-10235.
35. Becke, A. D. Density-functional thermochemistry. 3. The role of exact exchange *J. Chem. Phys.,* (1993), **98**, 5648-5652.
36. Lee, C. T., Yang, W. T.,Parr, R. G. Development of the Colle-Salvetti correlation-energy formula into a functional of the electron-density. *Phys. Rev. B,* (1988), **37**, 785-789.
37. Clark, T., Chandrasekhar, J., Spitznagel, G. W.,Schleyer, P. V. Efficient diffuse function-augmented basis-sets for anion calculations. 3. The 3-21+G basis set for 1st-row elements, LI-F. *J. Comput. Chem.,* (1983), **4**, 294-301.
38. Frisch, M. J., Pople, J. A.,Binkley, J. S. Self-consistent molecular-orbital methods. 25. Supplementary functions for gaussian-basis sets. *J. Chem. Phys.,* (1984), **80**, 3265-3269.
39. Frisch, M. J., G.W. Trucks, H.B. Schlegel, G.E. Scuseria, M.A. Robb, J.R. Cheeseman, J.A. Montgomery, T. Vreven, K.N. Kudin, J.C. Burant, J.M. Millam, S.S. Iyengar, ,J.Tomasi, V. B., B. Mennucci, M. Cossi, G. Scalmani, N. Rega, G.A. Petersson, H. Nakatsuji, M. Hada, M. Ehara, K. Toyota, R. Fukuda, J. Hasegawa, M. Ishida, T. Nakajima, Y. Honda, O. Kitao, H. Nakai, M. Klene, X. Li, J.E. Knox, H.P. Hratchian, J.B. Cross, V. Bakken, C. Adamo, J. Jaramillo, R. Gomperts, R.E. Stratmann, O. Yazyev, A.J. Austin, R. Cammi, C. Pomelli, J.W. Ochterski, P.Y. Ayala, K. Morokuma, G.A. Voth, P. Salvador, J.J. Dannenberg, V.G. Zakrzewski, S. Dapprich, A.D. Daniels, M.C. Strain, O.Farkas, D.K. Malick, A.D. Rabuck, K. Raghavachari, J.B. Foresman, J.V. Ortiz, Q. Cui, A.G. Baboul, S. Clifford, J. Cioslowski, B.B. Stefanov, G. Liu, A. Liashenko, P. Piskorz, I. Komaromi, R.L. Martin, D.J. Fox, T. Keith, M.A. Al-Laham, C.Y. Peng, A.

Nanayakkara, M. Challacombe, P.M.W. Gill, B. Johnson, W. Chen, M.W. Wong, C. Gonzalez, J.A. Pople, *Gaussian03*, C.02 ed.; Gaussian Inc.: Wallingford, CT, 2004.

40. Krishnan, R., Binkley, J. S., Seeger, R.,Pople, J. A. Self-consistent molecular-orbital methods. 20. Basis set for correlated wave-functions. *J. Chem. Phys.*, (1980), **72**, 650-654.
41. McLean, A. D.,Chandler, G. S. Contracted Gaussian-basis sets for molecular calculations.1. 2nd row atoms, Z=11-18. *J. Chem. Phys.*, (1980), **72**, 5639-5648.
42. Barone, V. Anharmonic vibrational properties by a fully automated second-order perturbative approach. *J. Chem. Phys.*, (2005), **122**, 10.
43. Zhou, S. M., Barnes, I., Zhu, T., Bejan, I., Albu, M.,Benter, T. Atmospheric chemistry of acetylacetone. *Environ. Sci. Technol.*, (2008), **42**, 7905-7910.
44. Havey, D. K., Feierabend, K. J.,Vaida, V. Vapor-phase vibrational spectrum of glycolic acid, $CH_2OHCOOH$, in the region 2000-8500 cm^{-1}. *J. Phys. Chem. A*, (2004), **108**, 9069-9073.
45. Plath, K. L., Takahashi, K., Skodje, R. T.,Vaida, V. Fundamental and overtone vibrational spectra of gas-phase pyruvic acid. *J. Phys. Chem. A*, (2009), **113**, 7294-7303.
46. Vaida, V., Feierabend, K. J., Rontu, N.,Takahashi, K. Sunlight-initiated photochemistry: Excited vibrational states of atmospheric chromophores. *Int. J. Photoenergy*, (2008, 1-13.
47. Vaida, V. Spectroscopy of photoreactive systems: Implications for atmospheric chemistry. *J. Phys. Chem. A*, (2009), **113**, 5-18.
48. Vaida, V., Daniel, J. S., Kjaergaard, H. G., Goss, L. M.,Tuck, A. F. Atmospheric absorption of near infrared and visible solar radiation by the hydrogen bonded water dimer. *Q. J. R. Meteorol. Soc.*, (2001), **127**, 1627-1643.
49. Vaida, V., Kjaergaard, H. G.,Feierabend, K. J. Hydrated complexes: Relevance to atmospheric chemistry and climate. *Int. Rev. Phys. Chem.*, (2003), **22**, 203-219.
50. Rothman, L. S., Gordon, I. E., Barbe, A., Benner, D. C., Bernath, P. E., Birk, M., Boudon, V., Brown, L. R., Campargue, A., Champion, J. P., Chance, K., Coudert, L. H., Dana, V., Devi, V. M., Fally, S., Flaud, J. M., Gamache, R. R., Goldman, A., Jacquemart, D., Kleiner, I., Lacome, N., Lafferty, W. J., Mandin, J. Y., Massie, S. T., Mikhailenko, S. N., Miller, C. E., Moazzen-Ahmadi, N., Naumenko, O. V., Nikitin, A. V., Orphal, J., Perevalov, V. I., Perrin, A., Predoi-Cross, A., Rinsland, C. P., Rotger, M., Simeckova, M., Smith, M. A. H., Sung, K., Tashkun, S. A., Tennyson, J., Toth, R. A., Vandaele, A. C.,Vander Auwera, J. The HITRAN 2008 molecular spectroscopic database. *J. Quant. Spectrosc. Radiat. Transf.*, (2009), **110**, 533-572.
51. Lange, K. R., Wells, N. P., Plegge, K. S.,Phillips, J. A. Integrated intensities of O-H stretching bands: Fundamentals and overtones in vapor-phase alcohols and acids. *J. Phys. Chem. A*, (2001), **105**, 3481-3486.
52. Miller, B. J., Kjaergaard, H. G., Hattori, K., Ishiuchi, S.,Fujii, M. The most stable conformer of benzyl alcohol. *Chem. Phys. Lett.*, (2008), **466**, 21-26.
53. Chen, Y. Q., Wang, W. J.,Zhu, L. Wavelength-dependent photolysis of methylglyoxal in the 290-440 nm region. *J. Phys. Chem. A*, (2000), **104**, 11126-11131.
54. Staffelbach, T. A., Orlando, J. J., Tyndall, G. S.,Calvert, J. G. The UV-visible absorption-spectrum and photolysis quantum yields of methylglyoxal *J. Geophys. Res.-Atmos.*, (1995), **100**, 14189-14198.

55. Meller, R., Raber, W., Crowley, J. N., Jenkin, M. E.,Moortgat, G. K. The UV-visible absorption-spectrum of methylglyoxal. *J. Photochem. Photobiol. A-Chem.*, (1991), **62**, 163-171.
56. Takahashi, K., Plath, K. L., Skodje, R. T.,Vaida, V. Dynamics of vibrational overtone excited pyruvic acid in the gas phase: Line broadening through hydrogen-atom chattering. *J. Phys. Chem. A*, (2008), **112**, 7321-7331.
57. Donaldson, D. J., Tuck, A. F.,Vaida, V. Atmospheric photochemistry via vibrational overtone absorption. *Chem. Rev.*, (2003), **103**, 4717-4729.
58. Mills, M. J., Toon, O. B., Vaida, V., Hintze, P. E., Kjaergaard, H. G., Schofield, D. P.,Robinson, T. W. Photolysis of sulfuric acid vapor by visible light as a source of the polar stratospheric CN layer. *J. Geophys. Res.-Atmos.*, (2005), **110**, 7.
59. Vaida, V., Kjaergaard, H. G., Hintze, P. E.,Donaldson, D. J. Photolysis of sulfuric acid vapor by visible solar radiation. *Science*, (2003), **299**, 1566-1568.

4. Spectroscopic analysis and reanalysis of methylglyoxal diol in the mid- and near-infrared

4.1 Introduction

In this study, I used mid- and near- infrared (IR) spectroscopic techniques to examine the vibrational spectroscopy of methylglyoxal diol. The methylglyoxal diol is formed through the reaction of methylglyoxal and water as seen in R4.1.

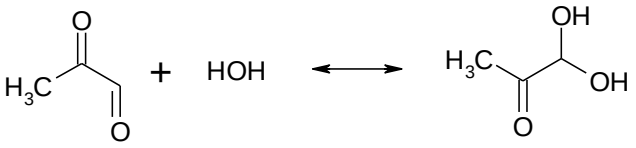

(R4.1)

The fundamental spectrum of a molecule can help identify and characterize the molecule by its normal vibrational modes. I previously used this experimental approach, along with theoretical calculations, to identify methylglyoxal diol (Chapter 1)[1]. The present study extends this investigation by obtaining spectra below 1000cm^{-1} to help identify methylglyoxal diols by changes in the carbon backbone. These features are more easily identifiable than the OH stretches of the diol, because of interference from water bands in the OH region, from 3300 – 3600 cm^{-1}. These carbon backbone changes have previously been used to identify glyoxylic acid diol from glyoxylic acid[2].

Water-mediated aldehyde chemistry may have important consequences to the formation of secondary organic aerosols (SOA)[1-3]. While the hydration of small aldehydes in aqueous

solutions is well known, their gas-phase hydration has not yet been considered in atmospheric models. The absence of gas phase hydration in atmospheric models is because it is commonly believed that there is not enough water present in the gas phase to make such reactions favorable. It has been seen more recently that aldehydes can hydrate in gas phase or in water restricted environments to form diols[1,2,4]. For instance, methylglyoxal has been observed to hydrate in the gas[1] and solution phase[5-7] to form methylglyoxal diol (Fig. 4.1).

Methylglyoxal diol (Fig 4.1b) contains two OH groups, one intramolecularly hydrogen bonded (OH_{Hb}) to the carbonyl oxygen of the ketone and one free (OH_{Fr}). An OH stretching vibration, such as those in methylglyoxal, lies at a higher frequency than other stretching vibrations of the molecule (3500 – 3600 cm^{-1}) and its potential is very anharmonic. The intensity of overtones makes their observation a challenge spectroscopically; however the OH stretching overtone has enough intensity to be observed. Therefore, probing the OH stretching overtones of methylglyoxal diol can give further information about the gas phase formation of methylglyoxal diol and insight into its photon mediated chemistry.

In this study, I used Fourier transform infrared spectroscopy (FTIR) and cavity ringdown spectroscopy (CRD) to analyze the spectral features of methylglyoxal diol. The FTIR was used to extend the spectroscopic study to the fingerprint region in the mid-IR. The CRD was used to observe and characterize the third and fourth OH stretching vibrational overtones, $4\nu_{OH}$ and $5\nu_{OH}$, of methylglyoxal diol in the near-IR. The combination of these techniques allows us to confirm the spectroscopic signatures of methylglyoxal diol and investigate its chemistry.

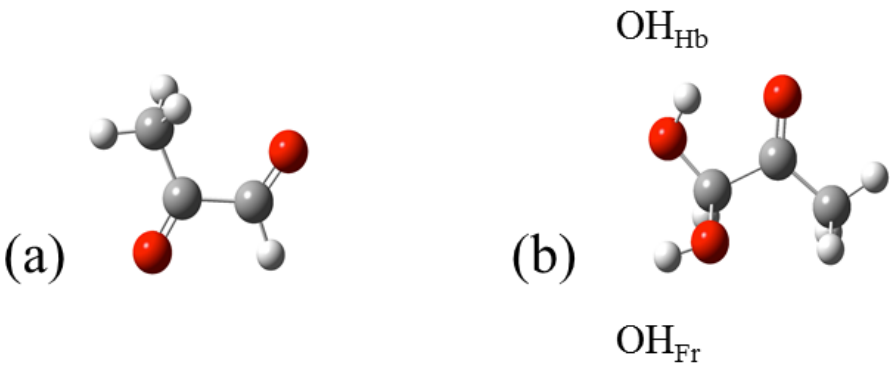

Figure 4.1 The schematic of the (a) trans methylglyoxal molecule and (b) methylglyoxal diol molecule.

4.2 Experimental

4.2.1 Sample Preparation

Methylglyoxal solution, ~40 wt% in water (Sigma-Aldrich) was dried and vacuum distilled as described in detail in Axson et al[1], with the exception that the methylglyoxal P_2O_5 mixture was only heated to 333 K to produce gas phase methylglyoxal in the vacuum distillation. Methylglyoxal diol was prepared in situ as described in Axson et al.[1] for the mid infrared study. For the CRD study, the methylglyoxal diol was prepared by rehydrating the purified methylglyoxal with 1 – 2 mL of NERL ultrapure water (Thermo scientific) and the new solution was agitated to ensure mixture. This solution was immediately introduced to the CRD cavity, where the solution would evaporate and methylglyoxal diol would be released. Acetic acid (Analytical Reagent) and formic acid (Sigma Aldrich) were used to provide reference spectra.

4.2.2 Fourier transform spectroscopy

The mid-IR absorption spectrum of methylglyoxal diol was measured from 600 –8000 cm^{-1} at 0.5 cm^{-1} resolution using FTIR spectroscopy. A commercial Bruker IFSv 66 spectrometer equipped with a globar source, KBr beamsplitter, and MCT detector was used in the mid-IR to obtain absorption spectra. The ~ 3 L, 71 cm glass spectroscopic cell had KBr windows to allow observation of transitions with frequencies down to 600 cm^{-1}. The cell was both pressure- and temperature-controlled and was pumped down to approximately 0.3 Torr and used as a static cell. The gas-phase methylglyoxal sample was introduced to the cell and water vapor was subsequently added from a temperature controlled water bulb. To ensure no photochemical

reactions, the methylglyoxal sample and the static cell were covered in black cloth. In addition, all experiments were performed at 298 K.

4.2.3 Cavity ring-down spectroscopy

The third overtone of methylglyoxal diol was collected using a pulsed CRD apparatus, whose set-up has been previously explained in detail.[8,9] The CRD is a more sensitive spectroscopic technique than traditional FTIR for viewing these low intensity OH overtone stretches, because it has effective path lengths of kilometers. In conventional FTIR, the pathlength is the physical length of the optical cell used. The cavity to observe the third overtone of methylglyoxal diol was formed using a set of highly reflective mirrors (Los Gatos Research Inc), each with 1 m radius of curvature. The mirrors were centered at 755 nm and have a reflectivity of 99.997%, giving an effective pathlength of roughly 31 km. An Nd:Yag (532 nm) pumped a dye laser with LDS 759 laser dye, and combined with the mirrors gave a range of 12500 – 13800 cm^{-1}. This combination of mirrors and dye gave an average time constant of 190 μs and a pathlength of 57 km. Prior to experiments, the apparatus was allowed to warm up for 20 minutes to ensure its stability. The cavity was wrapped in heating tape to maintain a temperature of 343 K. The cavity mirrors were purged with pure helium. The acetic acid and formic acid spectra were taken using the CRD at 298 K.

4.2.4 Nuclear magnetic resonance (NMR) spectroscopy

The aqueous phase methylglyoxal sample was separated to three aliquots for NMR analysis. One was covered and at room temperature for one hour. The solution was checked using NMR to verify the presence of methylglyoxal diol. All NMR spectra were taken in the University of Colorado NMR facility by Richard Shoemaker.

4.2.5 Theoretical Calculations

The methylglyoxal diol and the methylglyoxal diol water cluster local mode overtones were calculated by Zeb Kramer using a 1D PES for each OH and the hybrid density functional theory method of B3LYP [10,11] with the 6-31+G(d,p) basis set[12-16] using the Gaussian 03 program[16].

4.3 Results and Discussion

4.3.1 Mid infrared spectrum of methylglyoxal diol

In previous studies, the mixed methylglyoxal and methylglyoxal diol spectrum was measured in the mid infrared region from 1000 – 4000 cm^{-1}, which showed the OH_{Hb} and OH_{Fr} stretches as well as other diol features[1]. In this study, modifications in the cell design allowed probing the fingerprint region of the diol below 1000 cm^{-1}. Methylglyoxal diol was created in situ, using an excess of water to methylglyoxal in ratios up to 23:1. To examine the gas phase methylglyoxal diol, the cell was evacuated and the diol which adhered to the cell walls was

boiled off. The "dry" gas phase diol then reached equilibrium in the gas phase. The barrier for dehydration was theoretically calculated to be 43.7 kcal mol^{-1}, indicating that in the absence of water once the diol was formed it would not convert back to methylglyoxal (Fig 4.2). Therefore, I assert that Fig. 4.3 shows a better spectrum of the diol than that previously published.

Figure 4.3 shows the fundamental spectrum of methylglyoxal diol from 800 – 1800 cm^{-1}, with diol features and frequencies indicated by arrows. The spectrum shows a stretch and a bend associated with the diol at 1088 cm^{-1} for the C-OH stretch and 1254 cm^{-1} for the OH_{Hb} bend. In addition the diol will have backbone changes from methylglyoxal including the aldehyde H rocking (1177cm^{-1}) and ketone CH_3 (921, 945, and 1012 cm^{-1}). The broad feature centered around 1400 cm^{-1} is due to CH_3 asymmetric bending and was observed in the previous spectrum[1]. The methylglyoxal diol contains a ketone C=O group which is present at 1727 cm^{-1}. Not shown in Fig. 4.3 is the OH stretching region from 3300 – 3600 cm^{-1}. In the previous methylglyoxal diol spectrum[1], the OH stretching region showed the first overtone of the carbonyl, two OH vibrational stretching modes, and a diol water clustering region. The OH_{Hb} stretch was located at 3505 cm^{-1} and the OH_{Fr} stretch at 3585 cm^{-1}. I was unable to observe the OH stretches of the diol in this study because the region was dominated by diol forming clusters with water. The clustering is consistent with the previous spectra[1] and is favored to occur with the diol (Fig 4.2).

There no established gas-phase mechanism for the reaction of methylglyoxal and water to form methylglyoxal diol. The barrier for reaction of one water to methylglyoxal is suggested to be 40 kcal mol^{-1} or greater[17]. However, it is suggested that the excess amount of water molecules to methylglyoxal used in this experiment (up to 23:1) could have catalyzed the

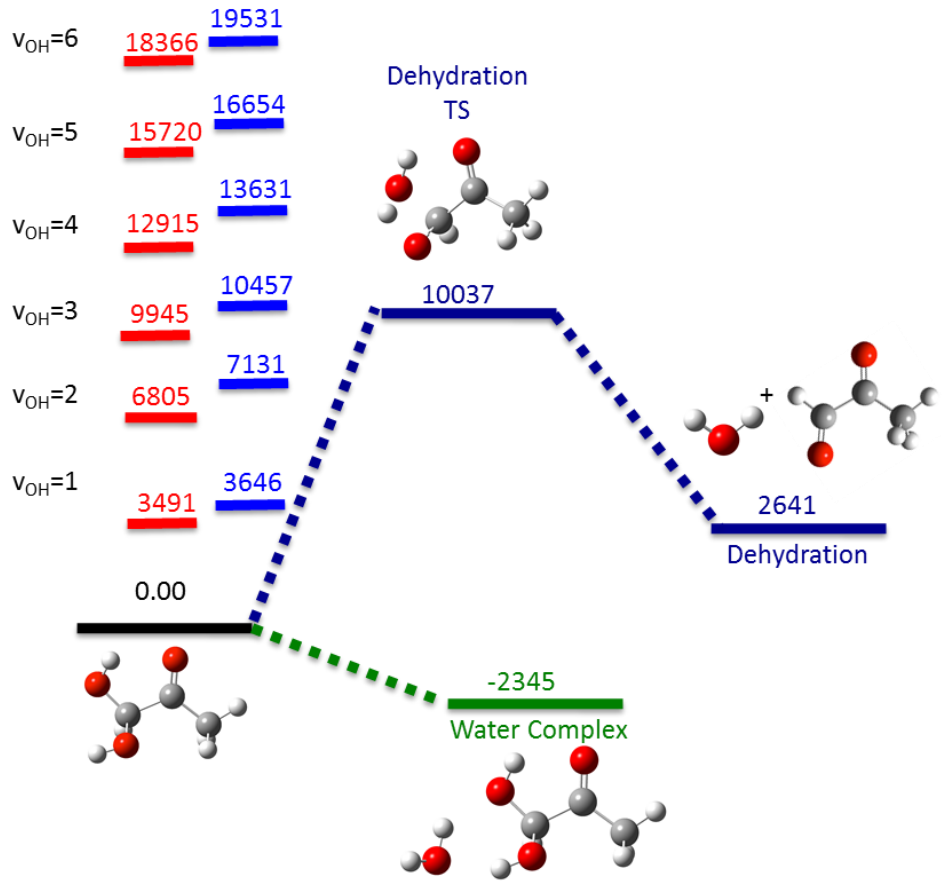

Figure 4.2 The potential energy diagram of methylglyoxal diol showing dehydration to methylglyoxal and water, and a diol water complex.

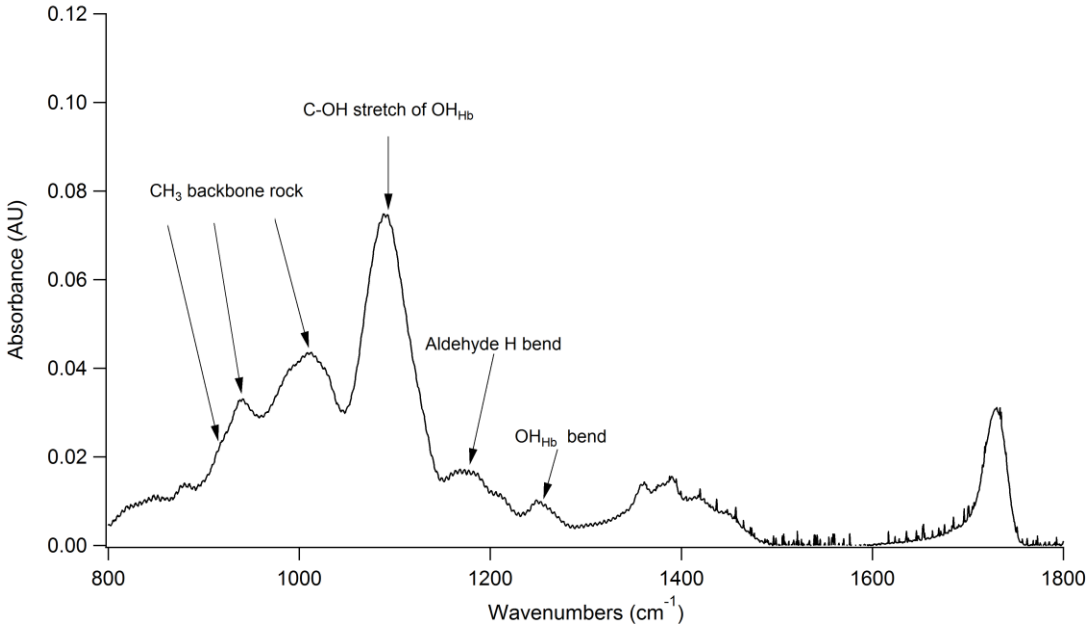

Figure 4.3 The fundamental spectrum of methylglyoxal diol from 800 – 1800 cm^{-1}. Methylglyoxal diol features and frequencies are indicated by arrows.

thermal hydration to form methylglyoxal diol by lowering the transition state energy for the reaction. This catalysis has been studied theoretically[18,19] and experimentally observed[20] to occur with single water molecules and with multiple water molecules[17,21-25]. The neutral hydration (no acid or base catalysis) of a carbonyl group is believed to occur via the carbonyl forming a hydrogen bonded complex with two or more water molecules[23,24]. Formation of the hydrogen bonded complex will reduce transition state energy by reducing the free energy of activation for the reaction[17]. The carbonyl water cluster is proposed to form cyclical rings, where the hydration reaction will proceed through a concerted reaction by proton movement along the hydrogen bonds. This theory of water cluster catalyzed carbonyl hydration could be extended to the formation of gas phase methylglyoxal diol.

4.3.2 Third overtone of methylglyoxal diol

The methylglyoxal diol $4\nu_{OH}$ seen at the bottom in Fig. 4.4, contains three overtone transitions which are identified as the OH_{Hb} and OH_{Fr} of the diol and methylglyoxal diol water cluster. The two possible overtones that can be observed in methylglyoxal diol are from CH and OH bonds. The C-H overtones of the aldehyde or methyl groups would occur at a higher frequency, >13400 cm^{-1}, outside of the observed range[26]. The intramolecular hydrogen bond will cause the OH_{Hb} bond to lengthen (0.976 Å) more than that of the OH_{Fr} (0.968 Å). Using theoretical calculations, I tentatively assign the OH_{Fr} of the diol at 13314 cm^{-1} (FWHM = 48 cm^{-1}) and the OH_{Hb} of the diol at 12900 cm^{-1} (FWHM = 64 cm^{-1}). The transition at 12791 cm^{-1} (FWHM = 57 cm^{-1}) is assumed to be the OH_{Hb} stretching overtone of clusters of the diol to water (diol$(H_2O)_n$). Additionally, the intensity for these methylglyoxal diol OH stretches is comparable

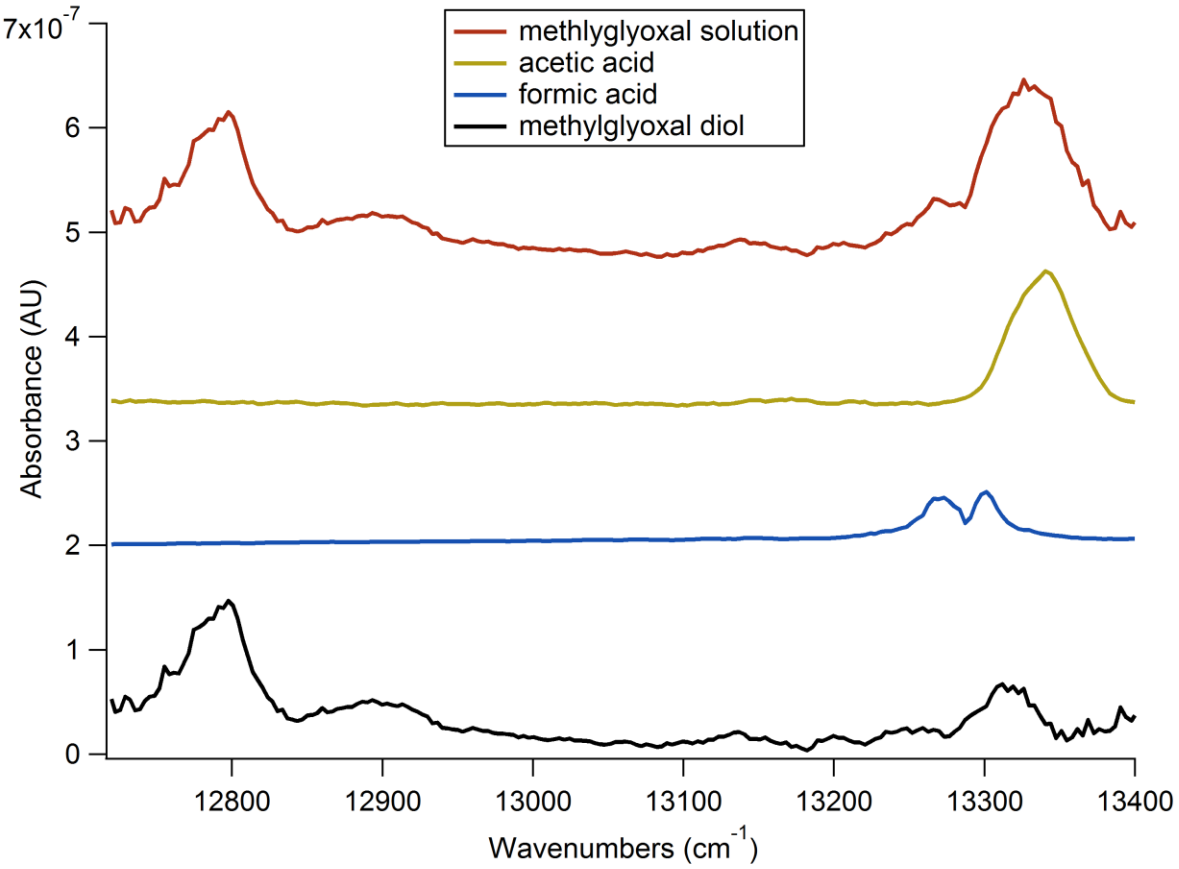

Figure 4.4 The $4\nu_{OH}$ spectrum of methylglyoxal solution, acetic acid, formic acid, and methylglyoxal diol from 12720 cm^{-1} – 13400 cm^{-1}.

to the intensity of OH stretches in other organic compounds[27]. The experimental results and the theoretical calculations are summarized in Table 4.1.

Intramolecular hydrogen bonding of an OH stretching mode can be observed spectroscopically. In the OH stretching overtones this is manifested by a red shift and broadening of the feature, which has been observed in a number of acids and alcohols[3,28-31]. For methylglyoxal diol, the intramolecular hydrogen bond is between the hydrogen of the diol OH and the oxygen of the ketone carbonyl (Fig 4.1b). Like other organic compounds, the OH_{Hb} feature of methylglyoxal diol is broadened and red shifted from the OH_{Fr} feature by 410 cm^{-1}. Additionally, there is an increase in the anharmonicity ($\omega_\varepsilon\chi_\varepsilon$) of the OH_{Hb} relative to that of the OH_{Fr} observed in methylglyoxal and other compounds, which is attributed to the intramolecular hydrogen bonding[30,31].

Figure 4.4 contains the spectrum from 12720 cm^{-1} – 13400 cm^{-1} of the $4\nu_{OH}$ methylglyoxal solution, the $4\nu_{OH}$ acetic acid, and the $4\nu_{OH}$ formic acid, with the difference producing the methylglyoxal diol spectrum. The acetic acid $4\nu_{OH}$ transition was measured in this study at 13340 cm^{-1} is consistent with the $3\nu_{OH}$ and $5\nu_{OH}$ transitions previously measured[32,33]. The formic acid $4\nu_{OH}$ has a transition at 13277 cm^{-1} which is consistent with previous experimental values[34,35]. In addition, methylglyoxal has no OH transition and any CH transition would not be visible in this region. The acetic and formic acid $4\nu_{OH}$ were subtracted from the methylglyoxal solution $4\nu_{OH}$ spectrum to yield the methylglyoxal $4\nu_{OH}$ spectrum.

The $5\nu_{OH}$ of methylglyoxal diol was examined and showed the OH_{Fr} stretching overtone transition centered at 16275 cm^{-1}. Like the $4\nu_{OH}$ of methylglyoxal diol, this overtone contains features from the formic acid ($6\nu_{CH}$ 16110 cm^{-1}, $5\nu_{OH}$ 16194 cm^{-1}, $4\nu_{OH+CH}$ 16221 cm^{-1})[34] and acetic acid ($5\nu_{OH}$ 16266 cm^{-1})[33] overtones. The OH_{Hb} $5\nu_{OH}$ of methylglyoxal diol was more

Table 4.1 The $4\nu_{OH}$ theoretical and experimental frequencies and the experimental full width at half max (FWHM) for the methylglyoxal diol OH_{Fr}, OH_{Hb} and diol·H_2O cluster. The anharmonicity ($\omega_\varepsilon\chi_\varepsilon$) for the diol OH_{Fr} and OH_{Hb} are calculated via Birge-Sponer plots (not shown).

Transition	Theoretical Frequency	Experimental Frequency	Experimental FWHM	Experimental $\omega_\varepsilon\chi_\varepsilon$	Theoretical $\omega_\varepsilon\chi_\varepsilon$
OH_{Fr}	13631	13314	48	83 (±2.5)	79 (±0.5)
OH_{Hb}	12915	12900	64	93 (±1.0)	87 (±0.5)
diol·(n)H_2O	12800	12791	57	–	–

*All values are in cm^{-1}

difficult to examine. This is likely due the order of magnitude decrease in intensity[27] when moving from the $4\nu_{OH}$ to $5\nu_{OH}$ as well as the large water interference (from 15200 – 15800 cm^{-1}) where the OH_{Hb} $5\nu_{OH}$ would be expected.

4.3.3 Examination of gas-phase acid formation from methylglyoxal diol

The fundamental methylglyoxal diol spectrum from Axson et al.[1] (Chapter 3) is now known to have contained traces of methanol (1035 cm^{-1}), formic acid (1105 cm^{-1}), acetic acid (1185 cm-1), and peracetic acid (1251 cm^{-1}). In this study, the gas phase methylglyoxal sample was purified to great extent to avoid impurities or initial acids. The methylglyoxal and water were allowed to react over the period of one day. Figure 4.5 shows the fingerprint region of the mixture's spectrum and there are clear indications that acetic acid, formic acid, and peracetic acid have been formed. Additionally, acetic and formic acid were observed in the third overtone spectrum of methylglyoxal diol (Fig. 4.4). The spectra were checked for other possible products, such as methanol, but none were identified.

The chemistry of diols has been previously discussed by Francisco et al, who suggests that gas phase diols can undergo reaction to form acids, though the calculated reaction barriers are too high to for these reactions to occur[17]. I propose that methylglyoxal diol water complexes may act as an intermediate in the acid formation. Methylglyoxal diol has been observed in this and previous work to form clusters with water. Previous studies have shown that hydrogen bonded complexes with water molecules can lower the transition state energy for a reaction[17-25]. In the absence of any initial acids, the formation of diol water complexes may have acted to

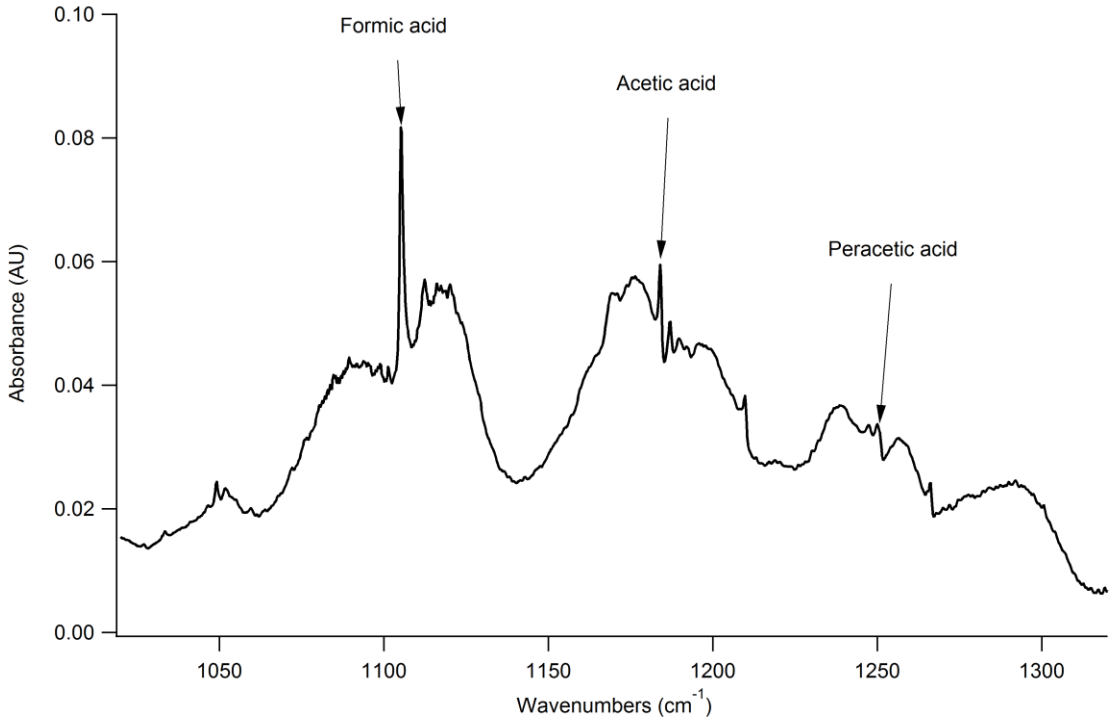

Figure 4.5 Acid products, inducing formic, acetic, and peracetic acid, formed from the reaction of methylglyoxal and water after one day.

lower the transition state energy and these acids, such as formic and acetic acid, were able to form.

To further examine the presence of these acids, nuclear magnetic resonance (NMR) spectra were taken of the prepared solution phase methylglyoxal. In solution methylglyoxal is roughly 60% diol and 40% tetrol[7]. The diol and tetrol of methylglyoxal was observed along with other, larger polyols. The dark, room temperature solution phase spectra also showed a line at 176.80 ppm, indicating the presence of a carboxylic acid, corresponding to acetic acid.

4.4 Conclusions

The new mid-IR fundamental and near-IR overtone spectra of methylglyoxal diol strengthen my argument that the diol is forming and is present in the gas phase. In both spectra there is evidence of gas phase acid evolution (acetic, formic, and peracetic acid). Although the mechanisms of formation remain unknown, I suggest that complexation of the methylglyoxal diol with water molecules may lower the transition state energy and allow for these acids to form[36]. Additionally, the formation of methylglyoxal diol can lead to greater gas to particle-phase partitioning because the diol has a lower vapor pressure and can more readily form hydrogen bonds than methylglyoxal. There would also be a change in the electronic state of the methylglyoxal upon forming the diol, by eliminating the $n \rightarrow \pi^*$ transition of the aldehyde carbonyl which is well known to undergo near-UV photochemistry.

Sunlight is a major driving force in atmospheric chemistry[37]. Most atmospheric photochemistry is considered to happen with UV radiation, which has enough energy to cause excited electronic state reactions and bond dissociation. However, a discrepancy between

atmospheric model predictions and field observations of SOA emphasizes the need for considering alternative photochemical processes not yet included in atmospheric models.[38-40] Recent experimental and theoretical studies have focused on excited ground electronic vibrational state photochemistry that can occur by absorption of red solar photons (λ > 400 nm)[27,37,41]. The photochemical reactions occur by pumping the ground electronic state vibrational overtones with near-IR and visible radiation, initiating a concerted, photochemical reaction and eventual bond dissociation to dehydrate or form new products[27,31,37,41-44]. This sunlight driven photochemical pathway may be relevant to methylglyoxal diol, given the OH stretching overtones available for overtone pumping.

4.5 References

1. Axson, J. L., Takahashi, K., De Haan, D. O.,Vaida, V. Gas-phase water-mediated equilibrium between methylglyoxal and its geminal diol. *Proc Natl Acad Sci USA*, (2010), **107**, 6687-6692.
2. Plath, K. L., Axson, J. L., Nelson, G. C., Takahashi, K., Skodje, R. T.,Vaida, V. Gas-phase vibrational spectra of glyoxylic acid and its gem diol monohydrate. Implications for atmospheric chemistry. *React. Kinet. Catal. Lett.*, (2009), **96**, 209-224.
3. Takahashi, K., Plath, K. L., Axson, J. L., Nelson, G. C., Skodje, R. T.,Vaida, V. Dynamics and spectroscopy of vibrational overtone excited glyoxylic acid and 2,2-dihydroxyacetic acid in the gas-phase. *J. Chem. Phys.*, (2010), **132**, 1-10.
4. Maron, M. K., Takahashi, K., Shoemaker, R. K.,Vaida, V. Hydration of pyruvic acid to its geminal-diol, 2,2-dihydroxypropanoic acid, in a water-restricted environment. *Chem. Phys. Lett.*, (2011), **513**, 184-190.
5. Betterton, E. A.,Hoffmann, M. R. Kinetics, mechanism, and thermodynamics of the reversable-reaction of methylglyoxal (CH_3COCHO) with S(IV). *J. Phys. Chem.*, (1987), **91**, 3011-3020.
6. Krizner, H. E., De Haan, D. O.,Kua, J. Thermodynamics and kinetics of methylglyoxal dimer formation: A computational study. *J. Phys. Chem. A*, (2009), **113**, 6994-7001.
7. Nemet, I., Vikic-Topic, D.,Varga-Defterdarovic, L. Spectroscopic studies of methylglyoxal in water and dimethylsulfoxide. *Bioorganic Chem.*, (2004), **32**, 560-570.
8. Havey, D. K., Feierabend, K. J., Takahashi, K., Skodje, R. T.,Vaida, V. Experimental and theoretical investigation of vibrational overtones of glycolic acid and its hydrogen bonding interactions with water. *J. Phys. Chem. A*, (2006), **110**, 6439-6446.
9. Brown, S. S., Wilson, R. W.,Ravishankara, A. R. Absolute intensities for third and fourth overtone absorptions in HNO_3 and H_2O_2 measured by cavity ring down spectroscopy. *J. Phys. Chem. A*, (2000), **104**, 4976-4983.
10. Becke, A. D. Density-functional thermochemistry. 3. The role of exact exchange *J. Chem. Phys.*, (1993), **98**, 5648-5652.
11. Lee, C. T., Yang, W. T.,Parr, R. G. Development of the Colle-Salvetti correlation-energy formula into a functional of the electron-density. *Phys. Rev. B*, (1988), **37**, 785-789.
12. Clark, T., Chandrasekhar, J., Spitznagel, G. W.,Schleyer, P. V. Efficient diffuse function-augmented basis-sets for anion calculations. 3. The 3-21+G basis set for 1st-row elements, LI-F. *J. Comput. Chem.*, (1983), **4**, 294-301.
13. Frisch, M. J., Pople, J. A.,Binkley, J. S. Self-consistent molecular-orbital methods. 25. Supplementary functions for gaussian-basis sets. *J. Chem. Phys.*, (1984), **80**, 3265-3269.
14. Krishnan, R., Binkley, J. S., Seeger, R.,Pople, J. A. Self-consistent molecular-orbital methods. 20. Basis set for correlated wave-functions. *J. Chem. Phys.*, (1980), **72**, 650-654.
15. McLean, A. D.,Chandler, G. S. Contracted Gaussian-basis sets for molecular calculations.1. 2nd row atoms, Z=11-18. *J. Chem. Phys.*, (1980), **72**, 5639-5648.
16. Frisch, M. J., G.W. Trucks, H.B. Schlegel, G.E. Scuseria, M.A. Robb, J.R. Cheeseman, J.A. Montgomery, T. Vreven, K.N. Kudin, J.C. Burant, J.M. Millam, S.S. Iyengar, ,J.Tomasi, V. B., B. Mennucci, M. Cossi, G. Scalmani, N. Rega, G.A. Petersson, H. Nakatsuji, M. Hada, M. Ehara, K. Toyota, R. Fukuda, J. Hasegawa, M. Ishida, T.

Nakajima, Y. Honda, O. Kitao, H. Nakai, M. Klene, X. Li, J.E. Knox, H.P. Hratchian, J.B. Cross, V. Bakken, C. Adamo, J. Jaramillo, R. Gomperts, R.E. Stratmann, O. Yazyev, A.J. Austin, R. Cammi, C. Pomelli, J.W. Ochterski, P.Y. Ayala, K. Morokuma, G.A. Voth, P. Salvador, J.J. Dannenberg, V.G. Zakrzewski, S. Dapprich, A.D. Daniels, M.C. Strain, O.Farkas, D.K. Malick, A.D. Rabuck, K. Raghavachari, J.B. Foresman, J.V. Ortiz, Q. Cui, A.G. Baboul, S. Clifford, J. Cioslowski, B.B. Stefanov, G. Liu, A. Liashenko, P. Piskorz, I. Komaromi, R.L. Martin, D.J. Fox, T. Keith, M.A. Al-Laham, C.Y. Peng, A. Nanayakkara, M. Challacombe, P.M.W. Gill, B. Johnson, W. Chen, M.W. Wong, C. Gonzalez, J.A. Pople, *Gaussian03*, C.02 ed.; Gaussian Inc.: Wallingford, CT, 2004.

17. Francisco, J. S.,Williams, I. H. Reaction pathways for gas-phase hydrolysis of formyl compounds HXCO (X = H, F, and CL). *J. Am. Chem. Soc.*, (1993), **115**, 3746-3751.
18. Aloisio, S.,Francisco, J. S. Radical-water complexes in Earth's atmosphere. *Accounts Chem. Res.*, (2000), **33**, 825-830.
19. Anglada, J. M.,Gonzalez, J. Different Catalytic Effects of a Single Water Molecule: The Gas-Phase Reaction of Formic Acid with Hydroxyl Radical in Water Vapor. *ChemPhysChem*, (2009), **10**, 3034-3045.
20. Vöhringer-Martinez, E., Hansmann, B., Hernandez, H., Francisco, J. S., Troe, J.,Abel, B. Water Catalysis of a Radical-Molecule Gas-Phase reaction. *Science*, (2011), **315**, 497-501.
21. Hsieh, Y. H., Weinberg, N., Yang, K., Kim, C. K., Shi, Z.,Wolfe, S. Hydration of the carbonyl group - Acetic acid catalysis in the co-operative mechanism. *Can. J. Chem.-Rev. Can. Chim.*, (2005), **83**, 769-785.
22. Shi, Z., Hsieh, Y. H., Weinberg, N.,Wolfe, S. The neutral hydrolysis of methyl acetate - Part 2. Is there a tetrahedral intermediate? *Can. J. Chem.-Rev. Can. Chim.*, (2009), **87**, 544-555.
23. Wolfe, S., Kim, C. K., Yang, K., Weinberg, N.,Shi, Z. Hydration of the carbonyl group - A theoretical-study of the cooperative mechanism. *J. Am. Chem. Soc.*, (1995), **117**, 4240-4260.
24. Williams, I. H., Spangler, D., Femec, D. A., Maggiora, G. M.,Schowen, R. L. Theoretical - Models for solvation and catalysis in carbonyl addition. *J. Am. Chem. Soc.*, (1983), **105**, 31-40.
25. Yang, K., Hsieh, Y. H., Kim, C. K., Zhang, H.,Wolfe, S. Hydration of acetone in the gas phase and in water solvent. *Can. J. Chem.-Rev. Can. Chim.*, (2010), **88**, 56-64.
26. Kjaergaard, H. G., Henry, B. R.,Tarr, A. W. Intensities in local mode overtone spectra of dimethyl ether and acetone. *J. Chem. Phys.*, (1991), **94**, 5844-5854.
27. Vaida, V., Feierabend, K. J., Rontu, N.,Takahashi, K. Sunlight-initiated photochemistry: Excited vibrational states of atmospheric chromophores. *Int. J. Photoenergy*, (2008, 1-13.
28. Howard, D. L.,Kjaergaard, H. G. Influence of intramolecular hydrogen bond strength on OH-stretching overtones. *J. Phys. Chem. A*, (2006), **110**, 10245-10250.
29. Howard, D. L., Jorgensen, P.,Kjaergaard, H. G. Weak intramolecular interactions in ethylene glycol identified by vapor phase OH-stretching overtone spectroscopy. *J. Am. Chem. Soc.*, (2005), **127**, 17096-17103.
30. Plath, K. L., Takahashi, K., Skodje, R. T.,Vaida, V. Fundamental and overtone vibrational spectra of gas-phase pyruvic acid. *J. Phys. Chem. A*, (2009), **113**, 7294-7303.

31. Havey, D. K., Feierabend, K. J.,Vaida, V. Vapor-phase vibrational spectrum of glycolic acid, $CH_2OHCOOH$, in the region 2000-8500 cm^{-1}. *J. Phys. Chem. A,* (2004), **108**, 9069-9073.
32. Lange, K. R., Wells, N. P., Plegge, K. S.,Phillips, J. A. Integrated intensities of O-H stretching bands: Fundamentals and overtones in vapor-phase alcohols and acids. *J. Phys. Chem. A,* (2001), **105**, 3481-3486.
33. Begashaw, I., Fiddler, M. N., Bililign, S.,Brown, S. S. Measurement of the Fourth O-H Overtone Absorption Cross Section in Acetic Acid Using Cavity Ring-Down Spectroscopy. *J. Phys. Chem. A,* (2011), **115**, 753-761.
34. Howard, D. L.,Kjaergaard, H. G. Resonance coupling in the fourth OH-stretching overtone spectrum of formic acid. *J. Chem. Phys.,* (2004), **121**, 136-140.
35. Freytes, M., Hurtmans, D., Kassi, S., Lievin, J., Auwera, J. V., Campargue, A.,Herman, M. Overtone spectroscopy of formic acid. *Chem. Phys.,* (2002), **283**, 47-61.
36. Vaida, V., Daniel, J. S., Kjaergaard, H. G., Goss, L. M.,Tuck, A. F. Atmospheric absorption of near infrared and visible solar radiation by the hydrogen bonded water dimer. *Q. J. R. Meteorol. Soc.,* (2001), **127**, 1627-1643.
37. Vaida, V. Spectroscopy of photoreactive systems: Implications for atmospheric chemistry. *J. Phys. Chem. A,* (2009), **113**, 5-18.
38. Heald, C. L., Jacob, D. J., Park, R. J., Russell, L. M., Huebert, B. J., Seinfeld, J. H., Liao, H.,Weber, R. J. A large organic aerosol source in the free troposphere missing from current models. *Geophys. Res. Lett.,* (2005), **32**, L18809.
39. Volkamer, R., Jimenez, J. L., San Martini, F., Dzepina, K., Zhang, Q., Salcedo, D., Molina, L. T., Worsnop, D. R.,Molina, M. J. Secondary organic aerosol formation from anthropogenic air pollution: Rapid and higher than expected. *Geophys. Res. Lett.,* (2006), **33**, 4.
40. Finlayson-Pitts, B. J. Reactions at surfaces in the atmosphere: integration of experiments and theory as necessary (but not necessarily sufficient) for predicting the physical chemistry of aerosols. *Phys. Chem. Chem. Phys.,* (2009), **11**, 7760-7779.
41. Donaldson, D. J., Tuck, A. F.,Vaida, V. Atmospheric photochemistry via vibrational overtone absorption. *Chem. Rev.,* (2003), **103**, 4717-4729.
42. Takahashi, K., Plath, K. L., Skodje, R. T.,Vaida, V. Dynamics of vibrational overtone excited pyruvic acid in the gas phase: Line broadening through hydrogen-atom chattering. *J. Phys. Chem. A,* (2008), **112**, 7321-7331.
43. Mills, M. J., Toon, O. B., Vaida, V., Hintze, P. E., Kjaergaard, H. G., Schofield, D. P.,Robinson, T. W. Photolysis of sulfuric acid vapor by visible light as a source of the polar stratospheric CN layer. *J. Geophys. Res.-Atmos.,* (2005), **110**, 7.
44. Vaida, V., Kjaergaard, H. G., Hintze, P. E.,Donaldson, D. J. Photolysis of sulfuric acid vapor by visible solar radiation. *Science,* (2003), **299**, 1566-1568.

5. The Absolute Ozone Absorption Cross Section in the Huggins Chappuis Minimum (350 – 470 nm) at 296 K

5.1 Introduction

Weak spectral absorptions play an important role in the radiative transfer of the Earth's atmosphere and accurate measurements of these are necessary for satellite retrievals of atmospheric trace gases[1-3]. It has recently been recognized that weak electronic features in the near-ultraviolet (UV), which are not well known, can be important for tropospheric radical production[4-6]. Ozone (O_3) plays a key role both chemically and radiatively throughout the atmosphere, acting as an absorber and blocker of harmful UV radiation (<300 nm) in the stratosphere and as the dominant source of OH radicals through its UV photolysis. Therefore, it is essential to have accurate O_3 absorption cross sections for satellite and ground based retrievals of vertical O_3 profiles and total O_3 columns, as well as to correctly model atmospheric O_3 concentrations[1-3].

Although the strong bands of O_3 have been well characterized, the absorption minimum between the Huggins and Chappuis bands at 350 – 470 nm is less well known, particularly the minimum region near 390 nm[7,8]. Measurement of the weak O_3 absorption cross-section has practical importance for two reasons. First, satellites use the adjoining Huggins and Chappuis bands for direct retrievals of O_3, relying on the strongly varying differential cross-section[9]. Second, quantifying weak O_3 absorptions is necessary for satellite retrievals of other trace gases in this spectral region. For example, at 404 nm O_3 and NO_2 cross-sections have been previously

reported to be 1.49×10^{-23} cm^2 $molecule^{-1}$ and 5.9×10^{-19} cm^2 $molecule^{-1}$ respectively[10,11]. For an O_3 column abundance of 8×10^{18} molecules cm^{-2} (~300 Dobson units) and an NO_2 column abundance of 4×10^{15} molecules cm^{-2}, the optical extinctions of the two molecules are 1×10^{-4} and 2×10^{-3}, respectively, and the O_3 extinction is both structured and significant (5% at 404 nm) in comparison to that of NO_2[10]. Furthermore, literature cross sections at 404 nm vary from 1.5×10^{-23} to 7×10^{-23} cm^2 $molecule^{-1}$, or 5 to 30% of the NO_2 column extinction for these conditions. More accurate O_3 measurements are therefore required across its absorption minimum.

Previous O_3 cross sections in this region have been measured using high resolution Fourier transform spectrometers and grating spectrometers[1,3,11-13]. These studies report cross sections that differ by more than an order of magnitude near the minimum, and also show some disagreement where the cross section is greater (e.g. 8% at 350 nm and 20% at 450 nm). These studies have also shown that the spectra, with their large discrepancies, are highly temperature dependent[1,3,12-14]. Table 5.1 summarizes the results of prior studies, and gives their spectral range, spectral resolution, temperature, and measured cross sections. The importance of O_3 absorption in the atmosphere, and the large discrepancies in the current literature over a wide spectral region around the O_3 absorption minimum, highlight the need for more accurate measurements of these very weak absorption cross sections.

In this investigation, an IBBCEAS instrument with three channels centered at 365, 405, and 455 nm channels was designed, constructed, and characterized to measure O_3 absorption cross sections in the region between the Huggins and Chappuis bands, from 350 to 470 nm. The increased sensitivity of this instrument compared to single-pass or multi-pass cells allows for the measurement of these weak absorption cross sections with higher signal-to-noise and accuracy.

Table 5.1 Measurements of O_3 absorption cross section between 350 – 470 nm.

Reference	Instrumental Technique	Spectral Region (nm)	Spectral Resolution (nm)	Temp (K)	Cross section at 365 nm ($\times 10^{-23}$ cm^2)	Cross section at 405 nm ($\times 10^{-23}$ cm^2)	Cross section at 455 nm ($\times 10^{-22}$ cm^2)
Burkholder and Talukdar (1994)[1]	Grating spectrometer	410–760	0.20	298	--	--	1.82
Brion et al. (1998)[2]	FTS	350–830	0.01	295	4.47	1.49	2.06
Burrows et al. (1999)	Grating spectrometer	231–794	0.2–0.3	293	6.26	4.27	2.29
Voigt et al. (2001)	FTS	230–851	0.027	293	7.81	7.19	2.24
Bogumil et al. (2003)	Grating spectrometer	230–1075	0.26	293	5.11	2.12	2.14
Fuchs et al. (2009)[1]	CRDS	404	0.5		--	1.49[3]	--
Chen and Venables (2011)[1]	IBBCEAS	335–375	0.26	296	4.92	--	--
This work	IBBCEAS	350-470	0.27-0.51	296	3.68	1.51	1.88

[1] λ_{air} converted to λ_{vacuum} using Ciddor (1996) Eqn. (1).
[2] Wavelength scale not specified.
[3] Cross-section reported at λ_{vacuum} = 404.1 nm.

Calibrations are based on 253.7 nm absorption of O_3 (Hg line) and Rayleigh scattering cross sections of pure gases, as described in section 2.3. Both analytical standards are known to high accuracy. These results are compared to the previous literature studies of O_3 cross sections in this region.

5.2 Experimental

5.2.1 Ozone generation, delivery, and measurement with a single-pass cell

The sampling set up for O_3 generation and delivery is shown in Fig. 5.1a. Ozone was generated by flowing O_2, between 1 – 50 standard cm^3 min^{-1} (SCCM) with a mass flow controller (Alicat Scientific, MC-20SSCM-D-DB15/5m), through a discharge source (OzoneLabs, OL80) capable of generating up to 2% O_3. The O_3 concentration was diluted by a controlled flow of 1.5 standard L min^{-1} (SLPM) of He via a second mass flow controller (Alicat Scientific, MC-5SLPM-D-DB15/5m) to produce O_3 concentrations in the range of 1.2×10^{15} – 2.4×10^{16} molecules cm^{-3} (58 – 1178 parts per million (ppm)). All experiments were conducted using a bath gas of He, which has a much smaller Rayleigh scattering cross section than N_2 or O_2 providing lower loss cavities with longer effective path lengths and higher sensitivity to optical absorption.[15] Zero air and O_2 were avoided as bath gases due to the formation of O_4, which is observable with the IBBCEAS instrument in the 350 – 470 nm region[16]. The O_4 absorption associated with the small concentration of O_2 resulting from the dilution of the flow from the discharge source provided a negligible absorption interference as described in section 5.2.3.

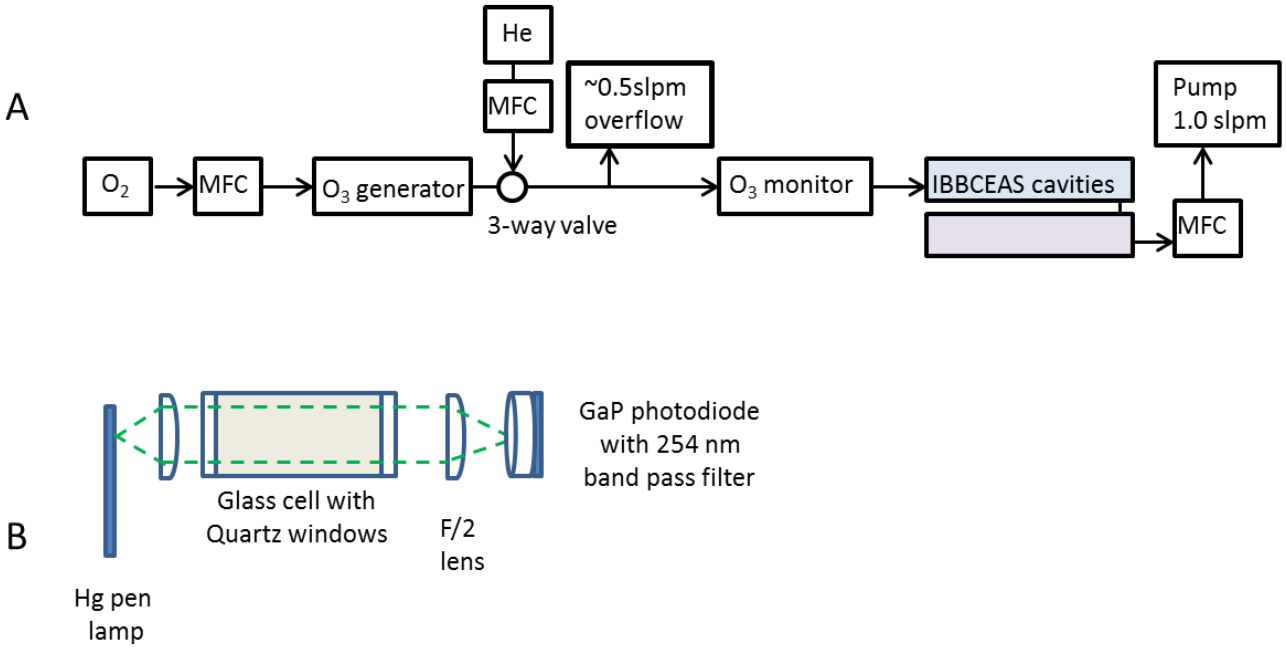

Figure 5.1 (a) Block diagram showing O_3 delivery system to the IBBCEAS and (b) a schematic of the ozone monitor, consisting of Hg light source and GaP photodiode.

A combination of a second mass flow controller and scroll pump controlled a 1.0 SLPM flow of gases through the IBBCEAS. The excess flow of approximately 0.5 SLPM was vented to the atmosphere to maintain near-ambient pressure during all experiments. Instrument zeros consisted of a spectrum of He and were recorded by diverting the small flow of O_3 in O_2 from the discharge source to the exhaust using a three way valve. The experiment was not affected by turbulence because the flow was laminar, with a calculated Reynolds number of 13 (1.5 SLPM of He in a 2.2 cm diameter tube), and because He has a small refractive index which would minimize any optical affects due to turbulence.

Ozone concentrations were measured simultaneously with the IBBCEAS spectral measurements using a single-pass absorption measurement at 254 nm that consisted of a 10.6 cm glass cell with quartz windows, a mercury pencil lamp (UVP 90-0012-01), and gallium phosphide (GaP) photodiode detector (Thorlabs SM05PD7A) with a 254 nm band pass filter (Fig. 5.1b). The intensity of the photodiode was measured using an analog to digital interface (Measurement Computing USB-1408FS) and recorded in the data acquisition software. A dark background of the GaP photodiode was first taken to determine its internal noise (i). Following this, the diode signal was recorded for each of the He blanks (I_0) and each of the O_3 spectra (I). The signal was then averaged and Eqn. 5.1 was used to determine the O_3 concentration, where d is the length of the absorption cell and the O_3 cross section, $\sigma_{O3} = 1.141 \times 10^{-17}$ cm^2 molecule^{-1} at 253.7 nm, was taken from Orphal[7].

$$[O_3] = \frac{\ln\left(\frac{I_0 - i}{I - i}\right)}{(d \times \sigma)} \qquad (5.1)$$

The quoted uncertainty in the literature O_3 absorption cross section is 0.9%[7]. My reported absorption cross section at 350 – 470 nm scales directly with the choice of cross section at 253.7 nm. The O_3 measurement was validated against a UV photometric O_3 instrument (Thermo Electron Corp., Model 49i, 102474-00) over the range of 50 – 165 ppm O_3 and the two agreed to within 1.0%, with a slope of 1.01±0.01 and r^2 = 0.9995. Thus, I anticipate error on the order of 2% for the determination of the O_3 concentration itself.

5.2.2 Operation of IBBCEAS Instrument

The IBBCEAS instrument required approximately 30 min of warm up to allow the temperature of the LEDs, O_3 generator, and spectrometer to stabilize. Dark background spectra were acquired to correct for the pixel-dependent dark signal. These were scaled to the integration time and subtracted from subsequent sample spectra. Following the acquisition of the dark background, spectra of He (I_{He}) and N_2 (I_{N2}) were taken to determine the mirror reflectivity associated with each of the IBBCEAS cavities[17].

Following calibration of mirror reflectivity, spectra of O_3 in He at various concentrations were acquired alternately with spectra of pure He, or zeros. Spectra were integrated for 1.5 s and the average of 180 spectra was recorded. The optimum integration time for the O_3 spectra between successive zeros in He was determined from an Allan deviation analysis which measures the stability of the measurement, due to noise, over time (Fig. 5.2a). It was determined that alternating 5 min He and O_3 spectra, at or just beyond the minimum in the Allan deviation plot, was optimal. The stability of the optical cavity alignment itself was most likely responsible for the upward trend in the Allan deviation plot after 5 min since independent tests of the stability of the LEDs by a separate photodiode showed its output to be stable over a longer

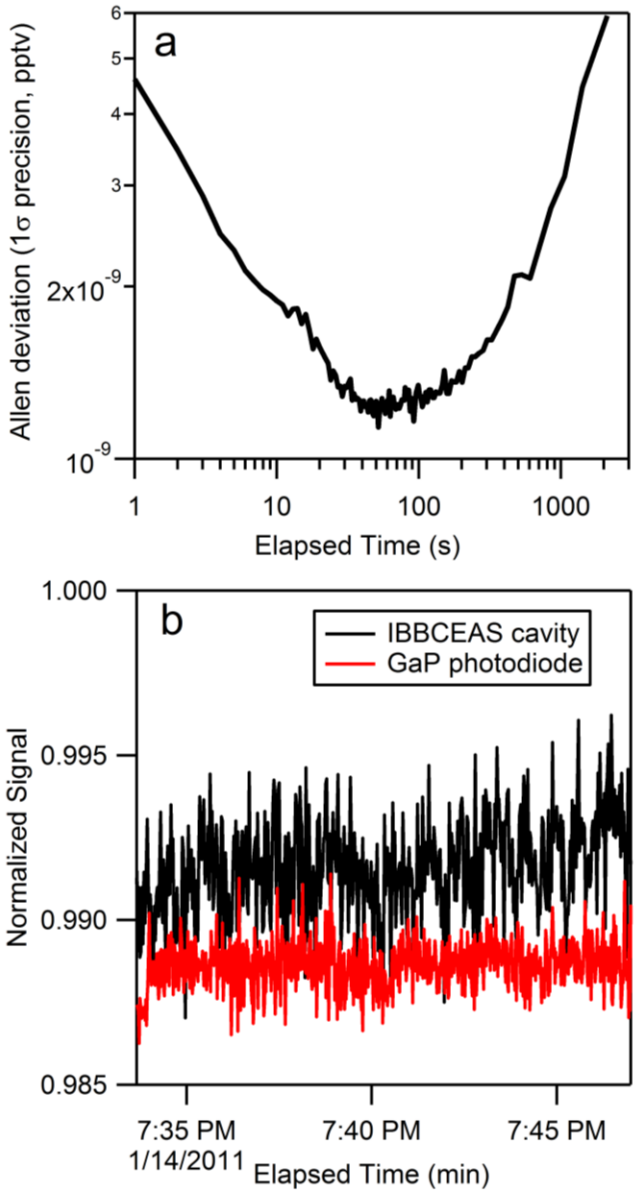

Figure 5.2 (a) Allan deviation plot of the optical density of the IBBCEAS for a single pixel at 370 nm in the 365 nm channel. The minimum near 5 min, was selected as the optimum sampling time between zeros. (b) Stability of the 365 nm LED intensity measured using a GaP photodiode, shown together with the stability of the IBBCEAS cavities for a single pixel at 376 nm.

period of time (Fig. 5.2b). Similar to the reflectivity spectra, O_3 spectra were integrated for 1.5 s and 180 spectra were averaged. The O_3 spectrum from this work was obtained by averaging roughly one hour of O_3 spectra recorded simultaneously for the 365nm and 405 nm cavities or the 405 nm and 455 nm cavities.

5.2.3 Consideration of O_4 interference

As noted in the previous section, collision induced oxygen dimers, or O_4, absorb in the UV and visible spectral regions, and are a potential spectroscopic interference for measurement of weak O_3 absorptions[16]. The O_2/O_3 flow from the discharge source was diluted with He (Fig. 5.1a), such that only up to 3.3% of flow through the IBBCEAS cells was from the O_3 source, of which, at most 1.8% of the flow could consist of O_4. Using Greenblatt et al. cross sections for O_4 of 4.1×10^{-46}, 2.4×10^{-46}, and 0.57×10^{-46} cm^5 $molecules^{-2}$ at 360.5, 380.2, and 446.7 nm respectively and the experimental temperature and pressure, I calculated the expected O_4 optical density[16]. For a maximum O_4 number density of 3.7×10^{17} molecules cm^{-3}, the corresponding optical extinctions, α_{O4}, are 5.6×10^{-11}, 3.3×10^{-11}, and 7.4×10^{-12} cm^{-1} at 360.5, 380.2, and 446.7 nm, respectively. These optical extinctions are more than five orders of magnitude smaller than those that would be observed for O_3 at the same concentration and therefore, any O_4 interferences were considered negligible.

5.3 Results and Discussion

5.3.1 Absolute absorption cross section of O_3

Fig. 5.3 shows the O_3 absorption cross section measured at 295 K and 820 hPa, together with previously measured cross sections obtained from the Mainz Spectral Database and plotted for vacuum wavelengths[1,3,11-13,18-20]. The Burkholder et al., Fuchs et al., and Chen and Venables spectra were corrected from air to vacuum wavelength using Eqn. (1) in Ciddor[13,18,19,21]. The wavelength scale reported by Brion et al. is not specified[11]. There were two sets of 405 nm spectra taken for the simultaneous measurement of the 365 nm and 405 nm cavities and the 405 nm and 455 nm cavities. Different band pass filters were used for the 405 nm cavity in each measurement to prevent out-of-band light from saturating the CCD detector. The sections were averaged in the wavelength regions where they overlap, and the final assembled spectrum is shown.

Plots of the optical extinction for single CCD pixels measured at various concentrations (Fig. 5.4) were used to compare the derived absorption cross sections to the experimental absorption cross sections seen in Fig. 5.3, and to test the linearity of the IBBCEAS response over a range larger than one order of magnitude in O_3. The cross sections determined from Fig. 5.3 are $\sigma_{O3} = 3.87 \times 10^{-23}$ cm^2 at 365.0 nm, $\sigma_{O3} = 1.47 \times 10^{-23}$ cm^2 at 405.0 nm, and $\sigma_{O3} = 1.86 \times 10^{-22}$ cm^2 at 455.0 nm.

From the slope and slope uncertainty in Fig. 5.4, we calculate precisions for the 365, 405, and 455nm channels of 2.3, 0.7, and 0.5% respectively. Similar linear fits for spectra acquired with the 365 nm channel at 380 nm and 390 nm near the absorption minimum, have precisions of 3.1% and 2.4%, respectively. The absolute accuracy is calculated to be 4% from quadrature

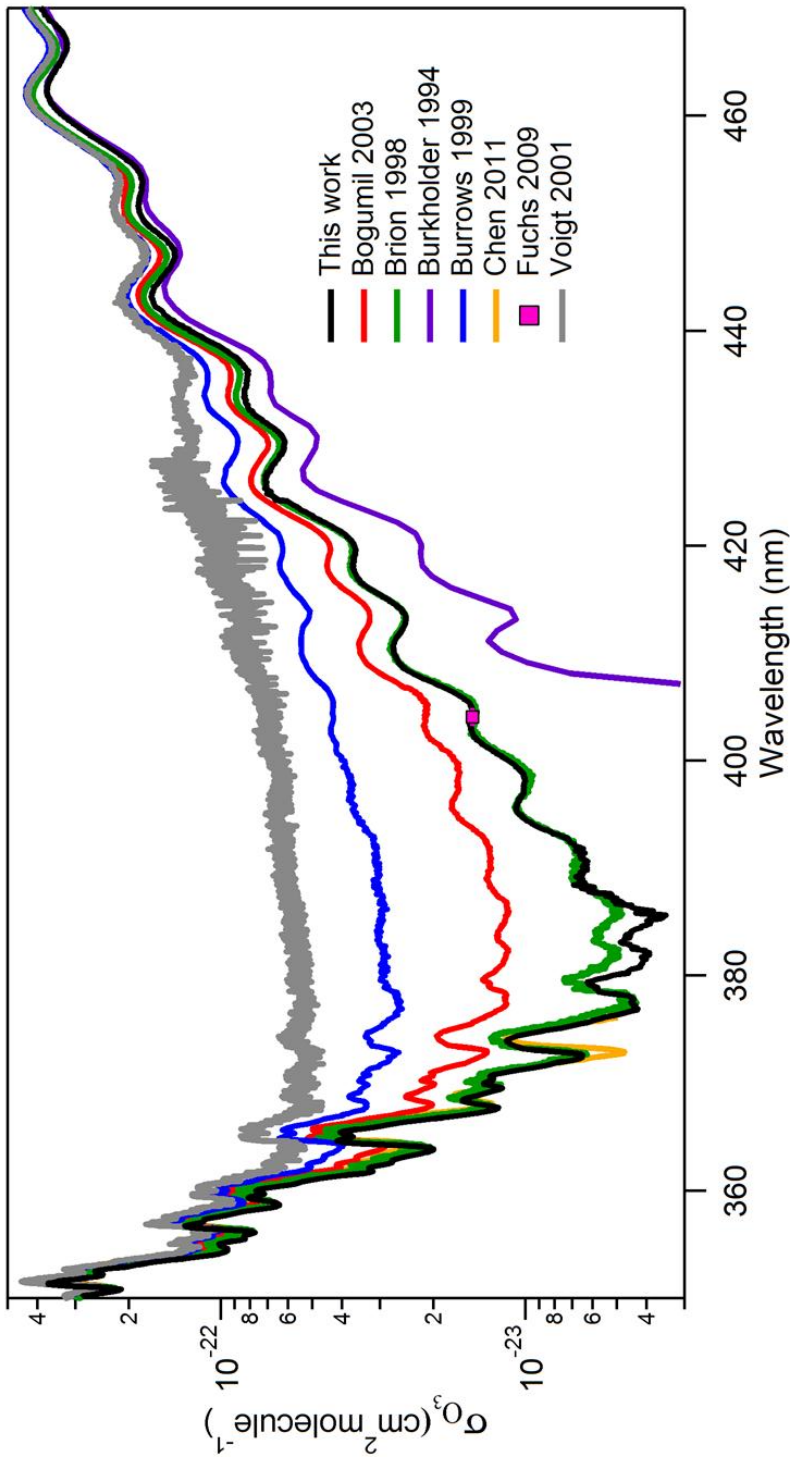

Figure 5.3 The O_3 cross section from 350 – 470 nm determined in this work compared to other published measurements.

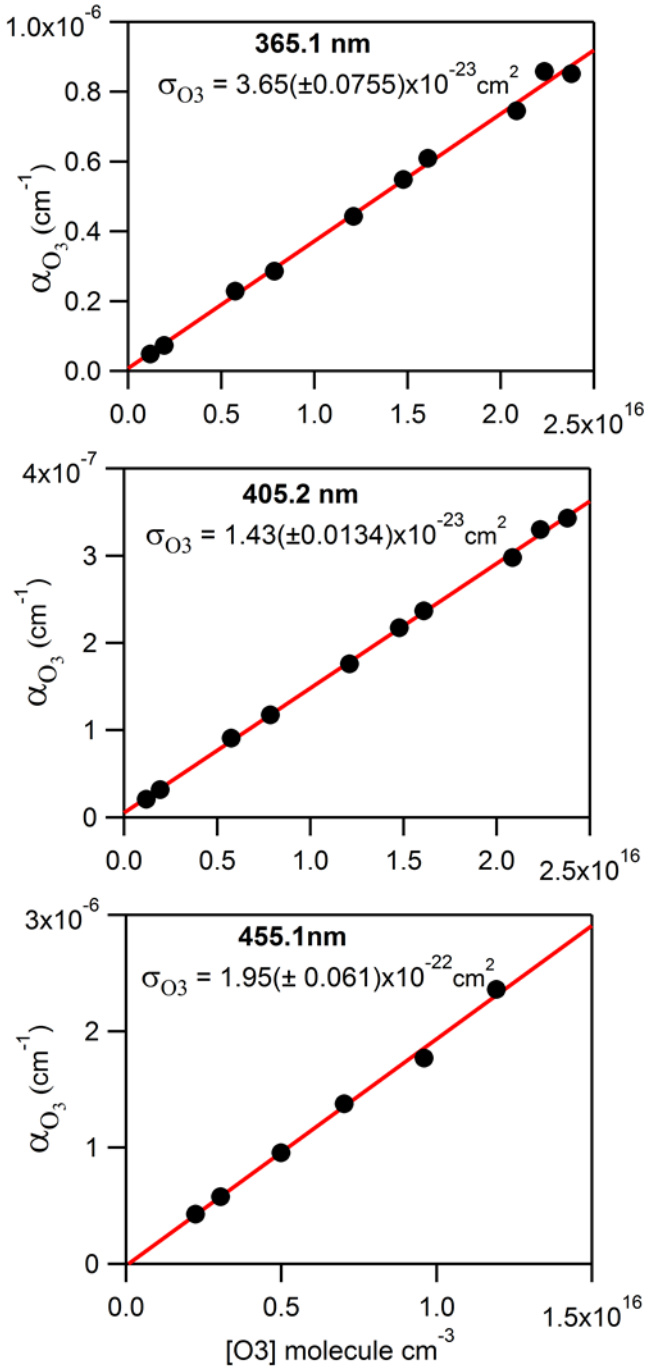

Figure 5.4 Optical extinction measurements at various O_3 concentrations whose slope is the absolute absorption cross sections

addition of the uncertainties in the reflectivity (±3%), O_3 concentration (±2%), pressure (±0.5%), and temperature (±0.7%). However, the absolute accuracy can also be evaluated by comparing the cross section differences where the spectral channels overlap. At 386 – 387 nm, near the minimum, observed discrepancies of $1 – 2 \times 10^{-24}$ cm^2 between the 365 nm channel and two 405 nm channels are equivalent to an absolute accuracy of ~30%, but this improves to less than 5% at 395 – 424 nm for the two 405 nm channel measurements, and is 3 – 10% at 424 – 442 nm in the overlap between the 405 nm and 455 nm channels.

In this very weakly absorbing region between the Huggins and Chappuis bands, there is more than an order of magnitude difference in the various reported O_3 cross sections[1,3,11,12]. My reported spectrum agrees quantitatively with prior literature values at the edges of the spectrum. The measurements are consistent most with Brion et al. with the exception of the minimum region from 375 – 390 nm, where my absorption cross section shows a lower minimum, but agrees within the combined uncertainty[11]. My measurements are also very consistent with those of Chen and Venables, but their measurements do not extend past 375 nm[18]. In addition, more defined O_3 structural features were observed in this work, Brion et al., and Chen and Venables when compared to the other literature cross sections[1,3,11,12,18]. The measurements also agree within 0.5% at 404 nm with Fuchs et al., in which CRDS was used to measure the O_3 cross section, with the highest precision currently available within this wavelength range, to quantify its interference associated with measurements of NO_2 at the single wavelength of a diode laser[19].

Though the O_3 cross sections derived in this work agree best with the data of Brion et al., there is some disagreement between their spectra and mine near the minimum absorption at 375 – 390 nm[11]. This is the region where the largest discrepancies have been reported. Prior to the measurements in this work, the lowest reported O_3 cross section were those of Brion et al. at

377.5 nm with a $\sigma_{O3} = 4.4 \times 10^{-24}$ cm^2 and a reported uncertainty of 4% near the absorption minimum Chen and Venables examined the near-UV region from 335 – 375 nm, just to the short wavelength side of the minimum[11,18]. These authors suggested that the absorption cross section in this region would be even lower than seen in previous studies.[1,3,11,12,18] In this work, the minimum was observed to be lower than the Brion et al. value, at 385.6 nm with $\sigma_{O3} = 3.4 \times 10^{-24}$ cm^2, although the two measurements are consistent within their combined uncertainty[11].

5.3.2 Pressure and relative humidity effect on O_3

It has been suggested that O_3 cross sections could be sensitive to the molecular environment[22-25]. At the low partial pressures of O_3 used, ranging from $1.2 \times 10^{15} – 2.4 \times 10^{16}$ molecules cm^{-3}, there was no evidence of nonlinear O_3 partial pressure dependence as shown by Fig. 5.4. Spectroscopic and theoretical studies of the ozone dimer indicate the ozone dimer photolysis cross section is much smaller than that of the monomer, and recent molecular beam studies by Chen et al. show the weak intermolecular interactions are not strong enough to affect the absorption spectra of the monomer[26-30]. In addition, Orphal notes in his review that there is no experimental or theoretical evidence of pressure dependence in the O_3 cross section in the region of interest[7].

Spectroscopic and photofragment experiments report increased OH formation from O_3 photolysis in the presence of water[31]. This increase could be due to stronger absorption of radiation in the region between 350 and 470 nm by $O_3 \cdot H_2O$ complexes than by monomeric ozone[4,22,25]. These complexes have been detected experimentally[32-34]. Limited information is

available from matrix isolation studies about the UV spectra and photochemistry of the $O_3 \cdot H_2O$ complex[35-42].

With the IBBCEAS instrument, I attempted to observe the change in cross section of O_3 using relative humidities (RH) of up to 90%, though I was unable to observe any changes in the O_3 absorption spectrum due to the presence of water. This indicates that the product of the cluster number density and its cross section at the wavelengths of interest here is below the signal to noise of the experiment, which was less than 5% at most wavelengths, passed on the precision of my measurements.

However, I can estimate upper limits for the cross section of the $O_3 \cdot H_2O$ complex in the wavelength region between 350 and 470 nm based on this result. Measured binding energies of the $O_3 \cdot H_2O$ complex range from -0.7 to -2.4 kcal mol^{-1}.[32] This translates to an equilibrium constant between 1.84×10^{-4} atm^{-1} and 3.55×10^{-4} atm^{-1} at room temperature.[22] At a relative humidity of 90%, the ratio of $O_3 \cdot H_2O$:O_3 will be between 5.0×10^{-6} and 9.65×10^{-5} based on the equilibrium constants given above. This gives an upper limit for the enhancement in the absorption cross section of 1.0×10^{4} or 5.0×10^{-2} for binding energies of -0.7 to -2.4 kcal mol^{-1}, respectively.

5.4 Conclusions

Using a newly developed, high sensitivity IBBCEAS instrument, I measured the O_3 absolute absorption cross section from 350 – 470 nm at 295 K and 820 hPa with low O_3 partial pressures. These measurements directly address the large discrepancy in current literature cross sections in this region and agree well with the most recent measurements that are based on cavity

enhanced methods which measured a portion of this spectral region. The effect of ozone concentration and relative humidity were investigated without any effect observed on the absorption cross section of O_3. The absorption cross sections obtained here may be useful for applications such as satellite retrievals, ground-based O_3 monitoring, and atmospheric radiative transfer models. Future work may include temperature dependent measurements, since the O_3 cross section across this minimum is known to be strongly temperature dependent.

5.5 References

1. Burrows, J. P., Richter, A., Dehn, A., Deters, B., Himmelmann, S.,Orphal, J. Atmospheric remote-sensing reference data from GOME - Part 2. Temperature-dependent absorption cross sections of O_3 in the 231-794 nm range. *J. Quant. Spectrosc. Radiat. Transf.,* (1999), **61**, 509-517.
2. Petropavlovskikh, I., Evans, R., Mcconville, G., Oltmans, S., Quincy, D., Lantz, K., Disterhoft, P., Stanek, M.,Flynn, L. Sensitifity of Dobson and Brewer Umkehr ozone profile retrievals to ozone cross-sections and stray light effects. *Atmos. Meas. Tech. Discuss,* (2011), **4**, 2007-2035.
3. Bogumil, K., Orphal, J., Homann, T., Voigt, S., Spietz, P., Fleischmann, O. C., Vogel, A., Hartmann, M., Kromminga, H., Bovensmann, H., Frerick, J.,Burrows, J. P. Measurements of molecular absorption spectra with the SCIAMACHY pre-flight model: Instrument characterization and reference data for atmospheric remote-sensing in the 230-2380 nm region. *J. Photochem. Photobiol. A-Chem.,* (2003), **157**, 167-184.
4. Vaida, V. Spectroscopy of photoreactive systems: Implications for atmospheric chemistry. *J. Phys. Chem. A,* (2009), **113**, 5-18.
5. Matthews, J., Sinha, A.,Francisco, J. S. The importance of weak absorption features in promoting tropospheric radical production. *Proc. Natl. Acad. Sci. U. S. A.,* (2005), **102**, 7449-7452.
6. Waschewsky, G. C. G., Horansky, R.,Vaida, V. Effect of dimers on the temperature-dependent absorption cross section of methyl iodide. *J. Phys. Chem.,* (1996), **100**, 11559-11565.
7. Orphal, J. A critical review of the absorption cross-sections of O_3 and NO_2 in the ultraviolet and visible. *J. Photochem. Photobiol. A-Chem.,* (2003), **157**, 185-209.
8. Gratien, A., Picquet-Varrault, B., Orphal, J., Doussin, J. F.,Flaud, J. M. New Laboratory Intercomparison of the Ozone Absorption Coefficients in the Mid-infrared (10 mu m) and Ultraviolet (300-350 nm) Spectral Regions. *J. Phys. Chem. A,* (2010), **114**, 10045-10048.
9. Kroon, M., de Haan, J. F., Veefkind, J. P., Froidevaux, L., Wang, R., Kivi, R.,Hakkarainen, J. J. Validation of operational ozone profiles from the Ozone Monitoring Instrument. *J. Geophys. Res.-Atmos.,* (2011), **116**, D18305.
10. Burrows, J. P., Weber, M., Buchwitz, M., Rozanov, V., Ladstatter-Weissenmayer, A., Richter, A., DeBeek, R., Hoogen, R., Bramstedt, K., Eichmann, K. U.,Eisinger, M. The global ozone monitoring experiment (GOME): Mission concept and first scientific results. *Journal of the Atmospheric Sciences,* (1999), **56**, 151-175.
11. Brion, J., Chakir, A., Charbonnier, J., Daumont, D., Parisse, C.,Malicet, J. Absorption spectra measurements for the ozone molecule in the 350-830 nm region. *J. Atmos. Chem.,* (1998), **30**, 291-299.
12. Voigt, S., Orphal, J., Bogumil, K.,Burrows, J. P. The temperature dependence (203-293 K) of the absorption cross sections of O_3 in the 230-850 nm region measured by Fourier-transform spectroscopy. *J. Photochem. Photobiol. A-Chem.,* (2001), **143**, 1-9.
13. Burkholder, J. B. and Talukdar, R. K. Temperature-dependence of the ozone absorption-spectrum over the wavelength range 410 to 760 nm. *Geophys. Res. Lett.,* (1994), **21**, 581-584.

14. Brion, J., Chakir, A., Daumont, D., Malicet, J.,Parisse, C. High-resolution laboratory absorption cross-section of O_3 - Temperature effect. *Chem. Phys. Lett.*, (1993), **213**, 610-612.
15. Bodhaine, B. A., Wood, N. B., Dutton, E. G.,Slusser, J. R. On Rayleigh optical depth calculations. *J. Atmos. Ocean. Technol.*, (1999), **16**, 1854-1861.
16. Greenblatt, G. D., Orlando, J. J., Burkholder, J. B.,Ravishankara, A. R. Absorption-measurements of oxygen between 330 nm and 1140 nm. *J. Geophys. Res.-Atmos.*, (1990), **95**, 18577-18582.
17. Washenfelder, R. A., Langford, A. O., Fuchs, H.,Brown, S. S. Measurement of glyoxal using an incoherent broadband cavity enhanced absorption spectrometer. *Atmos. Chem. Phys.*, (2008), **8**, 7779-7793.
18. Chen, J.,Venables, D. S. A broadband optical cavity spectrometer for measureing weak near-ultraviolet absorption spectra of gases. *Atmos. Meas. Tech.* , (2011), **4**, 425-436.
19. Fuchs, H., Dube, W. P., Lerner, B. M., Wagner, N. L., Williams, E. J.,Brown, S. S. A sensitive and versatile detector for atmospheric NO_2 and NO_x based on blue diode laser cavity ring-down spectroscopy. *Environ. Sci. Technol.*, (2009), **43**, 7831-7836.
20. Keller-Rudek, H.,Moortgat, G. K. MPI-Mainz-UV-VIS Spectral Atlas of Gaseous Molecules. (www.atmosphere.mpg.de/spectral-atlas-mainz.
21. Ciddor, P. E. Refractive index of air: New equations for the visible and near infrared. *Applied Optics*, (1996), **35**, 1566-1573.
22. Frost, G. J.,Vaida, V. Atmospheric implications of the photolysis of the ozone-water weakly bound complex. *J. Geophys. Res.-Atmos.*, (1995), **100**, 18803-18809.
23. Vaida, V., Donaldson, D. J., Strickler, S. J., Stephens, S. L.,Birks, J. W. A reinvestigation of the electronic-spectra of ozone condensed-phase effects. *J. Phys. Chem.*, (1989), **93**, 506-508.
24. Vaida, V.,Headrick, J. E. Physicochemical properties of hydrated complexes in the Earth's atmosphere. *J. Phys. Chem. A*, (2000), **104**, 5401-5412.
25. Vaida, V. Perspective: Water cluster mediated atmospheric chemistry. *J. Chem. Phys.*, (2011), **135**, 1-8.
26. Bahou, M., Schriver-Mazzuoli, L.,Schriver, A. Infrared spectroscopy and photochemistry at 266 nm of the ozone dimer trapped in an argon matrix. *J. Chem. Phys.*, (2001), **114**, 4045-4052.
27. Probst, M., Hermansson, K., Urban, J., Mach, P., Muigg, D., Denifl, G., Fiegele, T., Mason, N. J., Stamatovic, A.,Mark, T. D. Ionization energy studies for ozone and OClO monomers and dimers. *J. Chem. Phys.*, (2002), **116**, 984-992.
28. Sander, S. P., Finlayson-Pitts, B. J., Friedl, B. J., Golden, D. M., Huie, R. E., Keller-Rudek, H., Kolb, C. E., Kurylo, M. J., Molina, M. J., Moortgat, G. K., Orkin, V. L., Ravishankara, A. R.,Wine, P. H. Chemical Kinetics and Photochemical Data for Use in Atmospheric Studies 06-2, Jet Propulson Laboratory, Pasadena. (2006.
29. Slanina, Z.,Adamowicz, L. Computational studies of atmospheric chemistry species. 3. A computational study of the ozone dimer. *J. Atmos. Chem.*, (1993), **16**, 41-46.
30. Chen, I.-C., Chen, A. F., Huang, W.-T., Takahashi, K.,Lin, J. J. Photolysis cross section of ozone dimer. *Chem Asian J.*, (2011, doi.10.1002/asia.201100526.
31. Hurwitz, Y.,Naaman, R. Production of OH by dissociating ozone water complexes at 266 nm and 355 nm by reacting O(1D) with water dimers. *J. Chem. Phys.*, (1995), **102**, 1941-1943.

32. Gillies, J. Z., Gillies, C. W., Suenram, R. D., Lovas, F. J., Schmidt, T.,Cremer, D. A microwave spectral and abinitio investigation of O_3-H_2O. *J. Mol. Spectrosc.,* (1991), **146**, 493-512.
33. Schriver, L., Barreau, C.,Schriver, A. Infrared spectroscopic and photochemical study of water ozone complexes in solid argon. *Chem. Phys.,* (1990), **140**, 429-438.
34. Tsuge, M., Tsuji, K., Kawai, A.,Shibuya, K. Infrared spectroscopy of ozone-water complex in a neon matrix. *J. Phys. Chem. A,* (2007), **111**, 3540-3547.
35. Brasseur, G.,Solomon, S. Aeronomy of the Middle Atmosphere. *2nd ed.,* (1997), D. Reidel.
36. Dlugokencky, E. J.,Ravishankara, A. R. Laboratory measurements of direct ozone loss on ice and doped-ice surfaces. *Geophys. Res. Lett.,* (1992), **19**, 41-44.
37. Jaeger, K. Ph.D. Thesis. *University of Bremen,* (1991, 111 – 136.
38. Langenberg, S.,Schurath, U. Ozone destruction on ice. *Geophys. Res. Lett.,* (1999), **26**, 1695-1698.
39. Leu, M. T. Heterogeneous reactions of N_2O_5 with H_2O and HCL on ice surfaces - inplicatiosn for antartic ozone depletion. *Geophys. Res. Lett.,* (1988), **15**, 851-854.
40. Schriver, A., Schriver, L., Barreau, C., Carri re, D., Perchard, J. P., Jaeger, K.,Schrems, O. Ozone in the Atmosphere: Proceedings of the Quadrennial Ozone Symposium 1988 and Tropospheric Ozone Workshop. *A. Deepak Publishing,* (1989), 694– 697.
41. Sennikov, P. G., Ignatov, S. K.,Schrems, O. Complexes and clusters of water relevant to atmospheric chemistry: H_2O complexes with oxidants. *ChemPhysChem,* (2005), **6**, 392-412.
42. King, D. S., Sauder, D. G.,Casassa, M. P. Cluster effects in O_3/H_2O Photochemistry: Dynamics of the $O+H_2O \rightarrow 2OH$ reaction photoinitiated in the O3•H2O dimer. *J. Chem. Phys.,* (1994), **100**, 4200-4210.

6. Ultraviolet cross section changes in methylglyoxal as a factor of relative humidity: Photochemical implications

6.1 Introduction

The processing of organics in the atmosphere is complex and much remains unknown. Recent studies have shown that 20 – 90% of aerosols contain organics[1,2]. Several of these aerosols can contain a significant amount of organics, up to 90% of the particle[3-5]. This atmospheric organic matter can be chemically processed in a number of ways, including gas or aqueous-phase heterogeneous oxidation, photolysis, and aqueous phase cloud processing (photo-oxidation)[6-8]. Organic acids (i.e. oxalic and pyruvic acid) are found in secondary organic aerosols (SOA) and cloud droplets, though the origin of these acids is not predicted correctly by the gas-phase chemistry[6,8-10]. Recent modeling and experimental studies suggest that these acids are made in the aqueous phase, particularly in cloud water, by the oxidation of aldehydes like glyoxal and methylglyoxal with hydroxyl radicals and other aqueous radical species[6,7,11,12]. Methylglyoxal is one of the most abundant α–dicarbonyl present in the atmosphere from biogenic and anthropogenic sources[7,13-15]. While the gas-phase chemistry of such α–dicarbonyl is fairly well understood, the modeled concentration and role in atmospheric chemistry for these molecules is controversial[16,17].

More recently, mid- and near-IR spectroscopic studies (Chapter 3 and 4) have shown that hydration of methylglyoxal does happen in the gas phase to produce a geminal diol[18]. Methylglyoxal diol contains two OH groups that can or hydrogen bonds with gas or aqueous

phase water, allowing it to form clusters[18] or more readily partition in to the aqueous particle phase. The increased partitioning of methylglyoxal to the aqueous particle phase can lead to an increase in organic acids. This gas-phase hydration of methylglyoxal to form the diol, however, has not yet been considered in atmospheric models.

In addition to increasing the hydrogen bonding ability, the hydration of methylglyoxal will alter its electronic state and its photochemistry. The ultraviolet (UV) spectroscopy of small aldehydes and ketones has been studied in the gas and aqueous phases[19-27]. The aqueous phase hydration of α–dicarbonyls to form alcohols can change their electronic state by eliminating or suppressing one or both of the n→π* transitions of the carbonyl groups[24,26,27]. For methylglyoxal diol, aqueous phase studies show hydration forms diol (60%) and tetrol (40%) as primary products. The gas phase hydration study of methylglyoxal diol shows formation of only the diol[24]. This would leave the methylglyoxal diol ketone carbonyl still available for UV photolysis, but would effectively alter the UV photochemistry of methylglyoxal in the gas phase.

Though the electronic spectrum of the methylglyoxal diol is unknown, like most alcohols, it is expected to be at much higher energies that what is provided by the solar spectrum ($\lambda > 280$ nm). The hydration to form methylglyoxal diol is expected to modify the electronic spectrum of methylglyoxal in one of several ways. For instance, there can be a relative change in gas-phase methylglyoxal near-UV cross section (350 – 470 nm), such as a decrease in the relative cross section from the removal of the aldehyde carbonyl. The formation of methylglyoxal diol could alter the electronic state vibrational structure of the near-UV transition. Additionally, methylglyoxal diol water cluster formation could cause red shifting of the near-UV transition.

In this study, spectroscopic techniques were used to analyze the hydration of methylglyoxal in the gas and aqueous phases by observing changes in the UV cross section. The

aqueous phase methylglyoxal UV photochemistry was examined for product formation and to aid in understanding the UV photochemistry of gas phase methylglyoxal diol. A conventional UV-visible spectrometer was used to examine the near-UV cross section of aqueous phase methylglyoxal. The IBBCEAS instrument was used to investigate the changes in the methylglyoxal UV absorption cross section with increasing relative humidity. NMR techniques were then used to analyze UV photolysis products of aqueous phase methylglyoxal.

6.2 Experimental

6.2.1 Sample Preparation

The gas phase methylglyoxal UV cross section was obtained by drying and vacuum distilling the 40 wt% methylglyoxal solution as described in detail by Axson et al.[18]. The methylglyoxal gas was then transferred to an evacuated 12 L glass bulb wrapped in dark tape to avoid photolysis. The bulb was then pressurized to roughly 950 Torr with nitrogen. The sample lasted for two weeks at room temperature. The methylglyoxal gas and aqueous phase UV cross sections were measured at ambient temperature and pressure of 296 K and 837 mbar. The aqueous phase methylglyoxal for the NMR study was made by rehydrating the purified gas phase methylglyoxal. To obtain the aqueous phase methylglyoxal UV cross section, methylglyoxal solution (~40 wt% in water Sigma-Aldrich) was diluted to 0.02 M in NERL ultrapure water (Thermo scientific).

6.2.2 UV- visible spectrometer

The aqueous phase methylglyoxal UV cross section was obtained using an Ocean Optics ISS-UV-Vis spectrometer (CHEM2000, Ocean Optics Inc.). Prior to use the instrument lamp, consisting of a deuterium and tungsten bulb, was turned on and allowed to warm up 15 minutes to ensure stability. To avoid saturation the parameters for the experiment were 50 scans with an integration time of 100 ms. The spectra were then averaged.

6.2.3 Methylglyoxal delivery and measurement with IBBCEAS

The sampling set up for methylglyoxal delivery to the IBBCEAS is shown in Fig. 6.1. Methylglyoxal from the 12 L bulb was controlled to 5 SSCM by a mass flow controller and a three-way valve. The methylglyoxal concentration was diluted by a controlled flow of 4.0 SLPM of dry air by a second mass flow controller and three-way valve to give methylglyoxal concentrations in the range of 70 – 75 ppbv. Dry air was bubbled through water to produce water vapor of different relative humidities which was monitored using a RH probe. The static cell was constructed using ½ diameter Teflon tubing that was 9 m in length, which gave a resonance time of roughly 8 minutes.

The IBBCEAS for this experiment consisted of two channels with LEDs centered at 365 nm and 455 nm to span the spectral region from 440 – 470 nm and a CRD with a diode laser centered at 404 nm, whose set-up has been explained in detail in Washenfelder et al.[28]. The apparatus required approximately 30 min of warm up to allow the temperature of the LEDs and spectrometer to stabilize. Dark background spectra were acquired to correct for the pixel-depende nt dark signal. These were scaled to the integration time and subtracted from subsequent

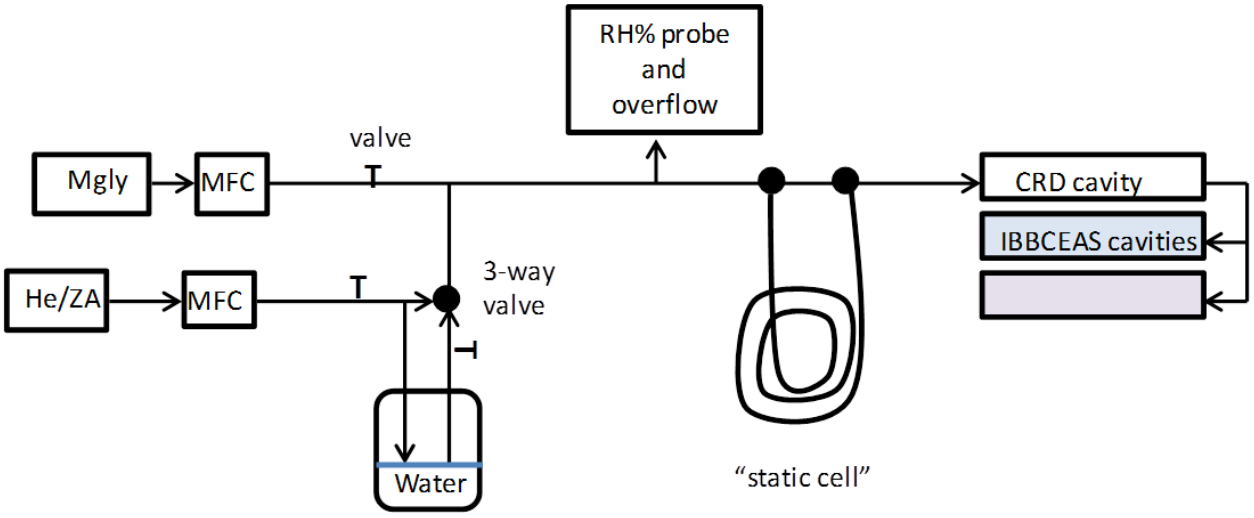

Figure 6.1 Block diagram showing the plumbing of the IBBCEAS instrument

sample spectra. Helium and dry air spectra obtained for each IBBCEAS cavity were used to calibrate mirror reflectivity using Eqn. 2.3.[29] The σ_{Ray} for helium and dry air were taken from Bodhaine et al. [30]. Spectra of methylglyoxal in air at various concentrations were acquired with alternating dry air zeros. Optical extinction due to methylglyoxal was then determined using Eqn. 2.4.[29]

6.2.4 Nuclear Magnetic Resonance (NMR)

The aqueous phase methylglyoxal sample was separated to three aliquots for NMR analysis. One was covered and at room temperature for one hour. During that hour, the remaining two aliquots were irradiated by a 450 W Xe Arc lamp from Newport, Inc. One of these was irradiated with UV-visible light and the second was placed in a quartz NMR tube so that only visible light passed through the sample. All NMR spectra were taken in the University of Colorado NMR facility by Richard Shoemaker.

6.3 Results and Discussion

6.3.1 Gas phase and aqueous phase UV cross sections of α-dicarbonyls

Figure 6.2 shows the previously measured gas-phase UV absorption cross sections from 250 – 500 nm of some atmospherically relevant α–dicarbonyls, glyoxal (CHOCHO), methylglyoxal (CH_3COCOH), and biacetyl ($CH_3COCOCH_3$) obtained from the Mainz Spectral Database[20-22,31]. Each of these α-dicarbonyls has two carbonyl $n \rightarrow \pi^*$ transitions. The glyoxal

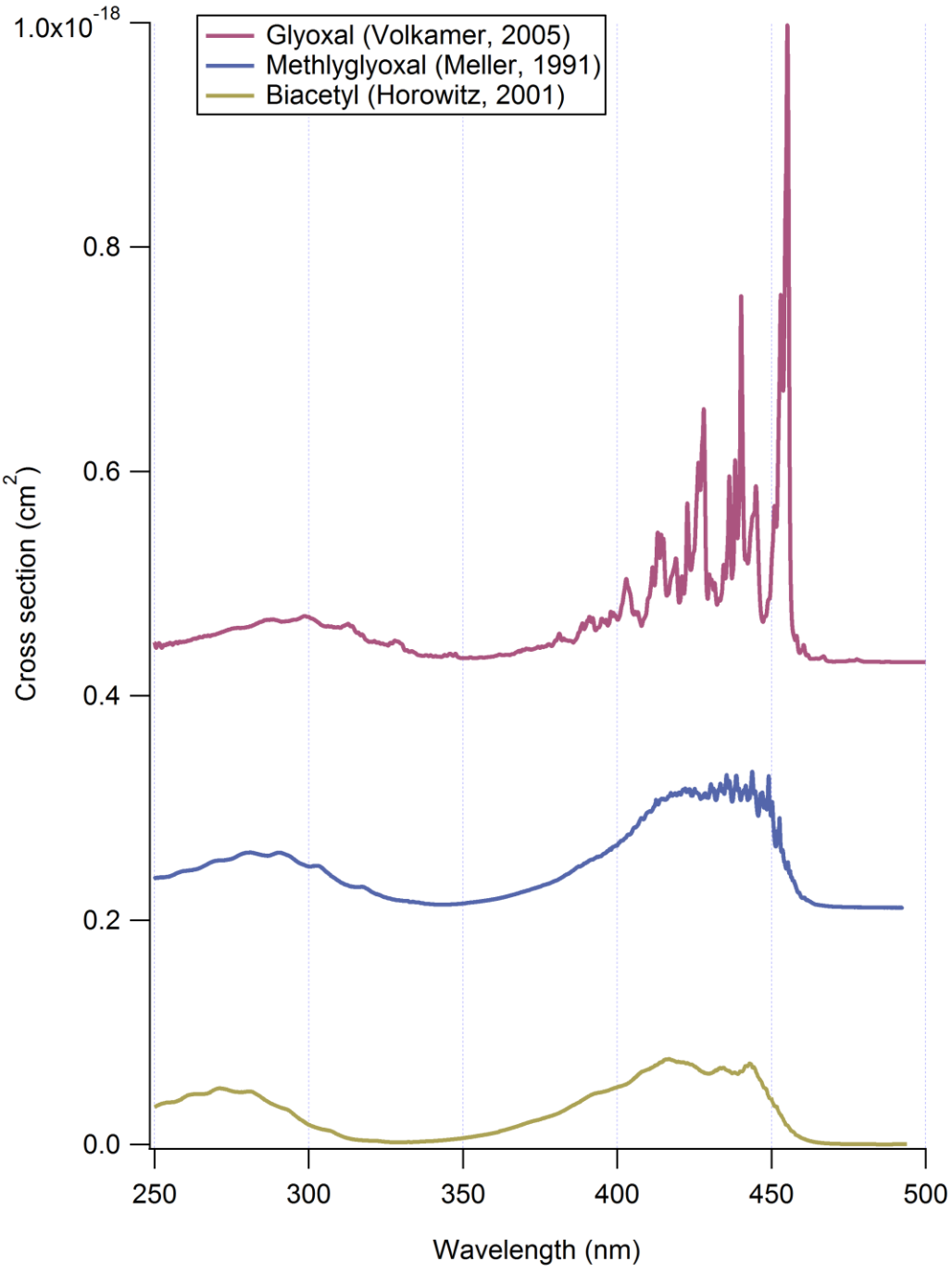

Figure 6.2 Gas-phase literature UV cross sections glyoxal, methylglyoxal, and biacetyl from 250 – 500 nm.[20,21,34]

UV cross section from Volkamer et al.[20] shows a very structured transition centered at 455 nm and a less structured transition at 300 nm. The Meller et al.[21] methylglyoxal UV cross section shows a more structured transitions centered at 440 nm and one at 280 nm. The Horowitz et al.[22] biacetyl UV cross sections, which are less structured and are centered at 420 nm and 270 nm.

Aqueous phase studies of these α-dicarbonyls shows hydration of one or more of the carbonyls, which results in changes to the UV cross section. The simplest of these a-dicarbonyls is glyoxal, which is comprised of two aldehyde groups. Glyoxal fully hydrates in aqueous phase to form a tetrol ($CH(OH)_2CH(OH)_2$). The OH groups on the glyoxal tetrol would not absorb light in the solar region (λ >280 nm), and therefore no transitions in this near-UV region should be observed. The aqueous phase UV cross section of glyoxal obtained in this study shows that the lower energy transition centered at 455 nm completely disappears and there is a very weak transition centered around 280 nm. Previous literature studies[26] confirm my experimental results and explain that the weak 280 nm transition may be from a very low concentration of the monohydrated glyoxal ($CH(OH)_2COH$) present in the solution. Methylglyoxal, a ketoaldehyde and next simplest dicarbonyl, is present at 60% methylglyoxal diol, with the aldehydic group hydrated, and 40% tetrol[18,24,32]. This suggests that in aqueous phase one of the carbonyl $n\rightarrow\pi^*$ transitions of methylglyoxal will be present. Figure 6.3 show a previously reported gas phase methylglyoxal UV cross section[21] along with an aqueous phase UV cross section of methylglyoxal acquired in this study. Similar to the aqueous phase glyoxal UV spectrum, the low energy transition has disappeared in the aqueous phase methylglyoxal UV cross section. The higher energy transition of methylglyoxal centered at 280 nm preserves some intensity. The weak intensity observed in aqueous phase for this band can be rationalized as being from the ketone carbonyl of the methylglyoxal diol.

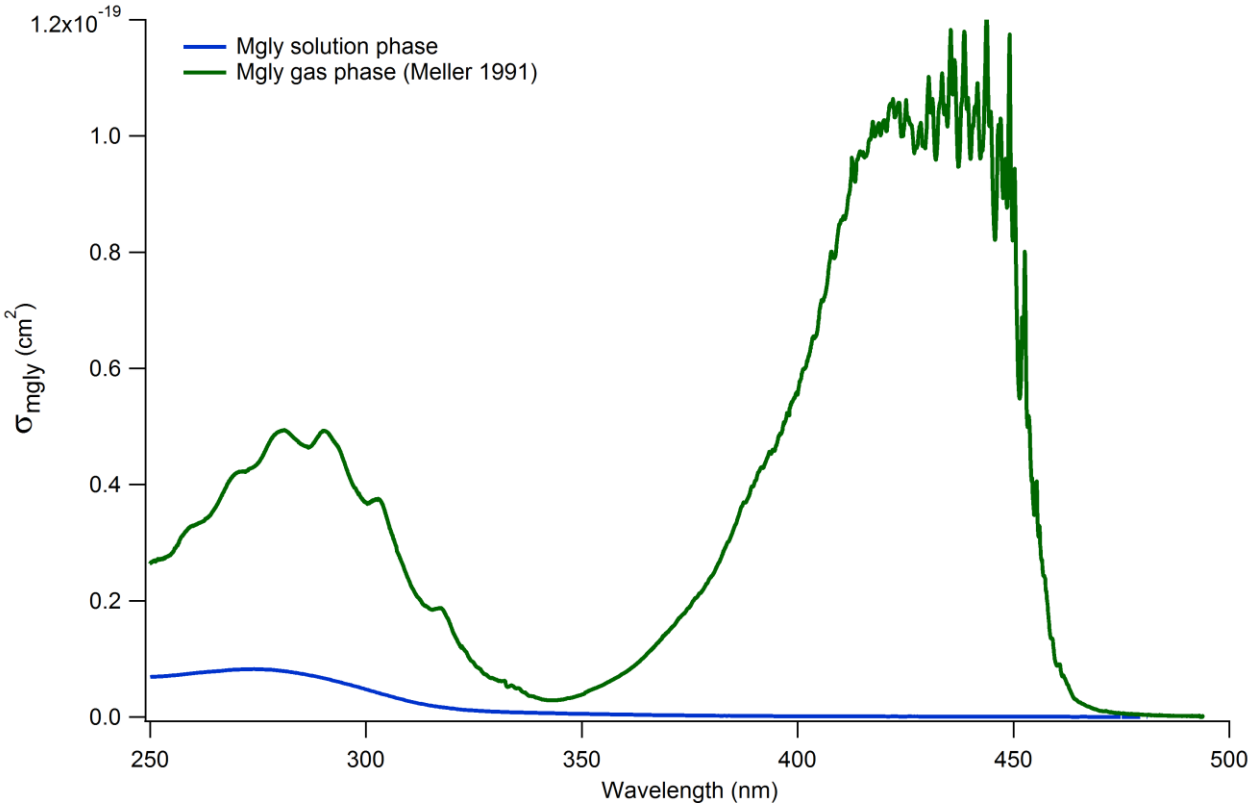

Figure 6.3 The gas-phase and solution-phase UV cross section of methylglyoxal from 250 – 500 nm.

Previous literature studies of the aqueous phase methylglyoxal UV spectrum[24] confirm my results. In aqueous phase, roughly 2/3 of biacetyl exists as the monohydrate and 1/3 as the dicarbonyl, consisting of two ketone groups[27,33]. Therefore, its aqueous phase spectrum retains its two transition features, at 420 nm and 270 nm[27]. I would expect that in comparison to the gas phase biacetyl UV cross section, the low energy transition would be slightly lower due to the formation of the monohydrate.

6.3.2 Gas phase methylglyoxal UV cross section as a function of RH%

With the IBBCEAS instrument, I measured the gas phase UV cross section of methylglyoxal from 440 – 470 nm and the relative changes in the cross section as a function of 20%, 40%, and 60% RH. In each of these relative humidity experiments, the static cell provided a resonance time of 8 minutes. Figure 6.4 shows three panels containing the UV cross section of methylglyoxal (green) and of methylglyoxal at each relative humidity (black). The top panel (Fig 6.4a) displaying the methylglyoxal cross section when exposed to 20% RH shows no change in the cross section of methylglyoxal. As the RH is increased to 40%, there is a 2% decrease in the methylglyoxal UV cross section (Fig 6.4b). In the 60%RH experiments (Fig 6.4c), there is a noticeable difference, ~3%, in the spectra hydrated and unhydrated methylglyoxal UV cross section.

It has been previously shown (Chapter 3 and 4) that methylglyoxal can hydrate in the gas phase to form methylglyoxal diol[18]. The hydration of methylglyoxal to form its diol changes the electronic state of the molecule by eliminating the aldehyde carbonyl $n \rightarrow \pi^*$ transition that undergoes near UV chemistry. This change is observed in the methylglyoxal UV cross section

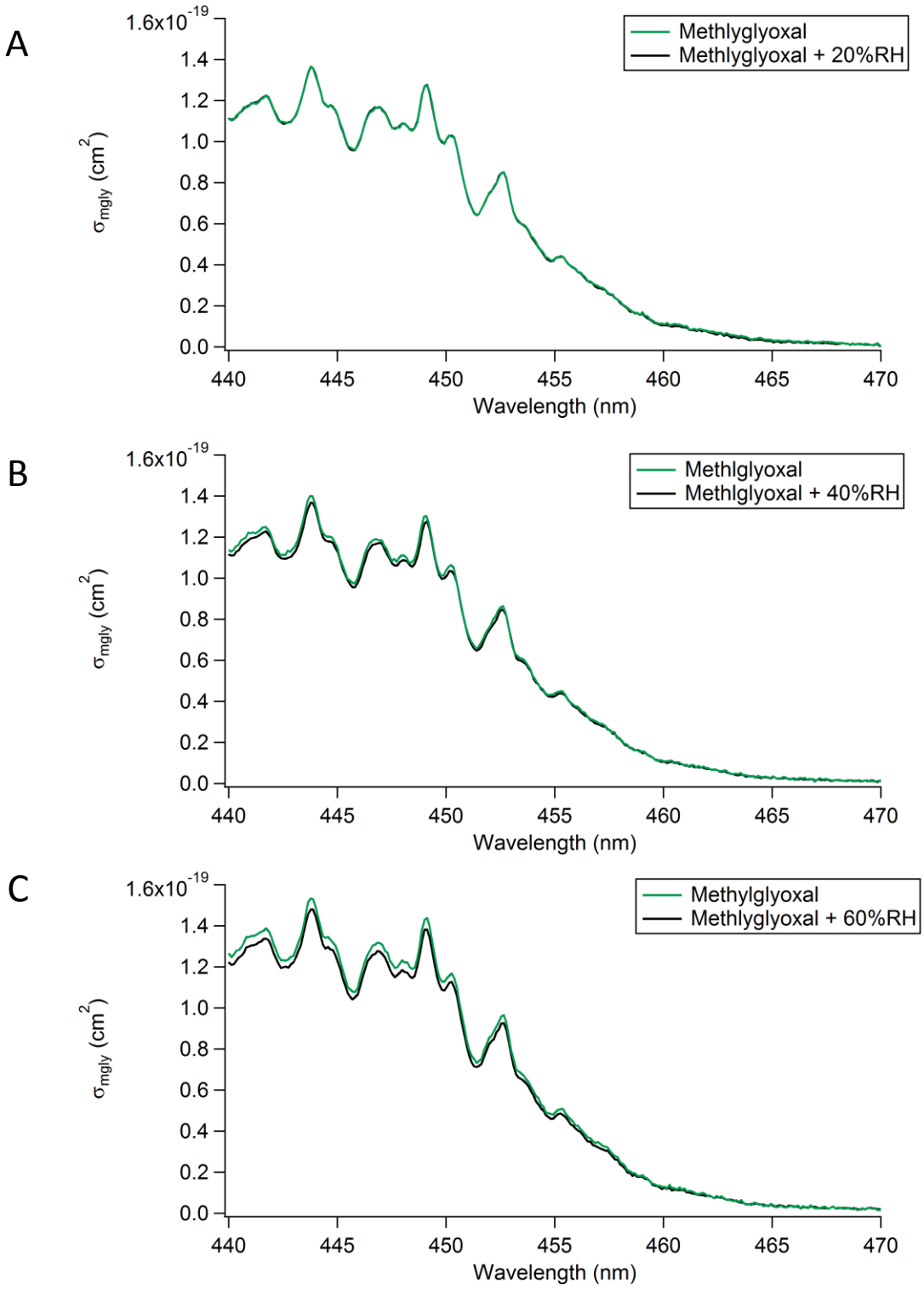

Figure 6.4 The gas phase UV spectrum from 440 – 470 nm of methylglyoxal and hydrated methylglyoxal at (a) 20% RH, (b) 40% RH, and (c) 60% RH taken with the IBBCEAS instrument.

where the strong transition centered at 450 nm disappears upon hydration in the aqueous phase (Fig. 6.3). This gas phase near-UV study shows the decrease in methylglyoxal cross section at a relative humidity > 40%.

Controls were run to ensure the sample, either the methylglyoxal or water vapor, was not adsorbing to the Teflon tubing. The control experiments were performed in the following manner, (1) the sample was inserted directly into the IBBCEAS instrument to measure the UV cross section and (2) the sample was inserted through the static cell and then the IBBCEAS instrument. When inserted separately, the methylglyoxal and water showed no observed change in the cross section. Therefore, I asserted there no loss of methylglyoxal or water vapor to the walls of the static cell. In addition to this, clusters/aerosol formation, when the methylglyoxal and water were sample together, was ruled out observing no cross sectional change when inserting and removing a filter between the static cell and the IBBCEAS. The only decrease in methylglyoxal UV cross section was observed when the methylglyoxal and water vapor were combined.

6.3.3 Aqueous phase UV photochemistry

The aqueous phase photolysis of α-dicarbonyls is not included in atmospheric models because the molecules are assumed to be fully hydrated removing any photolysis pathways. In aqueous phase, methylglyoxal has been observed to hydrate in the aqueous phase to primarily form the diol (60%)[24,32]. This partially hydrated form of methylglyoxal has a ketone carbonyl present that is still available for photochemistry. Figure 6.5 shows the NMR results of aqueous phase methylglyoxal taken in the absence of light, irradiated with only visible light, and

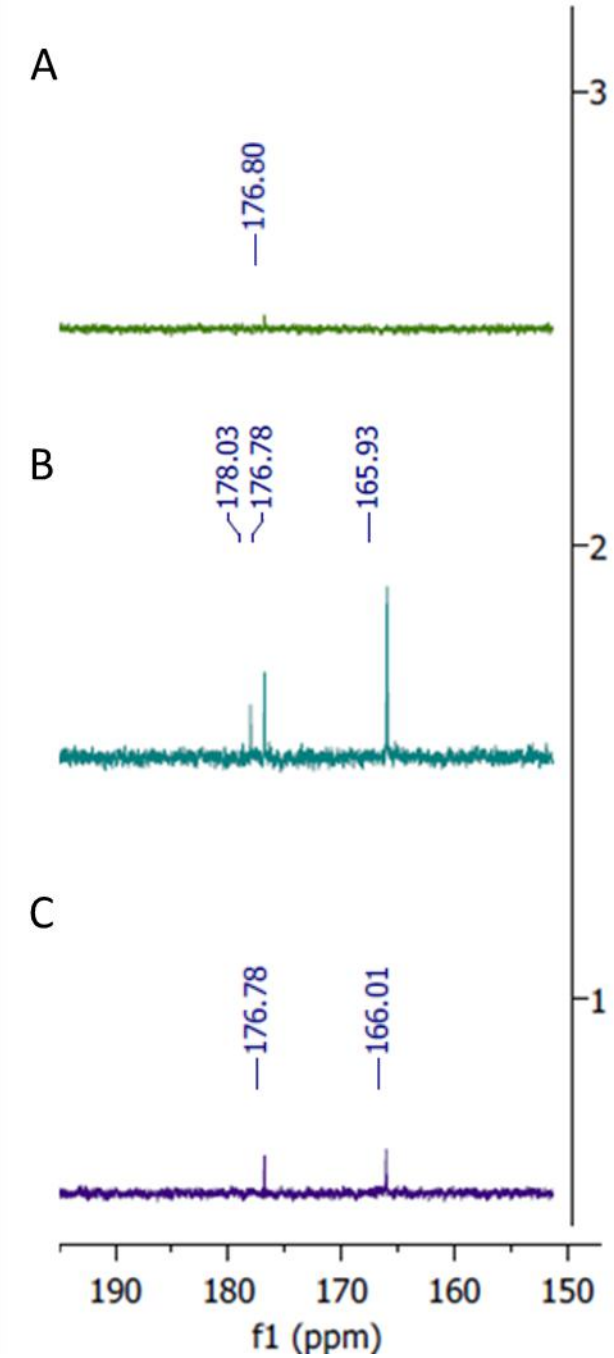

Figure 6.5 Aqueous phase methylglyoxal NMR spectrum where the solution was (a) kept in the dark at room temperature, (b) irradiated with visible light, and (c) irradiated with UV-visible light.

irradiated with UV-visible light. Carboxylic acid and ester carbonyl groups are typically located in the region from roughly 150 – 190 ppm. The NMR of aqueous phase methylglyoxal in the absence of light (Fig. 6.5a) shows the presence of a carboxylic acid group at 176 ppm corresponding to the acetic acid carbonyl. When irradiated with only visible light, the NMR spectrum of aqueous phase methylglyoxal shows three chemical shifts at 176 ppm and 165 ppm, corresponding to acetic acid, and formic acid, respectably (Fig 6.5b). There is an additional shift at 178 ppm from another carboxylic acid. Figure 6.5c is the NMR aqueous phase methylglyoxal of after irradiation with UV-visible light, showing the presence of acetic and formic acid.

In the absence of previous studies, the aqueous phase UV photolysis study of biacetyl[27] was used to understand the UV photolysis of aqueous phase methylglyoxal. Faust et at.[27] showed that the UV photolysis of aqueous phase biacetyl produced acetic acid and peracetic acid. They propose a schematic that shows a C-C bond cleavage between the two ketone groups to form acetyl radicals, which through a series of reactions form acetic acid and peracetic acid[27]. When this reaction scheme is applied to the aqueous phase methylglyoxal, which is ~60% diol, the C-C bond cleavage would lead to the formation of acetyl radicals and $CH(OH)_2$ radicals which could subsequently form formic acid, acetic acid, and peracetic acid.

Formation of gas phase methylglyoxal diol would alter methylglyoxal UV photochemistry, potentially effecting gas phase atmospheric radical chemistry. The radicals that could be formed from the UV photolysis of methylglyoxal diol could then exist in the gas phase and where it could react with other atmospheric species. This could also alter the methylglyoxal atmospheric lifetime by eliminating a photochemical pathway of the molecule, allowing the species to remain longer in the atmosphere, either in the gas or aqueous phase.

6.4 Conclusions

Small α-dicarbonyls, containing one or both aldehyde and ketone groups, show two UV transitions in the gas phase which decrease in intensity the aqueous phase. In the case of α-dicarbonyls with aldehyde groups, the lower energy transition completely disappears and the higher energy transition decreases by orders of magnitude. Using the IBBCEAS instrument, I followed a decrease in the gas-phase UV cross section of methylglyoxal as relative humidity was increased. The preliminary results suggest that the formation of gas phase methylglyoxal diol changes the electronic state of methylglyoxal by suppressing the aldehyde carbonyl n→π* transition at 450 nm. The resonance time for these experiments was about 8 minutes. Given a longer resonance time, there may have been more change observed.

In this study, I observed the formation of formic, acetic, and peracetic acids following the UV photolysis of aqueous phase methylglyoxal. This result points to the effect of hydration on the photochemistry of methylglyoxal and likely other aldehydes and ketones. This information is interpreted by analysis with aqueous phase biacetyl. The aqueous phase photolysis study of biacetyl by Faust et al.[27] shows the formation of carbon centered radicals which can go on to form acids and peroxides. Aqueous phase UV photolysis of methylglyoxal in this study showed the formation of acetic acid, formic acid, and other carboxylic acid containing groups. Assuming that 60% of the solution is methylglyoxal diol and using the schematic from Faust et al[27] these products along with peracetic acid would be expected to form. These acids and peroxides could also be present in the gas phase from the photolysis of gas phase methylglyoxal diol. The photolysis of the diol creates carbon centered radicals which have the potential to affect gas phase atmospheric radical chemistry.

6.5 References

1. Murphy, D. M., Cziczo, D. J., Froyd, K. D., Hudson, P. K., Matthew, B. M., Middlebrook, A. M., Peltier, R. E., Sullivan, A., Thomson, D. S.,Weber, R. J. Single-particle mass spectrometry of tropospheric aerosol particles. *J. Geophys. Res.-Atmos.*, (2006), **111**, 15.
2. Zhang, Q., Jimenez, J. L., Canagaratna, M. R., Allan, J. D., Coe, H., Ulbrich, I., Alfarra, M. R., Takami, A., Middlebrook, A. M., Sun, Y. L., Dzepina, K., Dunlea, E., Docherty, K., DeCarlo, P. F., Salcedo, D., Onasch, T., Jayne, J. T., Miyoshi, T., Shimono, A., Hatakeyama, S., Takegawa, N., Kondo, Y., Schneider, J., Drewnick, F., Borrmann, S., Weimer, S., Demerjian, K., Williams, P., Bower, K., Bahreini, R., Cottrell, L., Griffin, R. J., Rautiainen, J., Sun, J. Y., Zhang, Y. M.,Worsnop, D. R. Ubiquity and dominance of oxygenated species in organic aerosols in anthropogenically-influenced Northern Hemisphere midlatitudes. *Geophys. Res. Lett.*, (2007), **34**, L13801.
3. Kanakidou, M., Seinfeld, J. H., Pandis, S. N., Barnes, I., Dentener, F. J., Facchini, M. C., Van Dingenen, R., Ervens, B., Nenes, A., Nielsen, C. J., Swietlicki, E., Putaud, J. P., Balkanski, Y., Fuzzi, S., Horth, J., Moortgat, G. K., Winterhalter, R., Myhre, C. E. L., Tsigaridis, K., Vignati, E., Stephanou, E. G.,Wilson, J. Organic aerosol and global climate modelling: a review. *Atmos. Chem. Phys.*, (2005), **5**, 1053-1123.
4. Jimenez, J. L., Canagaratna, M. R., Donahue, N. M., Prevot, A. S. H., Zhang, Q., Kroll, J. H., DeCarlo, P. F., Allan, J. D., Coe, H., Ng, N. L., Aiken, A. C., Docherty, K. S., Ulbrich, I. M., Grieshop, A. P., Robinson, A. L., Duplissy, J., Smith, J. D., Wilson, K. R., Lanz, V. A., Hueglin, C., Sun, Y. L., Tian, J., Laaksonen, A., Raatikainen, T., Rautiainen, J., Vaattovaara, P., Ehn, M., Kulmala, M., Tomlinson, J. M., Collins, D. R., Cubison, M. J., Dunlea, E. J., Huffman, J. A., Onasch, T. B., Alfarra, M. R., Williams, P. I., Bower, K., Kondo, Y., Schneider, J., Drewnick, F., Borrmann, S., Weimer, S., Demerjian, K., Salcedo, D., Cottrell, L., Griffin, R., Takami, A., Miyoshi, T., Hatakeyama, S., Shimono, A., Sun, J. Y., Zhang, Y. M., Dzepina, K., Kimmel, J. R., Sueper, D., Jayne, J. T., Herndon, S. C., Trimborn, A. M., Williams, L. R., Wood, E. C., Middlebrook, A. M., Kolb, C. E., Baltensperger, U.,Worsnop, D. R. Evolution of Organic Aerosols in the Atmosphere. *Science*, (2009), **326**, 1525-1529.
5. Seinfeld, J. S.,Pandis, S. N. *Atmospheric Chemistry and Physics: From Air Pollution to Climate Change*, Second ed.; John Wiley & Sons, Inc., 2006.
6. Carlton, A. G., Turpin, B. J., Altieri, K. E., Seitzinger, S., Reff, A., Lim, H. J.,Ervens, B. Atmospheric oxalic acid and SOA production from glyoxal: Results of aqueous photooxidation experiments. *Atmos. Environ.*, (2007), **41**, 7588-7602.
7. Altieri, K. E., Seitzinger, S. P., Carlton, A. G., Turpin, B. J., Klein, G. C.,Marshall, A. G. Oligomers formed through in-cloud methylglyoxal reactions: Chemical composition, properties, and mechanisms investigated by ultra-high resolution FT-ICR mass spectrometry. *Atmos. Environ.*, (2008), **42**, 1476-1490.
8. Ervens, B., Feingold, G., Frost, G. J.,Kreidenweis, S. M. A modeling study of aqueous production of dicarboxylic acids: 1. Chemical pathways and speciated organic mass production. *J. Geophys. Res.-Atmos.*, (2004), **109**, 20.
9. Tervahattu, H., Juhanoja, J.,Kupiainen, K. Identification of an organic coating on marine aerosol particles by TOF-SIMS. *J. Geophys. Res.-Atmos.*, (2002), **107**, 7.

10. Veres, P., Roberts, J. M., Warneke, C., Welsh-Bon, D., Zahniser, M., Herndon, S., Fall, R.,de Gouw, J. Development of negative-ion proton-transfer chemical-ionization mass spectrometry (NI-PT-CIMS) for the measurement of gas-phase organic acids in the atmosphere. *Int. J. Mass Spectrom.*, (2008), **274**, 48-55.
11. Ervens, B., Carlton, A. G., Turpin, B. J., Altieri, K. E., Kreidenweis, S. M.,Feingold, G. Secondary organic aerosol yields from cloud-processing of isoprene oxidation products. *Geophys. Res. Lett.*, (2008), **35**, 5.
12. Warneck, P. In-cloud chemistry opens pathway to the formation of oxalic acid in the marine atmosphere. *Atmos. Environ.*, (2003), **37**, 2423-2427.
13. Fu, T. M., Jacob, D. J., Wittrock, F., Burrows, J. P., Vrekoussis, M.,Henze, D. K. Global budgets of atmospheric glyoxal and methylglyoxal, and implications for formation of secondary organic aerosols. *J. Geophys. Res.-Atmos.*, (2008), **113**, 17.
14. Jang, M. S.,Kamens, R. M. Characterization of secondary aerosol from the photooxidation of toluene in the presence of NO_x and 1-propene. *Environ. Sci. Technol.*, (2001), **35**, 3626-3639.
15. Tuazon, E. C., Macleod, H., Atkinson, R.,Carter, W. P. L. Alpha-dicarbonyl yields from the NO_X-air photooxidations of a aeries of aromatic-hydrocarbons in air. *Environ. Sci. Technol.*, (1986), **20**, 383-387.
16. Volkamer, R., Jimenez, J. L., San Martini, F., Dzepina, K., Zhang, Q., Salcedo, D., Molina, L. T., Worsnop, D. R.,Molina, M. J. Secondary organic aerosol formation from anthropogenic air pollution: Rapid and higher than expected. *Geophys. Res. Lett.*, (2006), **33**, 4.
17. Volkamer, R., Martini, F. S., Molina, L. T., Salcedo, D., Jimenez, J. L.,Molina, M. J. A missing sink for gas-phase glyoxal in Mexico City: Formation of secondary organic aerosol. *Geophys. Res. Lett.*, (2007), **34**, 5.
18. Axson, J. L., Takahashi, K., De Haan, D. O.,Vaida, V. Gas-phase water-mediated equilibrium between methylglyoxal and its geminal diol. *Proc Natl Acad Sci USA*, (2010), **107**, 6687-6692.
19. Coveleskie, R. A.,Yardley, J. T. Luminescence and Simplified Photophysicys of Methylglyoxal. *J. Am. Chem. Soc.*, (1974), **97**, 1667-1672.
20. Volkamer, R., Spietz, P., Burrows, J. P.,Platt, U. High-resolution absorption cross-sections of glyoxal in the UV-vis and IR spectral ranges. *J. Photochem. Photobiol. A: Chem.* , (2005), **172**, 35-36.
21. Meller, R., Raber, W., Crowley, J. N., Jenkin, M. E.,Moortgat, G. K. The UV-visible absorption-spectrum of methylglyoxal. *J. Photochem. Photobiol. A-Chem.*, (1991), **62**, 163-171.
22. Horowitz, A., Meller, R.,Moortgat, G. K. The UV-VIS absorption cross sections of the α-dicarbonyl compounds: pyruvic acid, biacetyl and glyoxal. *J. Photochem. Photobiol. A: Chem.*, (2001), **146**, 19-27.
23. Staffelbach, T. A., Orlando, J. J., Tyndall, G. S.,Calvert, J. G. The UV-visible absorption-spectrum and photolysis quantum yields of methylglyoxal *J. Geophys. Res.-Atmos.*, (1995), **100**, 14189-14198.
24. Nemet, I., Vikic-Topic, D.,Varga-Defterdarovic, L. Spectroscopic studies of methylglyoxal in water and dimethylsulfoxide. *Bioorganic Chem.*, (2004), **32**, 560-570.

25. Plum, C. N., Sanhueza, E., Atkinson, R., Carter, W. P. L.,Pitts, J. N. OH radical rate constants and photolysi rates of alpha-dicarbonyls. *Environ. Sci. Technol.*, (1983), **17**, 479-484.
26. Malik, M.,Joens, J. A. Temperature dependent near-UV molar absorptivities of glyoxal and gluteraldehyde in aqueous solution. *Spectrochimica Acta Part A*, (2000), **56**, 2653-2658.
27. Faust, B. C., Powell, K., Rao, C. J.,Anastasio, C. Aqueous-phase photolysis of biacetyl (an alpha-dicarbonyl compound): A sink for biacetyl, and a source of acetic acid, peroxyacetic acid, hydrogen peroxide, and the highly oxidizing acetylperoxyl radical in aqueous aerosols, fogs, and clouds. *Atmos. Environ.*, (1997), **31**, 497-510.
28. Washenfelder, R., Young, C.,Brown, S. S. A field instrument for NO_2, HONO, and CHOCHO using incoherent broadband cavity enhances absorption spectroscopy. *In preparation*.
29. Washenfelder, R. A., Langford, A. O., Fuchs, H.,Brown, S. S. Measurement of glyoxal using an incoherent broadband cavity enhanced absorption spectrometer. *Atmos. Chem. Phys.*, (2008), **8**, 7779-7793.
30. Bodhaine, B. A., Wood, N. B., Dutton, E. G.,Slusser, J. R. On Rayleigh optical depth calculations. *J. Atmos. Ocean. Technol.*, (1999), **16**, 1854-1861.
31. Keller-Rudek H.,Moortgat, G. K. MPI-Mainz-UV-VIS Spectral Atlas of Gaseous Molecules. (www.atmosphere.mpg.de/spectral-atlas-mainz.
32. Krizner, H. E., De Haan, D. O.,Kua, J. Thermodynamics and kinetics of methylglyoxal dimer formation: A computational study. *J. Phys. Chem. A*, (2009), **113**, 6994-7001.
33. Greenzai.P, Luz, Z.,Samuel, D. A nuclear magnetic resonance study of reversible hydration of aliphatic aldehydes and ketones I. Oxygen-17 and Proton spectra and equilibrium constants. *J. Am. Chem. Soc.*, (1967), **89**, 749-&.
34. Hurwitz, Y.,Naaman, R. Production of OH by dissociating ozone water complexes at 266 nm and 355 nm and by reacting $O(^1D)$ with water dimers. *J. Chem. Phys.*, (1995), **102**, 1941-1943.

7. Bibliography

Aloisio, S.,Francisco, J. S. Radical-water complexes in Earth's atmosphere. *Accounts Chem. Res.*, (2000), **33**, 825-830.

Altieri, K. E., Seitzinger, S. P., Carlton, A. G., Turpin, B. J., Klein, G. C.,Marshall, A. G. Oligomers formed through in-cloud methylglyoxal reactions: Chemical composition, properties, and mechanisms investigated by ultra-high resolution FT-ICR mass spectrometry. *Atmos. Environ.*, (2008), **42**, 1476-1490.

Anglada, J. M.,Gonzalez, J. Different Catalytic Effects of a Single Water Molecule: The Gas-Phase Reaction of Formic Acid with Hydroxyl Radical in Water Vapor. *ChemPhysChem*, (2009), **10**, 3034-3045.

Axson, J. L., Takahashi, K., De Haan, D. O.,Vaida, V. Gas-phase water-mediated equilibrium between methylglyoxal and its geminal diol. *Proc Natl Acad Sci USA*, (2010), **107**, 6687-6692.

Axson, J. L., Washenfelder, R. A., Young, C. J., Kahan, T. F., Vaida, V.,Brown, S. S. Absolute ozone absorption cross section in the Huggins and Chappuis minimum (350-450 nm) at 296 K. *Atmos. Chem. Phys.*, (2011), **11**, 1-10.

Back, R. A., Yamamoto, S. The gas-phase photochemistry and thermal-decomposition of glyoxylic acid. *Can. J. Chem.-Rev. Can. Chim.*, (1985), **63**, 542-548.

Bahou, M., Schriver-Mazzuoli, L.,Schriver, A. Infrared spectroscopy and photochemistry at 266 nm of the ozone dimer trapped in an argon matrix. *J. Chem. Phys.*, (2001), **114**, 4045-4052.

Bakri, B., Demaison, J., Margules, L.,Mollendal, H. The submillimeter-wave spectrum and quantum chemical calculations of glyoxylic acid. *J. Mol. Spectrosc.*, (2001), **208**, 92-100.

Balci, M. *Basic ^{1}H and ^{13}C-NMR Spectroscopy*; Elsevier, Inc.: Amsterdam, Netherlands, 2005.

Bao, L., Matsumoto, M., Kubota, T., Kazuhiko, S., Wang, Q.,Sakamoto, K. Gas/particle partioning of low-molecular-weight diacarboxylic acids at the suburban site in Saitama, Japan. *Atmos. Environ.*, (2009).

Barone, V. Anharmonic vibrational properties by a fully automated second-order perturbative approach. *J. Chem. Phys.*, (2005), **122**, 10.

Becke, A. D. Density-functional thermochemistry. 3. The role of exact exchange *J. Chem. Phys.*, (1993), **98**, 5648-5652.

Begashaw, I., Fiddler, M. N., Bililign, S.,Brown, S. S. Measurement of the Fourth O-H Overtone Absorption Cross Section in Acetic Acid Using Cavity Ring-Down Spectroscopy. *J. Phys. Chem. A*, (2011), **115**, 753-761.

Bell, R. P., Rand, M. H.,Wynnejones, K. M. A. Kinetics of the hydration of acetaldehyde. *Transactions of the Faraday Society,* (1956), **52**, 1093-1102.

Betterton, E. A.,Hoffmann, M. R. Kinetics, mechanism, and thermodynamics of the reversable-reaction of methylglyoxal (CH_3COCHO) with S(IV). *J. Phys. Chem.,* (1987), **91**, 3011-3020.

Bock, C. W., Redington, R. L. Isomerization and unimolecular dissociation channels of the glyoxylic acid monomer. *J. Phys. Chem.,* (1988), **92**, 1178-1187.

Bodhaine, B. A., Wood, N. B., Dutton, E. G.,Slusser, J. R. On Rayleigh optical depth calculations. *J. Atmos. Ocean. Technol.,* (1999), **16**, 1854-1861.

Bogumil, K., Orphal, J., Homann, T., Voigt, S., Spietz, P., Fleischmann, O. C., Vogel, A., Hartmann, M., Kromminga, H., Bovensmann, H., Frerick, J.,Burrows, J. P. Measurements of molecular absorption spectra with the SCIAMACHY pre-flight model: Instrument characterization and reference data for atmospheric remote-sensing in the 230-2380 nm region. *J. Photochem. Photobiol. A-Chem.,* (2003), **157**, 167-184

Brasseur, G.,Solomon, S. Aeronomy of the Middle Atmosphere. *2nd ed.,* (1997), D. Reidel.

Brion, J., Chakir, A., Daumont, D., Malicet, J.,Parisse, C. High-resolution laboratory absorption cross-section of O_3 - Temperature effect. *Chem. Phys. Lett.,* (1993), **213**, 610-612.

Brion, J., Chakir, A., Charbonnier, J., Daumont, D., Parisse, C.,Malicet, J. Absorption spectra measurements for the ozone molecule in the 350-830 nm region. *J. Atmos. Chem.,* (1998), **30**, 291-299.

Brown, S. S., Wilson, R. W.,Ravishankara, A. R. Absolute intensities for third and fourth overtone absorptions in HNO_3 and H_2O_2 measured by cavity ring down spectroscopy. *J. Phys. Chem. A,* (2000), **104**, 4976-4983.

Brown, S. S., Stark, H.,Ravishankara, A. R. Cavity ring-down spectroscopy for atmopheric trace gas detection: application to the nitrate radical (NO_3). *Applied Physics B: Lasers and Optics,* (2002), **75**, 173-182.

Brown, S. S. Absorption spectroscopy in high-finesse cavities for atmospheric studies. *Chem. Rev.,* (2003), **103**, 5219-5238.

Burkholder, J. B. and Talukdar, R. K. Temperature-dependence of the ozone absorption-spectrum over the wavelength range 410 to 760 nm. *Geophys. Res. Lett.,* (1994), **21**, 581-584.

Burrows, J. P., Richter, A., Dehn, A., Deters, B., Himmelmann, S.,Orphal, J. Atmospheric remote-sensing reference data from GOME - Part 2. Temperature-dependent absorption cross sections of O_3 in the 231-794 nm range. *J. Quant. Spectrosc. Radiat. Transf.,* (1999), **61**, 509-517.

Burrows, J. P., Weber, M., Buchwitz, M., Rozanov, V., Ladstatter-Weissenmayer, A., Richter, A., DeBeek, R., Hoogen, R., Bramstedt, K., Eichmann, K. U.,Eisinger, M. The global ozone monitoring experiment (GOME): Mission concept and first scientific results. *Journal of the Atmospheric Sciences,* (1999), **56**, 151-175.

Buschmann, H. J., Dutkiewicz, E.,Knoche, W. The reversable hydration of carbonyl-compounds in aqueous-solution.2. The kinetics of the keto gem-diol transition. *Ber. Bunsen-Ges. Phys. Chem. Chem. Phys.*, (1982), **86**, 129-134.

Busch, K. W.,Busch, M. A. *Cavity-Ringdown Spectroscopy: An Ultratrace-Absorption Measurement Technique*; American Chemical Society: Washington D.C., 1999.

Carlton, A. G., Turpin, B. J., Altieri, K. E., Seitzinger, S., Reff, A., Lim, H. J.,Ervens, B. Atmospheric oxalic acid and SOA production from glyoxal: Results of aqueous photooxidation experiments. *Atmos. Environ.*, (2007), **41**, 7588-7602.

Chen, C., Shyu, S. F. Theoretical study of glyoxylic and pyruvic acids: rotamers and intramolecular hydrogen bonding. *Journal of Molecular Structure-Theochem*, (2000), **503**, 201-211.

Chen, I.-C., Chen, A. F., Huang, W.-T., Takahashi, K.,Lin, J. J. Photolysis cross section of ozone dimer. *Chem Asian J.*, (2011, doi.10.1002/asia.201100526.

Chen, J.,Venables, D. S. A broadband optical cavity spectrometer for measureing weak near-ultraviolet absorption spectra of gases. *Atmos. Meas. Tech. ,* (2011), **4**, 425-436.

Chen, Y. Q., Wang, W. J.,Zhu, L. Wavelength-dependent photolysis of methylglyoxal in the 290-440 nm region. *J. Phys. Chem. A*, (2000), **104**, 11126-11131.

Ciddor, P. E. Refractive index of air: New equations for the visible and near infrared. *Applied Optics*, (1996), **35**, 1566-1573.

Clark, T., Chandrasekhar, J., Spitznagel, G. W.,Schleyer, P. V. Efficient diffuse function-augmented basis-sets for anion calculations. 3. The 3-21+G basis set for 1st-row elements, LI-F. *J. Comput. Chem.*, (1983), **4**, 294-301

Cooper, A. J. L., Redfield, A. G. Proton magnetic resonance studies of alpha-keto acids. *J. Biol. Chem.*, (1975), **250**, 527-532

Coveleskie, R. A.,Yardley, J. T. Luminescence and Simplified Photophysicys of Methylglyoxal. *J. Am. Chem. Soc.*, (1974), **97**, 1667-1672.

De Gouw, J. A., Middlebrook, A. M., Warneke, C., Goldan, P. D., Kuster, W. C., Roberts, J. M., Fehsenfeld, F. C., Worsnop, D. R., Canagaratna, M. R., Pszenny, A. A. P., Keene, W. C., Marchewka, M., Bertman, S. B.,Bates, T. S. Budget of organic carbon in a polluted atmosphere: Results from the New England Air Quality Study in 2002. *J. Geophys. Res.-Atmos.*, (2005), **110**, 22.

De Gouw, J.,Jimenez, J. L. Organic aerosols in the Earth's atmosphere. *Environ. Sci. Technol.*, (2009), **43**, 7614-7618.

De Haan, D. O., Corrigan, A. L., Tolbert, M. A., Jimenez, J. L., Wood, S. E.,Turley, J. J. Secondary Organic Aerosol Formation by Self-Reactions of Methylglyoxal and Glyoxal in Evaporating Droplets. *Environ. Sci. Technol.*, (2009), **43**, 8184-8190.

Dlugokencky, E. J.,Ravishankara, A. R. Laboratory measurements of direct ozone loss on ice and doped-ice surfaces. *Geophys. Res. Lett.*, (1992), **19**, 41-44.

Donaldson, D. J., Tuck, A. F.,Vaida, V. Atmospheric photochemistry via vibrational overtone absorption. *Chem. Rev.*, (2003), **103**, 4717-4729.

Dube, W. P., Brown, S. S., Osthoff, H. D., Nunley, M. R., Ciciora, S. J., Paris, M. W., McLaughlin, R. J.,Ravishankara, A. R. Aircraft instrument for simultaneous, in situ measurement of NO_3 and N_2O_5 via pulsed cavity ring-down spectroscopy. *Rev. Sci. Instrum.*, (2006), **77**.

Dunn, M. E., Shields, G. C., Takahashi, K., Skodje, R. T., Vaida, V. Experimental and theoretical study of the OH vibrational spectra and overtone chemistry of gas-phase vinylacetic acid. *J. Phys. Chem. A*, (2008), **112**, 10226-10235.

Eliason, T. L., Havey, D. K.,Vaida, V. Gas phase infrared spectroscopic observation of the organic acid dimers $(CH_3(CH_2)(6)COOH)(2)$, $(CH_3(CH_2)(7)COOH)(2)$, and $(CH_3(CH_2)(8)COOH)(2)$. *Chem. Phys. Lett.*, (2005), **402**, 239-244.

Ervens, B., Gligorovski, S., Herrmann, H. Temperature-dependent rate constants for hydroxyl radical reactions with organic compounds in aqueous solutions. *Phys. Chem. Chem. Phys.*, (2003), **5**, 1811-1824.

Ervens, B., Feingold, G., Frost, G. J., Kreidenweis, S. M. A modeling study of aqueous production of dicarboxylic acids: 1. Chemical pathways and speciated organic mass production. *J. Geophys. Res.-Atmos.*, (2004), **109**, 20.

Ervens, B., Kreidenweis, S. M. SOA formation by biogenic and carbonyl compounds: Data evaluation and application. *Environ. Sci. Technol.*, (2007), **41**, 3904-3910.

Ervens, B., Carlton, A. G., Turpin, B. J., Altieri, K. E., Kreidenweis, S. M., Feingold, G. Secondary organic aerosol yields from cloud-processing of isoprene oxidation products. *Geophys. Res. Lett.*, (2008), **35**, 5.

Ervens, B., Turpin, B. J.,Weber, R. J. Secondary organic aerosol formation in cloud droplets and aqueous particles (aqSOA): a review of laboratory, field and model studies. *Atmos. Chem. Phys.*, (2011), **11**, 11069-11102.

Fast, J., Aiken, A. C., Allan, J., Alexander, L., Campos, T., Canagaratna, M. R., Chapman, E., DeCarlo, P. F., de Foy, B., Gaffney, J., de Gouw, J., Doran, J. C., Emmons, L., Hodzic, A., Herndon, S. C., Huey, G., Jayne, J. T., Jimenez, J. L., Kleinman, L., Kuster, W., Marley, N., Russell, L., Ochoa, C., Onasch, T. B., Pekour, M., Song, C., Ulbrich, I. M., Warneke, C., Welsh-Bon, D., Wiedinmyer, C., Worsnop, D. R., Yu, X. Y.,Zaveri, R. Evaluating simulated primary anthropogenic and biomass burning organic aerosols during MILAGRO: Implications for assessing treatments of secondary organic aerosols. *Atmos. Chem. Phys.*, (2009), **9**, 6191-6215.

Faust, B. C., Powell, K., Rao, C. J.,Anastasio, C. Aqueous-phase photolysis of biacetyl (an alpha-dicarbonyl compound): A sink for biacetyl, and a source of acetic acid, peroxyacetic acid, hydrogen peroxide, and the highly oxidizing acetylperoxyl radical in aqueous aerosols, fogs, and clouds. *Atmos. Environ.*, (1997), **31**, 497-510.

Feierabend, K. J., Havey, D. K., Brown, S. S.,Vaida, V. Experimental absolute intensities of the 4v(9) and 5v(9) O-H stretching overtones of H_2SO_4. *Chem. Phys. Lett.*, (2006), **420**, 438-442.

Fiedler, S. E., Hese, A.,Ruth, A. A. Incoherent broad-band cavity-enhanced absorption spectroscopy. *Chem. Phys. Lett.*, (2003), **371**, 284-294.

Finlayson-Pitts, B. J.,Pitts, J. N. *Chemistry of the Upper and Lower Atmosphere: Theory, Experiments, and Applications*; Academic Press, 2000.

Finlayson-Pitts, B. J. Reactions at surfaces in the atmosphere: integration of experiments and theory as necessary (but not necessarily sufficient) for predicting the physical chemistry of aerosols. *Phys. Chem. Chem. Phys.*, (2009), **11**, 7760-7779.

Fleury, G., Tabacik, V. Glyoxylic acid - Asymmetry of free molecule vibration spectra and attribution. *J. Mol. Struct.*, (1971), **10**, 359.

Francisco, J. S.,Williams, I. H. Reaction pathways for gas-phase hydrolysis of formyl compounds HXCO (X = H, F, and CL). *J. Am. Chem. Soc.*, (1993), **115**, 3746-3751.

Freytes, M., Hurtmans, D., Kassi, S., Lievin, J., Auwera, J. V., Campargue, A.,Herman, M. Overtone spectroscopy of formic acid. *Chem. Phys.*, (2002), **283**, 47-61.

Frisch, M. J., Pople, J. A., Binkley, J. S. Self-consistent molecular-orbital methods. 25. Supplementary functions for gaussian-basis sets. *J. Chem. Phys.*, (1984), **80**, 3265-3269

Frisch, M. J., G.W. Trucks, H.B. Schlegel, G.E. Scuseria, M.A. Robb, J.R. Cheeseman, J.A. Montgomery, T. Vreven, K.N. Kudin, J.C. Burant, J.M. Millam, S.S. Iyengar, ,J.Tomasi, V. B., B. Mennucci, M. Cossi, G. Scalmani, N. Rega, G.A. Petersson, H. Nakatsuji, M. Hada, M. Ehara, K. Toyota, R. Fukuda, J. Hasegawa, M. Ishida, T. Nakajima, Y. Honda, O. Kitao, H. Nakai, M. Klene, X. Li, J.E. Knox, H.P. Hratchian, J.B. Cross, V. Bakken, C. Adamo, J. Jaramillo, R. Gomperts, R.E. Stratmann, O. Yazyev, A.J. Austin, R. Cammi, C. Pomelli, J.W. Ochterski, P.Y. Ayala, K. Morokuma, G.A. Voth, P. Salvador, J.J. Dannenberg, V.G. Zakrzewski, S. Dapprich, A.D. Daniels, M.C. Strain, O.Farkas, D.K. Malick, A.D. Rabuck, K. Raghavachari, J.B. Foresman, J.V. Ortiz, Q. Cui, A.G. Baboul, S. Clifford, J. Cioslowski, B.B. Stefanov, G. Liu, A. Liashenko, P. Piskorz, I. Komaromi, R.L. Martin, D.J. Fox, T. Keith, M.A. Al-Laham, C.Y. Peng, A. Nanayakkara, M. Challacombe, P.M.W. Gill, B. Johnson, W. Chen, M.W. Wong, C. Gonzalez, J.A. Pople, *Gaussian03*, C.02 ed.; Gaussian Inc.: Wallingford, CT, 2004.

Frost, G. J.,Vaida, V. Atmospheric implications of the photolysis of the ozone-water weakly bound complex. *J. Geophys. Res.-Atmos.*, (1995), **100**, 18803-18809.

Fu, T. M., Jacob, D. J., Wittrock, F., Burrows, J. P., Vrekoussis, M.,Henze, D. K. Global budgets of atmospheric glyoxal and methylglyoxal, and implications for formation of secondary organic aerosols. *J. Geophys. Res.-Atmos.*, (2008), **113**, 17.

Fuchs, H., Dube, W. P., Lerner, B. M., Wagner, N. L., Williams, E. J.,Brown, S. S. A sensitive and versatile detector for atmospheric NO_2 and NO_x based on blue diode laser cavity ring-down spectroscopy. *Environ. Sci. Technol.*, (2009), **43**, 7831-7836.

George, P., Bock, C. W., Trachtman, M. An ab initio study of the geometry and energy of the 4 planar conformers of glyoxylic acid and the glyoxylate ion. *Theochem-J. Mol. Struct.*, (1982), **4**, 1-18.

Gherman, T., Venables, D. S., Vaughan, S., Orphal, J.,Ruth, A. A. Incoherent broadband cavity-enhanced absorption spectroscopy in the near-ultraviolet: Application to HONO and NO_2. *Environ. Sci. Technol.*, (2008), **42**, 890-895.

Gillies, J. Z., Gillies, C. W., Suenram, R. D., Lovas, F. J., Schmidt, T.,Cremer, D. A microwave spectral and abinitio investigation of O_3-H_2O. *J. Mol. Spectrosc.*, (1991), **146**, 493-512.

Gratien, A., Picquet-Varrault, B., Orphal, J., Doussin, J. F.,Flaud, J. M. New Laboratory Intercomparison of the Ozone Absorption Coefficients in the Mid-infrared (10 mu m) and Ultraviolet (300-350 nm) Spectral Regions. *J. Phys. Chem. A,* (2010), **114**, 10045-10048.

Greenblatt, G. D., Orlando, J. J., Burkholder, J. B.,Ravishankara, A. R. Absorption-measurements of oxygen between 330 nm and 1140 nm. *J. Geophys. Res.-Atmos.*, (1990), **95**, 18577-18582.

Greenzai.P, Luz, Z.,Samuel, D. A nuclear magnetic resonance study of reversible hydration of aliphatic aldehydes and ketones I. Oxygen-17 and Proton spectra and equilibrium constants. *J. Am. Chem. Soc.*, (1967), **89**, 749-&.

Griffiths, P. R.,J.A., D. *Fourier Transform Infrared Spectroscopy*, 2nd ed.; John Wiley and Sons, Inc: New Jersey, 2007.

Grosjean, D., Williams, E. L.,Grosjean, E. Atmospheric chemistry of isoprene and of its carbonyl products. *Environ. Sci. Technol.*, (1993), **27**, 830-840.

Gurnick, M., Chaiken, J., Benson, T.,McDonald, J. D. Vibrational and rotational spectroscopy of the 1st electronically allowed transition of alpha-dicarbonyls. *J. Chem. Phys.*, (1981), **74**, 99-105.

Hallquist, M., Wenger, J. C., Baltensperger, U., Rudich, Y., Simpson, D., Claeys, M., Dommen, J., Donahue, N. M., George, C., Goldstein, A. H., Hamilton, J. F., Herrmann, H., Hoffmann, T., Iinuma, Y., Jang, M., Jenkin, M. E., Jimenez, J. L., Kiendler-Scharr, A., Maenhaut, W., McFiggans, G., Mentel, T. F., Monod, A., Prevot, A. S. H., Seinfeld, J. H., Surratt, J. D., Szmigielski, R.,Wildt, J. The formation, properties and impact of secondary organic aerosol: current and emerging issues. *Atmos. Chem. Phys.*, (2009), **9**, 5155-5236.

Havey, D. K., Feierabend, K. J.,Vaida, V. Vapor-phase vibrational spectrum of glycolic acid, $CH_2OHCOOH$, in the region 2000-8500 cm^{-1}. *J. Phys. Chem. A,* (2004), **108**, 9069-9073.

Havey, D. K., Feierabend, K. J., Takahashi, K., Skodje, R. T.,Vaida, V. Experimental and theoretical investigation of vibrational overtones of glycolic acid and its hydrogen bonding interactions with water. *J. Phys. Chem. A*, (2006), **110**, 6439-6446.

Heald, C. L., Jacob, D. J., Park, R. J., Russell, L. M., Huebert, B. J., Seinfeld, J. H., Liao, H.,Weber, R. J. A large organic aerosol source in the free troposphere missing from current models. *Geophys. Res. Lett.*, (2005), **32**, L18809.

Hennigan, C. J., Bergin, M. H., Dibb, J. E.,Weber, R. J. Enhanced secondary organic aerosol formation due to water uptake by fine particles. *Geophys. Res. Lett.*, (2008), **35**.

Hollenstein, H., Ha, T. K., Gunthard, H. H. IR induced conversion of rotamers, matrix spectra, ab initio calculations of conformers, assignment, and valent force-field of trans glycolic acid. *J. Mol. Struct.*, (1986), **146**, 289-307.

Horowitz, A., Meller, R.,Moortgat, G. K. The UV-VIS absorption cross sections of the α-dicarbonyl compounds: pyruvic acid, biacetyl and glyoxal. *J. Photochem. Photobiol. A: Chem.*, (2001), **146**, 19-27.

Howard, D. L.,Kjaergaard, H. G. Resonance coupling in the fourth OH-stretching overtone spectrum of formic acid. *J. Chem. Phys.*, (2004), **121**, 136-140.

Howard, D. L., Jorgensen, P., Kjaergaard, H. G. Weak intramolecular interactions in ethylene glycol identified by vapor phase OH-stretching overtone spectroscopy. *J. Am. Chem. Soc.*, (2005), **127**, 17096-17103.

Howard, D. L., Kjaergaard, H. G. Influence of intramolecular hydrogen bond strength on OH-stretching overtones. *J. Phys. Chem. A*, (2006), **110**, 10245-10250.

Hsieh, Y. H., Weinberg, N., Yang, K., Kim, C. K., Shi, Z.,Wolfe, S. Hydration of the carbonyl group - Acetic acid catalysis in the co-operative mechanism. *Can. J. Chem.-Rev. Can. Chim.*, (2005), **83**, 769-785.

Hurwitz, Y.,Naaman, R. Production of OH by dissociating ozone water complexes at 266 nm and 355 nm and by reacting $O(^1D)$ with water dimers. *J. Chem. Phys.*, (1995), **102**, 1941-1943.

Jaeger, K. Ph.D. Thesis. *University of Bremen,* (1991), 111 – 136.

Jang, M. S.,Kamens, R. M. Characterization of secondary aerosol from the photooxidation of toluene in the presence of NO_x and 1-propene. *Environ. Sci. Technol.*, (2001), **35**, 3626-3639.

Jimenez, J. L., Canagaratna, M. R., Donahue, N. M., Prevot, A. S. H., Zhang, Q., Kroll, J. H., DeCarlo, P. F., Allan, J. D., Coe, H., Ng, N. L., Aiken, A. C., Docherty, K. S., Ulbrich, I. M., Grieshop, A. P., Robinson, A. L., Duplissy, J., Smith, J. D., Wilson, K. R., Lanz, V. A., Hueglin, C., Sun, Y. L., Tian, J., Laaksonen, A., Raatikainen, T., Rautiainen, J., Vaattovaara, P., Ehn, M., Kulmala, M., Tomlinson, J. M., Collins, D. R., Cubison, M. J., Dunlea, E. J., Huffman, J. A., Onasch, T. B., Alfarra, M. R., Williams, P. I., Bower, K., Kondo, Y., Schneider, J., Drewnick, F., Borrmann, S., Weimer, S., Demerjian, K., Salcedo, D., Cottrell, L., Griffin, R., Takami, A., Miyoshi, T., Hatakeyama, S., Shimono, A., Sun, J. Y., Zhang, Y. M., Dzepina, K., Kimmel, J. R., Sueper, D., Jayne, J. T., Herndon, S. C., Trimborn, A. M., Williams, L. R., Wood, E. C., Middlebrook, A. M., Kolb, C. E., Baltensperger, U.,Worsnop, D. R. Evolution of Organic Aerosols in the Atmosphere. *Science,* (2009), **326**, 1525-1529.

Kanakidou, M., Seinfeld, J. H., Pandis, S. N., Barnes, I., Dentener, F. J., Facchini, M. C., Van Dingenen, R., Ervens, B., Nenes, A., Nielsen, C. J., Swietlicki, E., Putaud, J. P., Balkanski, Y., Fuzzi, S., Horth, J., Moortgat, G. K., Winterhalter, R., Myhre, C. E. L., Tsigaridis, K., Vignati, E., Stephanou, E. G.,Wilson, J. Organic aerosol and global climate modelling: a review. *Atmos. Chem. Phys.*, (2005), **5**, 1053-1123.

Kawamura, K., Kasukabe, H.,Barrie, L. A. Source and reaction pathways of dicarboxylic acids, ketoacids and dicarbonyls in arctic aerosols: One year of observations. *Atmos. Environ.*, (1996), **30**, 1709-1722.

Kawamura, K.,Yasui, O. Diurnal changes in the distribution of dicarboxylic acids, ketocarboxylic acids and dicarbonyls in the urban Tokyo atmosphere. *Atmos. Environ.,* (2005), **39**, 1945-1960.

Keller-Rudek H.,Moortgat, G. K. MPI-Mainz-UV-VIS Spectral Atlas of Gaseous Molecules. (www.atmosphere.mpg.de/spectral-atlas-mainz.

Kent, D. R., Widicus, S. L., Blake, G. A., Goddard, W. A. A theoretical study of the conversion of gas phase methanediol to formaldehyde. *J. Chem. Phys.,* (2003), **119**, 5117-5120.

King, D. S., Sauder, D. G.,Casassa, M. P. Cluster effects in O_3/H_2O Photochemistry: Dynamics of the $O+H_2O \rightarrow 2OH$ reaction photoinitiated in the O3•H2O dimer. *J. Chem. Phys.,* (1994), **100**, 4200-4210.

Kjaergaard, H. G., Henry, B. R.,Tarr, A. W. Intensities in local mode overtone spectra of dimethyl ether and acetone. *J. Chem. Phys.,* (1991), **94**, 5844-5854.

Krishnan, R., Binkley, J. S., Seeger, R.,Pople, J. A. Self-consistent molecular-orbital methods. 20. Basis set for correlated wave-functions. *J. Chem. Phys.,* (1980), **72**, 650-654.

Krizner, H. E., De Haan, D. O.,Kua, J. Thermodynamics and kinetics of methylglyoxal dimer formation: A computational study. *J. Phys. Chem. A,* (2009), **113**, 6994-7001

Kroon, M., de Haan, J. F., Veefkind, J. P., Froidevaux, L., Wang, R., Kivi, R.,Hakkarainen, J. J. Validation of operational ozone profiles from the Ozone Monitoring Instrument. *J. Geophys. Res.-Atmos.,* (2011), **116**, D18305.

Lange, K. R., Wells, N. P., Plegge, K. S.,Phillips, J. A. Integrated intensities of O-H stretching bands: Fundamentals and overtones in vapor-phase alcohols and acids. *J. Phys. Chem. A,* (2001), **105**, 3481-3486.

Langenberg, S.,Schurath, U. Ozone destruction on ice. *Geophys. Res. Lett.,* (1999), **26**, 1695-1698.

Lane, J. R., Kjaergaard, H. G., Plath, K. L.,Vaida, V. Overtone spectroscopy of sulfonic acid derivatives. *J. Phys. Chem. A,* (2007), **111**, 5434-5440.

Langridge, J. M., Ball, S. M.,Jones, R. L. A compact broadband cavity enhanced absorption spectrometer for detection of atmospheric NO_2 using light emitting diodes. *Analyst,* (2006), **131**, 916-922.

Langridge, J. M., Ball, S. M., Shillings, A. J. L.,Jones, R. L. A broadband absorption spectrometer using light emitting diodes for ultrasensitive, in situ trace gas detection. *Rev. Sci. Instrum.,* (2008), **79**, 123110.

Lee, C. T., Yang, W. T.,Parr, R. G. Development of the Colle-Salvetti correlation-energy formula into a functional of the electron-density. *Phys. Rev. B,* (1988), **37**, 785-789.

Leu, M. T. Heterogeneous reactions of N_2O_5 with H_2O and HCL on ice surfaces - inplicatiosn for antartic ozone depletion. *Geophys. Res. Lett.,* (1988), **15**, 851-854.

Limbeck, A., Puxbaum, H., Otter, L., Scholes, M. C. Semivolatile behavior of dicarboxylic acids and other polar organic species at a rural background site (Nylsvley, RSA). *Atmos. Environ.*, (2001), **35**, 1853-1862.

Loeffler, K. W., Koehler, C. A., Paul, N. M.,De Haan, D. O. Oligomer formation in evaporating aqueous glyoxal and methylglyoxal solutions. *Environ. Sci. Technol.*, (2006), **40**, 6318-6323.

Macomber, R. S. *A Complete Introduction to Modern NMR Spectroscopy*; John Wiley & Sons, Inc.: New York, 1998.

Malik, M.,Joens, J. A. Temperature dependent near-UV molar absorptivities of glyoxal and gluteraldehyde in aqueous solution. *Spectrochimica Acta Part A*, (2000), **56**, 2653-2658.

Maron, M. K., Takahashi, K., Shoemaker, R. K.,Vaida, V. Hydration of pyruvic acid to its geminal-diol, 2,2-dihydroxypropanoic acid, in a water-restricted environment. *Chem. Phys. Lett.*, (2011), **513**, 184-190.

Marstokk, K. M. and Mollenda, H. Microwave spectrum, conformation, dipole moment and centrifugal distortion of glyoxylic acid. *J. Mol. Struct.*, (1973), **15**, 137-150.

Matsunaga, S., Mochida, M.,Kawamura, K. Variation on the atmospheric concentrations of biogenic carbonyl compounds and their removal processes in the northern forest at Moshiri, Hokkaido Island in Japan. *J. Geophys. Res.-Atmos.*, (2004), **109**, 9.

Matthews, J., Sinha, A.,Francisco, J. S. The importance of weak absorption features in promoting tropospheric radical production. *Proc. Natl. Acad. Sci. U. S. A.*, (2005), **102**, 7449-7452.

McLean, A. D.,Chandler, G. S. Contracted Gaussian-basis sets for molecular calculations.1. 2nd row atoms, Z=11-18. *J. Chem. Phys.*, (1980), **72**, 5639-5648.

Meller, R., Raber, W., Crowley, J. N., Jenkin, M. E.,Moortgat, G. K. The UV-visible absorption-spectrum of methylglyoxal. *J. Photochem. Photobiol. A-Chem.*, (1991), **62**, 163-171.

Miller, B. J., Kjaergaard, H. G., Hattori, K., Ishiuchi, S.,Fujii, M. The most stable conformer of benzyl alcohol. *Chem. Phys. Lett.*, (2008), **466**, 21-26.

Mills, M. J., Toon, O. B., Vaida, V., Hintze, P. E., Kjaergaard, H. G., Schofield, D. P.,Robinson, T. W. Photolysis of sulfuric acid vapor by visible light as a source of the polar stratospheric CN layer. *J. Geophys. Res.-Atmos.*, (2005), **110**, 7.

Mugnai, M., Cardini, G., Schettino, V., Nielsen, C. J. Ab initio molecular dynamics study of aqueous formaldehyde and methanediol. *Mol. Phys.*, (2007), **105**, 2203-2210.

Murphy, D. M., Cziczo, D. J., Froyd, K. D., Hudson, P. K., Matthew, B. M., Middlebrook, A. M., Peltier, R. E., Sullivan, A., Thomson, D. S.,Weber, R. J. Single-particle mass spectrometry of tropospheric aerosol particles. *J. Geophys. Res.-Atmos.*, (2006), **111**, 15.

Naus, H.,Ubachs, W. Experimental verification of Rayleigh scattering cross sections. *Opt. Lett.*, (2000), **25**, 347-349.

Nemet, I., Vikic-Topic, D.,Varga-Defterdarovic, L. Spectroscopic studies of methylglyoxal in water and dimethylsulfoxide. *Bioorganic Chem.,* (2004), **32**, 560-570.

Orphal, J. A critical review of the absorption cross-sections of O_3 and NO_2 in the ultraviolet and visible. *J. Photochem. Photobiol. A-Chem.,* (2003), **157**, 185-209.

Petropavlovskikh, I., Evans, R., Mcconville, G., Oltmans, S., Quincy, D., Lantz, K., Disterhoft, P., Stanek, M.,Flynn, L. Sensitifity of Dobson and Brewer Umkehr ozone profile retrievals to ozone cross-sections and stray light effects. *Atmos. Meas. Tech. Discuss,* (2011), **4**, 2007-2035.

Plath, K. L., Axson, J. L., Nelson, G. C., Takahashi, K., Skodje, R. T.,Vaida, V. Gas-phase vibrational spectra of glyoxylic acid and its gem diol monohydrate. Implications for atmospheric chemistry. *React. Kinet. Catal. Lett.,* (2009), **96**, 209-224.

Plath, K. L., Takahashi, K., Skodje, R. T.,Vaida, V. Fundamental and overtone vibrational spectra of gas-phase pyruvic acid. *J. Phys. Chem. A,* (2009), **113**, 7294-7303.

Plum, C. N., Sanhueza, E., Atkinson, R., Carter, W. P. L.,Pitts, J. N. OH radical rate constants and photolysi rates of alpha-dicarbonyls. *Environ. Sci. Technol.,* (1983), **17**, 479-484.

Probst, M., Hermansson, K., Urban, J., Mach, P., Muigg, D., Denifl, G., Fiegele, T., Mason, N. J., Stamatovic, A.,Mark, T. D. Ionization energy studies for ozone and OClO monomers and dimers. *J. Chem. Phys.,* (2002), **116**, 984-992.

Redington, R. L., Liang, C. K. J. Vibrational spectra of glyoxylic acid monomers. *J. Mol. Spectrosc.,* (1984), **104**, 25-39.

Rincon, A. G., Guzman, M. I., Hoffmann, M. R.,Colussi, A. J. Optical absorptivity versus molecular composition of model organic aerosol matter. *J. Phys. Chem. A,* (2009), **113**, 10512-10520.

Rontu, N., Vaida, V. Vibrational spectroscopy of perfluoroproplonic acid in the region between 1000 and 11000 cm^{-1}. *J. Mol. Spectrosc.,* (2006), **237**, 19-26.

Rontu, N., Vaida, V. Vibrational spectroscopy of perfluorocarboxylic acids from the infrared to the visible regions. *J. Phys. Chem. B,* (2008), **112**, 276-282.

Rodler, M. Ab inito studies of the structures and energies of methanediol and 1,1-ethenediol. *Chem. Phys.,* (1986), **105**, 345-353.

Rothman, L. S., Gordon, I. E., Barbe, A., Benner, D. C., Bernath, P. E., Birk, M., Boudon, V., Brown, L. R., Campargue, A., Champion, J. P., Chance, K., Coudert, L. H., Dana, V., Devi, V. M., Fally, S., Flaud, J. M., Gamache, R. R., Goldman, A., Jacquemart, D., Kleiner, I., Lacome, N., Lafferty, W. J., Mandin, J. Y., Massie, S. T., Mikhailenko, S. N., Miller, C. E., Moazzen-Ahmadi, N., Naumenko, O. V., Nikitin, A. V., Orphal, J., Perevalov, V. I., Perrin, A., Predoi-Cross, A., Rinsland, C. P., Rotger, M., Simeckova, M., Smith, M. A. H., Sung, K., Tashkun, S. A., Tennyson, J., Toth, R. A., Vandaele, A. C.,Vander Auwera, J. The HITRAN 2008 molecular spectroscopic database. *J. Quant. Spectrosc. Radiat. Transf.,* (2009), **110**, 533-572.

Rosado-Reyes, C. M., Francisco, J. S. Atmospheric oxidation pathways of acetic acid. *J. Phys. Chem. A,* (2006), **110**, 4419-4433.

Sander, S. P., Finlayson-Pitts, B. J., Friedl, B. J., Golden, D. M., Huie, R. E., Keller-Rudek, H., Kolb, C. E., Kurylo, M. J., Molina, M. J., Moortgat, G. K., Orkin, V. L., Ravishankara, A. R.,Wine, P. H. Chemical Kinetics and Photochemical Data for Use in Atmospheric Studies 06-2, Jet Propulson Laboratory, Pasadena. (2006.

Sansonetti, C. J., Salit, M. L.,Reader, J. Wavelengths of spectral lines in mercury pencil lamps. *Applied Optics,* (1996), **35**, 74-77.

Sareen, N., Schwier, A. N., Shapiro, E. L., Mitroo, D.,McNeill, V. F. Secondary organic material formed by methylglyoxal in aqueous aerosol mimics. *Atmos. Chem. Phys.*, (2010), **10**, 997-1016.

Scharge, T., Luckhaus, D., Suhm, M. A. Observation and quantification of the hydrogen bond effect on O-H overtone intensities in an alcohol dimer. *Chem. Phys.*, (2008), **346**, 167-175.

Schriver, L., Barreau, C.,Schriver, A. Infrared spectroscopic and photochemical study of water ozone complexes in solid argon. *Chem. Phys.*, (1990), **140**, 429-438.

Schriver, A., Schriver, L., Barreau, C., Carri re, D., Perchard, J. P., Jaeger, K.,Schrems, O. Ozone in the Atmosphere: Proceedings of the Quadrennial Ozone Symposium 1988 and Tropospheric Ozone Workshop. *A. Deepak Publishing*, (1989), 694– 697.

Scherer, J. J., Paul, J. B., Okeefe, A.,Saykally, R. J. Cavity ringdown laser absorption spectroscopy: History, development, and application to pulsed molecular beams. *Chem. Rev.*, (1997), **97**, 25-51.

Seinfeld, J. S.,Pandis, S. N. *Atmospheric Chemistry and Physics: From Air Pollution to Climate Change*, Second ed.; John Wiley & Sons, Inc., 2006.

Sennikov, P. G., Ignatov, S. K.,Schrems, O. Complexes and clusters of water relevant to atmospheric chemistry: H_2O complexes with oxidants. *ChemPhysChem*, (2005), **6**, 392-412.

Shi, Z., Hsieh, Y. H., Weinberg, N.,Wolfe, S. The neutral hydrolysis of methyl acetate - Part 2. Is there a tetrahedral intermediate? *Can. J. Chem.-Rev. Can. Chim.*, (2009), **87**, 544-555.

Slanina, Z.,Adamowicz, L. Computational studies of atmospheric chemistry species. 3. A computational study of the ozone dimer. *J. Atmos. Chem.*, (1993), **16**, 41-46.

Smith, B. C. *Fundamentals of Fourier Transform Infrared Spectroscopy*; CRC Press: New York, 1996.

Sneep, M.,Ubachs, W. Direct measurement of the Rayleigh scattering cross section in various gases. *J. Quant. Spectrosc. Radiat. Transf.*, (2005), **92**, 293-310.

Solomon, S., Qin, D., Manning, M., Chen, Z., Marquis, M., Averyt, K. B., Tignor, M.,Miller, H. L. e. *IPCC, 2007: Climate Change 2007: The Physical Science Basis. Contribution of Working Group I to the Fourth Assessment Report of the Intergovernmental Panel on Climate Change* Cambridge University Press: Cambridge, United Kingdom and New York, NY, USA, 2007.

Sorensen, P. E., Bruhn, K., Lindelov, F. Kinetics and equilibria for reversible hydration of aldehyde group in glyoxylic acid. *Acta Chemica Scandinavica Series a-Physical and Inorganic Chemistry*, (1974), **A 28**, 162-168.

Staffelbach, T. A., Orlando, J. J., Tyndall, G. S.,Calvert, J. G. The UV-visible absorption-spectrum and photolysis quantum yields of methylglyoxal *J. Geophys. Res.-Atmos.*, (1995), **100**, 14189-14198.

Takahashi, K., Plath, K. L., Skodje, R. T., Vaida, V. Dynamics of vibrational overtone excited pyruvic acid in the gas phase: Line broadening through hydrogen-atom chattering. *J. Phys. Chem. A*, (2008), **112**, 7321-7331.

Takahashi, K., Plath, K. L., Axson, J. L., Nelson, G. C., Skodje, R. T., Vaida, V. Dynamics and spectroscopy of vibrational overtone excited glyoxylic acid and 2,2-dihydroxyacetic acid in the gas-phase. *J. Chem. Phys.*, (2010), **132**, 1-10.

Tan, Y., Carlton, A. G., Seitzinger, S. P.,Turpin, B. J. SOA from methylglyoxal in clouds and wet aerosols: Measurement and prediction of key products. *Atmos. Environ.*, (2010), **44**, 5218-5226.

Tervahattu, H., Juhanoja, J.,Kupiainen, K. Identification of an organic coating on marine aerosol particles by TOF-SIMS. *J. Geophys. Res.-Atmos.*, (2002), **107**, 7.

Thalman, R.,Volkamer, R. Inherent calibration of a blue LED-CE-DOAS instrument to measure iodine oxide, glyoxal, methyl glyoxal, nitrogen dioxide, water vapour and aerosol extinction in open cavity mode. *Atmos. Meas. Tech.*, (2010), **3**, 1797-1814.

Tsuge, M., Tsuji, K., Kawai, A.,Shibuya, K. Infrared spectroscopy of ozone-water complex in a neon matrix. *J. Phys. Chem. A*, (2007), **111**, 3540-3547.

Tuazon, E. C., Macleod, H., Atkinson, R.,Carter, W. P. L. Alpha-dicarbonyl yields from the NO_X-air photooxidations of a aeries of aromatic-hydrocarbons in air. *Environ. Sci. Technol.*, (1986), **20**, 383-387.

Vaida, V., Donaldson, D. J., Strickler, S. J., Stephens, S. L.,Birks, J. W. A reinvestigation of the electronic-spectra of ozone condensed-phase effects. *J. Phys. Chem.*, (1989), **93**, 506-508.

Vaida, V.,Headrick, J. E. Physicochemical properties of hydrated complexes in the Earth's atmosphere. *J. Phys. Chem. A*, (2000), **104**, 5401-5412.

Vaida, V., Daniel, J. S., Kjaergaard, H. G., Goss, L. M.,Tuck, A. F. Atmospheric absorption of near infrared and visible solar radiation by the hydrogen bonded water dimer. *Q. J. R. Meteorol. Soc.*, (2001), **127**, 1627-1643.

Vaida, V., Kjaergaard, H. G., Hintze, P. E.,Donaldson, D. J. Photolysis of sulfuric acid vapor by visible solar radiation. *Science*, (2003), **299**, 1566-1568.

Vaida, V., Kjaergaard, H. G.,Feierabend, K. J. Hydrated complexes: Relevance to atmospheric chemistry and climate. *Int. Rev. Phys. Chem.*, (2003), **22**, 203-219.

Vaida, V., Feierabend, K. J., Rontu, N.,Takahashi, K. Sunlight-initiated photochemistry: Excited vibrational states of atmospheric chromophores. *Int. J. Photoenergy*, (2008), 1-13.

Vaida, V. Spectroscopy of photoreactive systems: Implications for atmospheric chemistry. *J. Phys. Chem. A,* (2009), **113**, 5-18.

Vaida, V. Perspective: Water cluster mediated atmospheric chemistry. *J. Chem. Phys.*, (2011), **135**, 1-8.

Vaneijck, B. P., Vanduijneveldt, F. B. Molecular structure and rotational isomerism in glyoxylic acid from microwave spectroscopy and ab inito calculations. *J. Mol. Struct.*, (1977), **39**, 157-163

Vaughan, S., Gherman, T., Ruth, A. A.,Orphal, J. Incoherent broad-band cavity-enhanced absorption spectroscopy of the marine boundary layer species I_2, IO and OIO. *Phys. Chem. Chem. Phys.*, (2008), **10**, 4471-4477.

Venables, D. S., Gherman, T., Orphal, J., Wenger, J. C.,Ruth, A. A. High sensitivity in situ monitoring of NO_3 in an atmospheric simulation chamber using incoherent broadband cavity-enhanced absorption spectroscopy. *Environ. Sci. Technol.*, (2006), **40**, 6758-6763.

Veres, P., Roberts, J. M., Warneke, C., Welsh-Bon, D., Zahniser, M., Herndon, S., Fall, R.,de Gouw, J. Development of negative-ion proton-transfer chemical-ionization mass spectrometry (NI-PT-CIMS) for the measurement of gas-phase organic acids in the atmosphere. *Int. J. Mass Spectrom.*, (2008), **274**, 48-55.

Vöhringer-Martinez, E., Hansmann, B., Hernandez, H., Francisco, J. S., Troe, J.,Abel, B. Water Catalysis of a Radical-Molecule Gas-Phase reaction. *Science*, (2011), **315**, 497-501.

Voigt, S., Orphal, J., Bogumil, K.,Burrows, J. P. The temperature dependence (203-293 K) of the absorption cross sections of O_3 in the 230-850 nm region measured by Fourier-transform spectroscopy. *J. Photochem. Photobiol. A-Chem.*, (2001), **143**, 1-9.

Volkamer, R., Spietz, P., Burrows, J. P.,Platt, U. High-resolution absorption cross-sections of glyoxal in the UV-vis and IR spectral ranges. *J. Photochem. Photobiol. A: Chem.* , (2005), **172**, 35-36.

Volkamer, R., Jimenez, J. L., San Martini, F., Dzepina, K., Zhang, Q., Salcedo, D., Molina, L. T., Worsnop, D. R.,Molina, M. J. Secondary organic aerosol formation from anthropogenic air pollution: Rapid and higher than expected. *Geophys. Res. Lett.*, (2006), **33**, 4.

Volkamer, R., Martini, F. S., Molina, L. T., Salcedo, D., Jimenez, J. L.,Molina, M. J. A missing sink for gas-phase glyoxal in Mexico City: Formation of secondary organic aerosol. *Geophys. Res. Lett.*, (2007), **34**, 5.

Volkamer, R., Ziemann, P. J.,Molina, M. J. Secondary organic aerosol formation from acetylene (C_2H_2): seed effect on SOA yields due to organic photochemistry in the aerosol aqueous phase. *Atmos. Chem. Phys.*, (2009), **9**, 1907-1928.

Warneck, P. In-cloud chemistry opens pathway to the formation of oxalic acid in the marine atmosphere. *Atmos. Environ.*, (2003), **37**, 2423-2427.

Warneck, P. Multi-phase chemistry of C-2 and C-3 organic compounds in the marine atmosphere. *J. Atmos. Chem.*, (2005), **51**, 119-159.

Waschewsky, G. C. G., Horansky, R.,Vaida, V. Effect of dimers on the temperature-dependent absorption cross section of methyl iodide. *J. Phys. Chem.*, (1996), **100**, 11559-11565.

Washenfelder, R. A., Langford, A. O., Fuchs, H.,Brown, S. S. Measurement of glyoxal using an incoherent broadband cavity enhanced absorption spectrometer. *Atmos. Chem. Phys.*, (2008), **8**, 7779-7793.

Washenfelder, R., Young, C.,Brown, S. S. A field instrument for NO_2, HONO, and CHOCHO using incoherent broadband cavity enhances absorption spectroscopy. *In preparation*.

Wheeler, M. D., Newman, S. M., Orr-Ewing, A. J.,Ashfold, M. N. R. Cavity ring-down spectroscopy. *J. Chem. Soc.-Faraday Trans.*, (1998), **94**, 337-351.

Williams, I. H., Spangler, D., Femec, D. A., Maggiora, G. M.,Schowen, R. L. Theoretical - Models for solvation and catalysis in carbonyl addition. *J. Am. Chem. Soc.*, (1983), **105**, 31-40.

Wolfe, S., Kim, C. K., Yang, K., Weinberg, N.,Shi, Z. Hydration of the carbonyl group - A theoretical-study of the cooperative mechanism. *J. Am. Chem. Soc.*, (1995), **117**, 4240-4260.

Yang, K., Hsieh, Y. H., Kim, C. K., Zhang, H.,Wolfe, S. Hydration of acetone in the gas phase and in water solvent. *Can. J. Chem.-Rev. Can. Chim.*, (2010), **88**, 56-64.

Yasmeen, F., Sauret, N., Gal, J. F., Maria, P. C., Massi, L., Maenhaut, W.,Claeys, M. Characterization of oligomers from methylglyoxal under dark conditions: a pathway to produce secondary organic aerosol through cloud processing during nighttime. *Atmos. Chem. Phys.*, (2010), **10**, 3803-3812.

Yoshida, H., Ehara, A., Matsuura, H. Density functional vibrational analysis using wavenumber-linear scale factors. *Chem. Phys. Lett.*, (2000), **325**, 477-483

Zalicki, P.,Zare, R. N. Cavity ring-down spectroscopy for quantitative absorption measurements. *J. Chem. Phys.*, (1994), **102 (7)**, 2708-2717.

Zhang, Q., Jimenez, J. L., Canagaratna, M. R., Allan, J. D., Coe, H., Ulbrich, I., Alfarra, M. R., Takami, A., Middlebrook, A. M., Sun, Y. L., Dzepina, K., Dunlea, E., Docherty, K., DeCarlo, P. F., Salcedo, D., Onasch, T., Jayne, J. T., Miyoshi, T., Shimono, A., Hatakeyama, S., Takegawa, N., Kondo, Y., Schneider, J., Drewnick, F., Borrmann, S., Weimer, S., Demerjian, K., Williams, P., Bower, K., Bahreini, R., Cottrell, L., Griffin, R. J., Rautiainen, J., Sun, J. Y., Zhang, Y. M.,Worsnop, D. R. Ubiquity and dominance of oxygenated species in organic aerosols in anthropogenically-influenced Northern Hemisphere midlatitudes. *Geophys. Res. Lett.*, (2007), **34**, L13801.

Zhou, S. M., Barnes, I., Zhu, T., Bejan, I., Albu, M.,Benter, T. Atmospheric chemistry of acetylacetone. *Environ. Sci. Technol.*, (2008), **42**, 7905-7910.

8. Appendix A: Gas-phase Vibrational Spectra of Glyoxylic Acid and Its Gem Diol Monohydrate: Implications for Atmospheric Chemistry

8.1 Introduction

Highly oxidized organic molecules, in particular aldehydes and ketones, have a unique and complex role in water uptake and aerosol formation in the atmosphere. These compounds are found in the highly oxidized material of secondary organic aerosols (SOA)[1-9]. Aldehydes, and to a lesser extent ketones, are known to form a gem diol in the presence of water[10,11]. The gem diol drastically changes the physical and chemical properties of the molecules, which impacts the partitioning between gas and particle phase as well as the chemistry of such molecules in the atmosphere. The conversion of glyoxylic acid to the diol form of glyoxylic acid gem diol, 2,2-dihydroxyacetic acid, is heavily influenced by the presence of water. Due to the gem diol's tendency to form strong intermolecular hydrogen bonds, it will partition predominantly to the condensed phase. The aldehyde form of glyoxylic acid also has the ability to form hydrogen bonds; however it has a much higher vapor pressure and is more likely to remain in the gas-phase than its diol analogue. Both glyoxylic acid and glyoxylic acid gem diol have several rotational conformers that are populated at temperatures less than 100 °C[12-14]. Using these two molecules and their many conformers the effects of inter- and intramolecular hydrogen-bonding are studied to understand the water mediated equilibrium between the aldehyde and diol forms of glyoxylic acid and its environmental implications[15,16].

Intramolecular hydrogen bonds can have a large impact on the physical and chemical properties of a molecule. One interesting case of intramolecular hydrogen bonding is that of geminal diols due to the increased strain imposed by the two alcohol groups on a single carbon. The gem diol is well-known in aqueous solution through NMR investigations, however it has not been observed in the gas-phase in any system[10,11,17]. The gem diol forms intermolecular hydrogen bonds consequently lowering the vapor pressure compared to the carbonyl analogues. The readiness of glyoxylic acid to form glyoxylic acid gem diol reduces the presence of glyoxylic acid in the gas phase. The reduction of glyoxylic acid the gas phase may explain the discrepancy between atmospheric model predictions of the abundance of aldehydes and ketones in the atmosphere and results of field measurements of such molecules[18]. In this work, the first recorded gas-phase infrared (IR) spectrum of a gem diol, glyoxylic acid gem diol, along with a reinvestigation of the IR spectrum of glyoxylic acid is presented. The experiments were conducted with Dr. Kathryn Plath and the theoretical calculations were provided by Prof. Rex Skodje, Dr. Kaito Takahashi, and Galen Nelson. Varying the experimental conditions allows for a better understanding of the gas-phase equilibrium of glyoxylic acid and glyoxylic acid gem diol. Intramolecular hydrogen bonds cause shifts in the vibrational modes, primarily in the OH stretching mode and carbonyl stretching mode. These shifts have a typical magnitude of <100 cm^{-1}. In contrast, intermolecular hydrogen bonds cause larger shifts (200 – 500 cm^{-1}) in the vibrational spectrum. By altering the experimental conditions it is also possible to probe the strength of the intermolecular hydrogen bonds, which provides insight into a molecule's tendency to form aggregates.

Glyoxylic acid has been studied as a simple difunctionalized organic compound. The microwave spectrum provided the geometry for glyoxylic acid[13,14]. A theoretical investigation of

the rotamers and intramolecular hydrogen bonding previously discussed its ability to form hydrogen bond[12]. Spectroscopically, glyoxylic acid was recorded in the IR in gas-phase and matrix environments, along with CCl_4 solutions[19-21]. The electronic state photochemical unimolecular reactions have been studied both theoretically and experimentally[12,22]. The glyoxylic acid gem diol has been recorded by NMR spectroscopy in the aqueous phase[23]. The rate constant for dehydration of aldehyde hydrates has been discussed, including the equilibrium between glyoxylic acid and glyoxylic acid gem diol in aqueous phase[24,25]. The work of Sorenson et. al. found that the equilibrium constant favors the glyoxylic acid gem diol over glyoxylic acid[25]. While gem diols have been observed in aqueous solutions, they have been postulated to exist in the gas-phase, but never observed. Due to their ability to form intermolecular hydrogen bonds the gem diols would have a low vapor pressure, yet by careful control of the experimental conditions the gem diol was observed in the gas-phase in this work.

Diols with alcohol groups on separate carbons are stable and their vibrational spectroscopy has been studied previously[26-28]. The spectroscopic work on diols provides an excellent opportunity to study the difference between intramolecular hydrogen bonded alcohol groups and free alcohol groups. Gem diols are expected to engage in intramolecular hydrogen bonding similar to other diols. If aldehydes and ketones form diols as readily in the atmosphere as has been seen in the laboratory, then the current treatment of these compounds in atmospheric models does not accurately describe their behavior. This may be the cause of the discrepancy between atmospheric field measurements of aldehydes and ketones and the values derived from atmospheric models[18].

8.2 Experimental

8.2.1 Sample preparation

Glyoxylic acid (HCOCOOH, 98%) was purchased from Sigma-Aldrich. It exists as the monohydrate due to its large hydrophilicity and was comprised almost completely of the diol form ($HC(OH)_2COOH$), 2,2-dihydroxyacetic acid. In order to increase the population of glyoxylic acid relative to glyoxylic acid gem diol the sample was processed and dried. The difficulty associated with this issue has been noted in nearly all experimental studies of glyoxylic acid[19-21,25,29,30]. Activated molecular sieves were added to the sample and sealed at ambient conditions for 5 – 7 days. The sample was attached to a vacuum line (~30 mTorr) and gently heated to 313 K for 12 – 48 hours. This method produced the cleanest sample of the aldehyde, though with any introduction of water the sample quickly formed the diol. Glyoxylic acid was assumed to have a higher vapor pressure than glyoxylic acid gem diol, making it easier to observe in the gas-phase. The vapor pressures for either molecule are not known values. Both forms existed throughout the experiment, but by changing the temperature, flow rate, and relative humidity there was some measure of control over the relative populations of either form. The relative populations were estimated using the peak intensities of transitions that were assigned to each substance. The aldehyde and diol forms were distinguishable by the difference in melting points. As an aldehyde, glyoxylic acid melts at ~318 K. The glyoxylic acid gem diol had a greater melting point at ~343 K. This melting point information suggests the glyoxylic acid gem diol's tendency to form intermolecular hydrogen bonds.

8.2.2 Fourier Transform Infra-Red Spectra

The mid- infrared absorption spectra of glyoxylic acid and glyoxylic acid gem diol were measured between 800 and 5000 cm^{-1} using FTIR at 370 K and 1 cm^{-1} resolution. A Bruker Tensor 27 with a permanent set-up of a globar, KBr beamsplitter, and MCT detector allowed for optimal mid-IR absorption spectroscopy. The set-up for this experiment has been described previously[31-35]. The glass cell had a path length of 75 cm. Nitrogen (N_2) gas was bubbled through a molten sample of glyoxylic acid and glyoxylic acid gem diol to force the sample through the cell. The cell was wrapped in heating tape for temperature control. The temperature of the cell varied between 365 and 373 K. N_2 gas was also used to create a purge volume between the cooler windows and the hot sample to prevent condensation of the sample. The FTIR technique allows for the simultaneous measurement of all wavelengths of light, producing accurate relative intensities of the various peaks in the fundamental vibrational range.

8.2.3 Theoretical calculations

Prof. Rex Skodje, Dr. Kaito Takahashi, and Galen Nelson calculated the structures and fundamental vibrational mode frequencies of glyoxylic acid and glyoxylic acid gem diol using the hybrid density functional theory method of B3LYP with the 6-311++G(3df,3pd) basis set using the Gaussian 03 program[36-42]. The frequencies were scaled using the wavenumber linear scaling method of Yoshida et. al[43]. The optimized structures with bond lengths are given in Fig. 8.1 and **Error! Reference source not found.**8.2. The most stable structure (Tc) revealed an ntramolecular hydrogen bonding causing the elongation of the OH bond compared to the Tt

conformer. The calculated frequencies and integrated cross-sections are presented in Table 8.1 and Table 8.2. Previously,

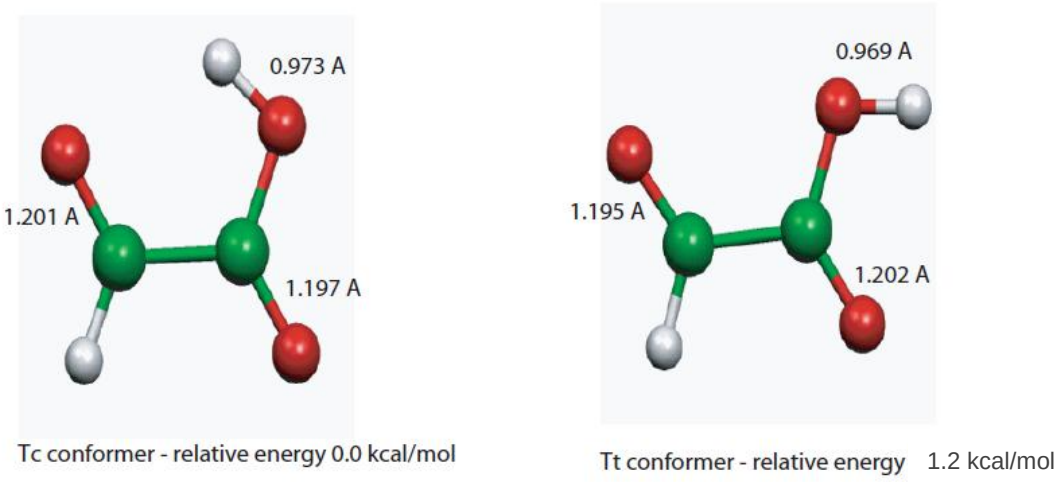

Figure 8.1 The theoretically calculated structures for the two lowest energy conformers of glyoxylic acid. Several bond lengths are included to highlight difference relating to the OH bond.

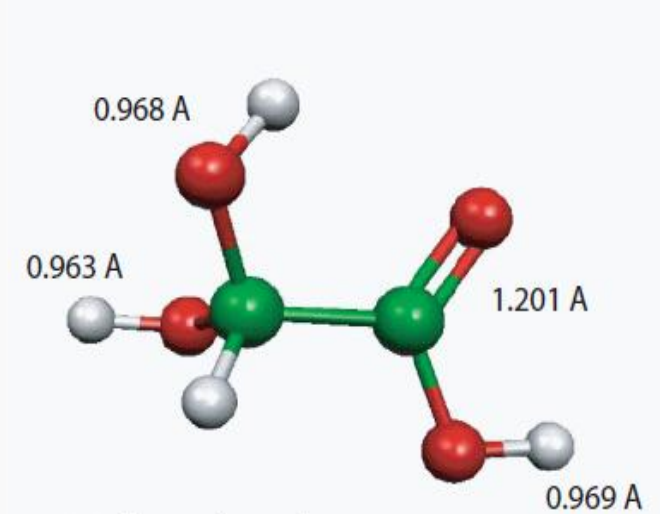

Figure 8.2 The theoretically calculated structure of the most stable conformer of glyoxylic acid gem diol. Bond lengths are provided for comparison with the glyoxylic acid results.

Table 8.1 The results of the re-examination of the glyoxylic acid spectrum. The experimental frequencies, FWHM's, the theoretical frequencies and intensities, and the literature frequencies for the fundamental modes, as well as the mode descriptions.

Theo Freq (cm^{-1})	Exptl Freq (cm^{-1})	Lit Freq[19] (cm^{-1})	Theo Int (km/mol)	Exptl FWHM (cm^{-1})	Mode Descriptions[19]*
3561	3584	--	80.5	49	OH stretch (Tt conformer)
3490	3501	3510	99.9	45	OH stretch (Tc conformer)
2881	2878	2860	38.7	51	CH stretch
1791	1807	1809	238.4	22	C=O acid stretch
1749	1751	1755	103.3	68	C=O aldehyde stretch
1335	1351	1348	324.5	53	dCCH + dCOH
1319	1323	1305	23.4	19.5	C-O stretch + C-C stretch + dCOH
1184	1206	1205	3.5	36	dCOH + C-O stretch + C-Cstretch
998	1006	--	3.6	50	--
862	896	876	50	21	C-C stretch + C-O stretch
676	--	--	15	--	frame bend
493	--	--	6.2	--	C=O bend
276	--	--	33.3	--	frame bend
--	--	773	--	--	dCCOacid + dCCO aldehyde
--	957	948	--	88	YCC(=H)-O
674	--	--	76.5	--	OH outplane bend (A")
568	--	--	29.9	--	COOH torsion (A")
164	--	--	29.1	--	CHO torsion (A")

* The mode descriptions for transitions less than 700 cm^{-1} are from this chapter's theoretical calculations. Mode descriptions for transitions greater than 800 cm^{-1} are from the work of Fleury and Tabacik.[19]

Table 8.2 The theoretical and experimental results for the fundamental spectrum of glyoxylic acid gem diol.

Theoretical Frequency (cm^{-1})	Experimental Frequency (cm^{-1})	Theoretical Intensity (km/mol)	Experimental FWHM (cm^{-1})	Mode Descriptions
3624	--	53.8	--	OH stretch
3557	--	58.7	--	OH stretch
3555	--	75.6	--	OH stretch
2931	--	27.1	--	CH stretch
1771	1742	291.3	69	OHC=O stretch
1452	1434	17.6	65	CH bend
1364	1390	30	19	CH bend
1314	1320	77.7	97	OH bend
1265	--	14.1	--	OH bend
1196	1206	69.9	46	CH bend
1148	--	137.7	--	C-OH stretch
1079	1101	257.4	96	C-OH stretch
1023	1065	142.6	--	C-OH stretch
843	--	63.6	--	C-C str+OH bend
759	--	54.5	--	C-C stretch
661	--	27.5	--	Torsion
593	--	89	--	OH rock
558	--	61.3	--	OH rock
459	--	56.6	--	OH rock
390	--	30.2	--	OH rock
291	--	32.4	--	frame bend
256	--	45.1	--	OH rock
222	--	50.9	--	OH rock
66	--	1.1	--	Torsion

this method calculated the results of pyruvic acid and was in excellent agreement with experimental results and the results obtained with CCSD(T) methods[33,44].

8.3 Results and Discussion

This work presents the fundamental vibrational spectra of glyoxylic acid and glyoxylic acid gem diol in order to gain insight into these molecules structure, ability to form intra- and inter-molecular hydrogen bonds, relative vapor pressures, atmospheric aerosol partitioning, and tendency for uptake into water. While the gas-phase IR spectrum of glyoxylic acid has been measured previously[19] this study provides the first gas-phase IR spectrum of glyoxylic acid gem diol. Theoretical calculations acted as a guide to assign the glyoxylic acid gem diol spectrum. The theoretical structures of glyoxylic acid and glyoxylic acid gem diol elucidated differences in the structures, which were confirmed by the observed spectral shifts. The structures are presented in Fig. 8.1 and Fig. 8.2. The gas-phase vibrational spectrum of glyoxylic acid is shown in Fig. 8.3 and Table 8.1 gives the comparison of the glyoxylic acid recorded spectrum and theoretical calculations with the previously observed spectrum[19]. The glyoxylic acid gem diol spectrum and assignments are available in Fig. 8.4 and Table 8.2.

8.3.1 Spectrum of Glyoxylic Acid

A reexamination of the IR spectrum of glyoxylic acid with new theoretical results reveals new insight into gas-phase glyoxylic acid (Table 8.1 and Fig. 8.3). In the experiment, thermal energy was sufficient enough to populate the Tt conformer of glyoxylic acid in addition to the

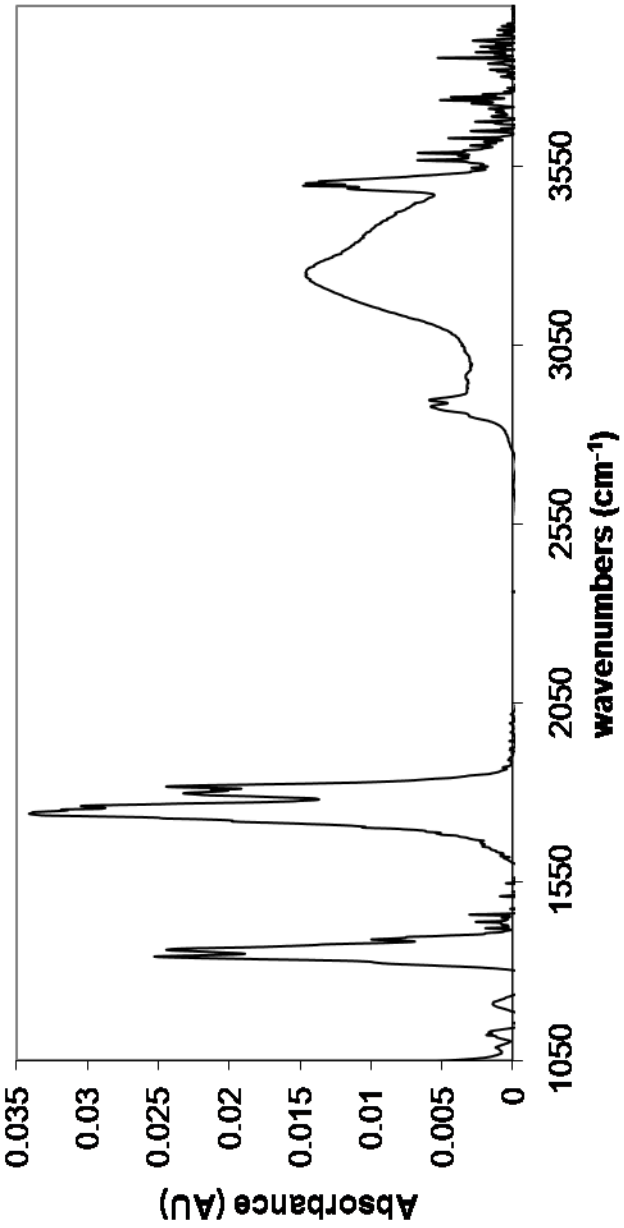

Figure 8.3 The fundamental IR spectrum of glyoxylic acid. The OH stretching transitions for both the Tc and Tt conformers are observed. The spectrum was collected at 365 K with 1 cm^{-1} resolution.

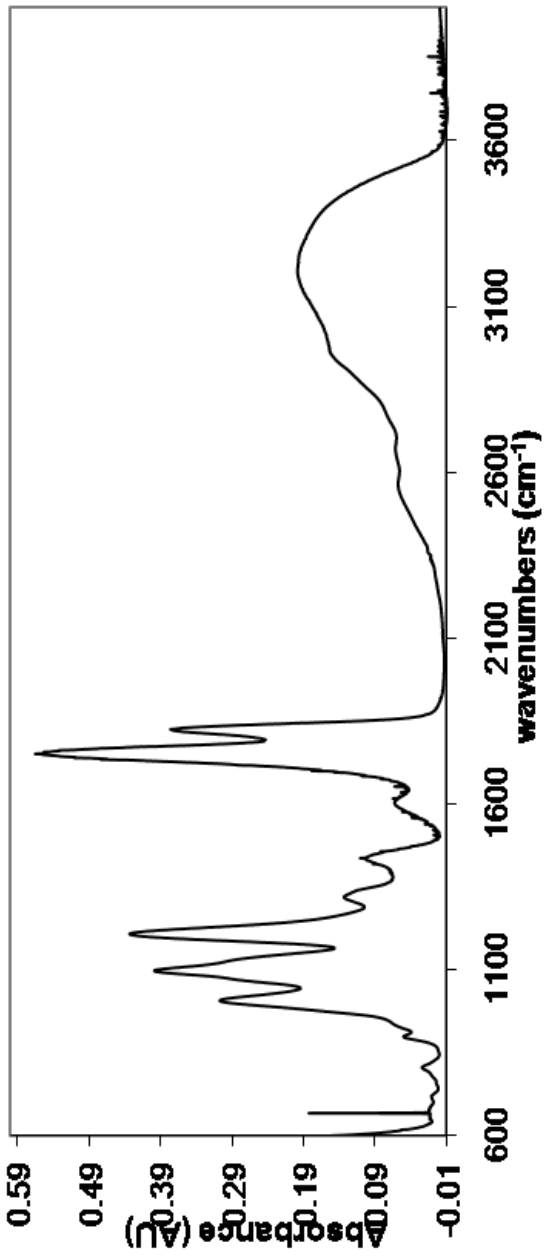

Figure 8.4 The fundamental IR spectrum of glyoxylic acid gem diol. The large broad feature toward high energy represents the OH stretching modes engaged in intermolecular hydrogen bonding. The spectrum was collected at 370 K and 1 cm^{-1} resolution.

most stable Tc conformer. According to the theoretical calculations, the Tt conformer is 1.2 kcal mol^{-1} higher in energy relative to the Tc conformer. The major difference between these two structures was in the orientation of the hydrogen atom of the carboxylic acid group. In the Tc conformer, the OH group is oriented toward the aldehyde group creating an intramolecular hydrogen bond. Based on the selected bond lengths shown in Fig. 8.1, the Tc conformer shows a longer OH bond length compared to the Tt conformer. Using the C=O bond lengths, it appears that in the Tc conformer there is an interaction between the OH group and the aldehyde group, while in the Tt conformer the trend of C=O bond lengths suggests that the OH is interacting with the C=O of the carboxylic acid group. The differences in the C=O bond lengths suggest where the intramolecular interactions occur, however the OH bond length reveals that the intramolecular hydrogen bond in the Tc conformer is stronger than that of the Tt conformer. These structures are reminiscent of those seen in pyruvic acid, where two similar conformers were observed in the gas phase[12,33,44]. From the frequency and intensity changes observed in the vibrational spectrum, the subtle structural differences were confirmed and the relative strength of the intramolecular forces was investigated.

There were several vibrational bands identified and assigned to glyoxylic acid. A distinct doublet feature at 1351 cm^{-1} was assigned as the glyoxylic acid fundamental C-O stretching mode. This feature is in good agreement with Fleury and Tabacik[19] (1348 cm^{-1}) and with the theoretical calculations (1335 cm^{-1}). The theoretical intensity for the C-O stretching mode was calculated to be 324.5 km mol^{-1}, which was evident in the strength of this mode. The clear doublet structure of the C-O stretching mode, which is also seen in the Fleury and Tabacik[19] spectrum, is a distinct feature that was used to identify a majority concentration of the aldehyde form of glyoxylic acid in the spectrum.

The carbonyl stretches of the molecules were difficult to separate because their frequencies change very little. In glyoxylic acid, the aldehyde C=O stretch is slightly lower in frequency than the C=O of the carboxylic acid functional group, as was the case for pyruvic acid[33,44]. The aldehyde C=O stretch was assigned at 1751 cm^{-1} which is in good agreement with the Fleury and Tabacik[19] and the theoretical calculations, 1755 cm^{-1} and 1749 cm^{-1} respectively. The predicted intensity of the aldehyde C=O stretch was 103.3 km mol^{-1}, suggesting that it would be one of the more intense vibrational modes of glyoxylic acid. The theoretical predictions suggest that the C=O stretch of the carboxylic acid functional group has a larger cross section, 238.4 km mol^{-1}. The carboxylic acid C=O stretch was observed at 1807 cm^{-1}, which is in good agreement with Fleury and Tabacik[19] and the theoretical calculations, 1809 cm^{-1} and 1791 cm^{-1} respectively. Fleury and Tabacik assign this transition as having a PQR structure, which was confirmed this work. However, in this work, the lower energy transition was observed to have more intensity and a larger linewidth. This was attributed to overlapping transitions of multiple species. One of these overlapping transitions could be the aldehyde carbonyl stretching transition of the Tt conformer of the glyoxylic acid, which should have a slightly blue shifted frequency due to the lack of intramolecular hydrogen bonding that was present in the Tc conformer of glyoxylic acid. Using several data sets, the two transitions were modeled using Gaussian functions and it was found that a typical function used to fit the peak at 1751 cm^{-1} has a line-width of 65 cm^{-1}, while the peak at 1807 cm^{-1} has a line-width of ~35 cm^{-1}. The linewidth is evidence that the lower energy peak was the result of multiple transitions.

The OH stretch of the glyoxylic acid aldehyde was unique and easily assigned at 3501 cm^{-1}. The theoretical results were 3490 cm^{-1} and 99.9 km mol^{-1}, while Fleury and Tabacik[19] assign the OH stretch at 3510 cm^{-1}. At the elevated temperatures of these experiments, the Tt

conformer was observed, with an OH stretch present at 3584 cm^{-1}. Theoretical predictions place this transition at 3561 cm^{-1}. The predicted intensity was less than that of the Tc conformer (80.5 km mol^{-1}), which combined with the lower population, suggests the small intensity was of the Tt conformer's OH stretch. These results fit the trend of the similar molecule, pyruvic acid, where the OH stretches of the two conformers are separated by 120 cm^{-1}.[33,44] The difference in the frequencies was attributed to an intramolecular hydrogen bond and was supported by the calculated structures (in Fig. 8.1) showing the Tc conformer's longer OH bond compared to the Tt conformer[45].

The spectrum provided by Fleury and Tabacik[19] was invaluable in understanding the spectra collected in this work; however there are several vibrational mode assignments that do not agree. There was a mode at 948 cm^{-1} that Fleury and Tabacik[19] observed which was not observed in this work or predicted by the calculations. This peak is not believed to be due to a fundamental transition of glyoxylic acid. It was not predicted in either of the conformers of glyoxylic acid or in the glyoxylic acid gem diol fundamental transitions. With minor discrepancies, the gas-phase spectra of glyoxylic acid obtained in this work and theoretical results agree well with those obtained by Fleury and Tabacik[19].

8.3.2 Spectrum of the Gem Diol form of Glyoxylic Acid Monohydrate

In addition to obtaining and reexamining the IR spectrum of glyoxylic acid, the fundamental spectrum of glyoxylic acid gem diol was obtained. To the best of my knowledge, this species has not been seen in the gas phase before. The results are presented in Table 8.2 and the spectrum is displayed in Fig. 8.4. The glyoxylic acid gem diol vibrational modes have

several frequencies that are unique and were used to identify the presence of glyoxylic acid gem diol in the spectrum. These vibrational modes occurred mainly in the fingerprint region of the spectrum (< 1500 cm^{-1}). The spectral assignments were done using the frequencies and intensities from B3LYP calculations reported here. The glyoxylic acid previously published and presently obtained spectrum serves as a calibration for the assignment of the glyoxylic acid gem diol features[19]. The theoretical results and experimental data from this work reveal a confidence in the vibrational frequency of within 20 cm^{-1}. The agreement between glyoxylic acid gem diol's experimental and theoretical frequencies is within 30 cm^{-1}.

The theoretical results predicted that the transition at 1006 cm^{-1} can be attributed to either glyoxylic acid gem diol or glyoxylic acid. In this case, the predicted glyoxylic acid vibrational mode was not recorded by the Fleury and Tabacik paper or in this work[19]. The glyoxylic acid mode was calculated at 998 cm^{-1} with an integrated intensity of 3.6 km mol^{-1}. This low intensity may be the reason why no such mode was observed. The feature at 1006 cm^{-1} in Fig. 8.4 was relatively intense, unlike the calculated intensity for the glyoxylic acid vibrational mode. However, the glyoxylic acid gem diol calculations predict the C-OH stretch vibrational transition centered at 1023 cm^{-1} with an intensity of 142.6 km mol^{-1}. This glyoxylic acid gem diol frequency fits better with the observed data and was tentatively assigned to the diol.

A large feature in the spectrum of the glyoxylic acid gem diol lies at 1101 cm^{-1}. This peak was completely absent from the glyoxylic acid spectrum. Theoretical results place two modes in this vicinity: one at 1079 cm^{-1} with an intensity of 257.4 km mol^{-1} and the other at 1148 cm^{-1} and an intensity of 137.7 km mol^{-1}. The shape of the peak fits well with the idea that there are multiple transitions contained within it. A shoulder exists to the high energy side of the peak (~1130 cm^{-1}), which was tentatively assigned as the higher energy mode predicted at 1148 cm^{-1}.

The feature at 1206 cm^{-1} was present in all spectra regardless of sample composition, though spectra with a large population of glyoxylic acid gem diol revealed this feature relatively larger than in the spectrum of glyoxylic acid. This agrees with the calculated intensities. For the glyoxylic acid transition, the calculated frequency of the OH bending vibrational mode was 1184 cm^{-1} (Fleury and Tabacik[19] assign it at 1205 cm^{-1}) with an intensity of 3.5 km mol^{-1} and for glyoxylic acid gem diol the calculated frequency was 1196 cm^{-1} with an intensity of 69.9 km mol^{-1}. The combination of experimental spectra and theoretical calculations suggest that two distinct modes belonging to separate molecules overlap and the assignment of a particular peak to one molecule must be done by comparing the intensity to the intensity of peaks of known vibrational modes. Thus, by comparing the intensity of the peak at 1206 cm^{-1} to the intensity of the carboxylic acid C=O stretch of glyoxylic acid the feature was assigned. If the 1206 cm^{-1} peak was less intense, as was the case in Fig. 8.3, then the 1206 cm^{-1} feature would be due to the glyoxylic acid OH bend vibrational mode. However, in cases where the intensity of the 1206 cm^{-1} transition was equal to or greater than the 1807 cm^{-1} C=O stretch, the feature was the result of the glyoxylic acid gem diol CH bending vibrational mode. This assignment is supported by Fleury and Tabacik's assignment of a feature at 1205 cm^{-1} as the dCOH + C-O stretch + CC stretch vibrational mode of glyoxylic acid observed with a low intensity in their spectrum.[19]

The OH bending mode was observed at 1320 cm^{-1} which was based on the theoretically predicted frequency for the mode at 1314 cm^{-1}. This mode helps to show the majority species are due to its proximity to the 1351 cm^{-1} glyoxylic acid vibrational mode. These two transitions were easily distinguishable due to the differing band shapes. The glyoxylic acid doublet was a very strong mode in the spectrum and as the glyoxylic acid gem diol population was increased the doublet disappears and a structureless peak arose at 1320 cm^{-1}. While the 1351 cm^{-1}

transition had a very large calculated intensity (324.5 km mol^{-1}) the glyoxylic acid gem diol vibrational mode transition had a much smaller calculated intensity of 77.7 km mol^{-1}. This suggested that the population of gas-phase glyoxylic acid gem diol in Fig. 8.4 was greater than the gas-phase population of glyoxylic acid in Fig. 8.3.

Overlapping of transitions made it difficult to ascertain the absolute peak position for the glyoxylic acid gem diol C=O stretch, however the mode was assigned a frequency at 1742 cm^{-1}. The theoretical calculations predicted a frequency of 1771 cm^{-1} and an intensity of 291.3 km mol^{-1}, which was more intense than the predicted carbonyl stretches of glyoxylic acid. By taking several spectra at different conditions and assigning certain peaks as being uniquely glyoxylic acid diol or glyoxylic acid, a spectrum was obtained that contains a majority of glyoxylic acid diol compared to glyoxylic acid. From the spectrum the frequency of the glyoxylic acid diol C=O stretching mode was determined. When compared to the glyoxylic acid carboxylic acid C=O stretch, the glyoxylic acid diol C=O stretch was significantly red-shifted. The red shifting of the glyoxylic acid C=O was attributed to increased hydrogen bonding when compared to the glyoxylic acid carboxylic acid C=O. This increased intramolecular interaction results in lessened electron density between the carbon and oxygen atoms. As seen in Fig. 8.4, the transition centered at 1750 cm^{-1} had some structure but does not have as clear of a PQR structure as the higher energy transition. According to Fleury and Tabacik,[19] the PQ and RQ branches were observed for the glyoxylic acid C=O stretch and were observed in this work as well. There was a third structural feature at 1742 cm^{-1}, which was believed to be the glyoxylic acid diol C=O stretching mode transition next to and commingled with the glyoxylic acid aldehyde C=O stretch. In spectra where the vast majority of the population was in the glyoxylic acid gem diol form, the structure of the carbonyl stretches disappears and the 1742 cm^{-1} transition dominated.

The larger shift in the glyoxylic acid gem diol C=O stretching frequency than the glyoxylic acid carboxylic acid C=O stretching frequency suggested that the intramolecular hydrogen bond formed in glyoxylic acid gem diol was stronger than that of glyoxylic acid. This was manifested in the theoretical calculations with the longer C=O bond length (1.201 Å).

The OH stretching modes of glyoxylic acid gem diol monomer were not observed with certainty in this spectrum (Fig. 8.4). The predicted frequencies for the OH stretches were 3555, 3557, and 3624 cm^{-1}, with the intensities being lower than the glyoxylic acid OH stretches (75.6, 58.7, and 53.8 km mol^{-1} respectively). In the spectrum, there was a large, broad feature between 3000 cm^{-1} and 3500 cm^{-1}. This type of feature is often seen in spectra of compounds that dimerize or form clusters. The height of the feature scales with the population of glyoxylic acid gem diol present. The broad feature fits with intermolecular hydrogen bonded OH stretching modes. Calculations on the HCOCOOH· H_2O cluster reveal that the OH group involved in the intermolecular hydrogen bond was red-shifted to 3146 cm^{-1} and the intensity was predicted to be 902 km mol^{-1}. It was assumed that there would be a similar result for the glyoxylic acid gem diol·H_2O cluster. The results show a much larger perturbation to the OH stretching mode than is typically seen in intramolecular hydrogen bonds, such as pyruvic acid, glyoxylic acid, or glycolic acid[33,46]. The low vapor pressure and high melting point of glyoxylic acid gem diol reinforce the concept that glyoxylic acid gem diol forms strong intermolecular interactions. These greatly shifted hydrogen bonded transitions would account for the lack of monomeric glyoxylic acid gem diol OH stretching mode transitions observed.

Proof for hydrated complexes in this experiment was limited, though the increased intensity and large frequency shifts were observed under the right experimental conditions. Both glyoxylic acid and glyoxylic acid gem diol were prone to forming clusters and intermolecular

hydrogen bonds, though the glyoxylic acid gem diol appears to form stronger intermolecular interactions than glyoxylic acid. This was consistent with the observation that the melting point of glyoxylic acid was ~315 K and glyoxylic acid gem diol was ~343 K. Additionally, the vapor pressure of glyoxylic acid is predicted to be higher than that of glyoxylic acid gem diol, though it is possible to get a large population of glyoxylic acid gem diol into the vapor phase at ~370 K. In data sets with a large amount of vapor phase water there also exists a feature at 1610 cm^{-1} that was attributed to these hydrated complexes (this feature is shown in Fig. 8.4). The feature was only observed in spectra that were predominantly glyoxylic acid gem diol. It was impossible to assign this feature to a specific molecule. The peak position was red-shifted from typical C=O stretching frequencies due to a strong hydrogen bond. The water molecule creates a stronger hydrogen bond with glyoxylic acid gem diol because it was not constrained by the geometry of the molecule, provoking larger shifts in the spectrum than result from intramolecular hydrogen bonding.

8.3.3 Gas-Phase Equilibrium between Glyoxylic Acid and Glyoxylic Acid Gem Diol

It was evident that the equilibrium between glyoxylic acid and glyoxylic acid gem diol was highly dependent on the temperature and water partial pressure. Using the calculated intensities of transitions, the population ratio of glyoxylic acid gem diol to glyoxylic acid was estimated. The glyoxylic acid mode at 1351 cm^{-1} and the glyoxylic acid gem diol transition at 1390 cm^{-1} were observed in all of the spectra. Spectra, such as that of Fig. 8.3, had a large number density of glyoxylic acid, a ratio of ~2 for glyoxylic acid gem diol : glyoxylic acid. Fig. 8.4 shows a spectrum with a much larger population of glyoxylic acid gem diol, a ratio of ~500

glyoxylic acid diol : glyoxylic . From these ratios it was concluded that the glyoxylic acid gem diol : glyoxylic acid ratio favors glyoxylic acid gem diol to a large extent.

If the equilibrium is assumed to be solely due to the gas phase reaction of the isolated glyoxylic acid and a water molecule to form gas-phase glyoxylic acid gem diol, then the theoretically calculated free energy change gives an equilibrium constant favoring the reactants. A larger relative population of glyoxylic acid gem diol was observed in this work, implying that the simple assumed equilibrium is not correct in describing the observations. The discrepancy between the calculated equilibrium constant and the experimentally derived result can be understood with reference to the involvement of hydrogen bonded complexes. These spectroscopic observations of complexes are evidence that glyoxylic acid and to a larger extent glyoxylic acid gem diol form hydrogen bonded complexes. The complexes must be incorporated into the equilibrium to acquire accurate results. Based on the spectra and population ratio estimations in this work, it was concluded that the gas-phase equilibrium between glyoxylic acid gem diol and glyoxylic acid is water-mediated and involves hydrated complexes of glyoxylic acid and glyoxylic acid gem diol.

8.4 Atmospheric Implications

Glyoxylic acid is a known product of the aqueous phase oxidation of glyoxal and is incorporated into atmospheric models[2,3]. Based on these experiments, it appears that at relevant atmospheric conditions glyoxylic acid can form glyoxylic acid gem diol and in a short amount of time due to the large amount of water present in the atmosphere. Once glyoxylic acid gem diol forms it is unlikely to remain in the gas phase and will partition to aerosols and cloud droplets

due to its propensity for forming intermolecular hydrogen bonds[47]. The ability to form hydrated clusters affects the molecule's transport and chemistry in the troposphere. These experimental results can be extrapolated further, to temperatures relevant to the atmosphere, showing that glyoxylic acid gem diol will have a nearly negligible vapor pressure, though the glyoxylic acid will still have an appreciable vapor pressure. The reaction of glyoxylic acid to form glyoxylic acid gem diol is inevitable if glyoxylic acid partitions to the aerosol. These experiments showed that in the gas phase the glyoxylic acid gem diol was favored. Following the uptake of glyoxylic acid to the aerosol and cloud droplets, the subsequent reaction to form glyoxylic acid gem diol, and the low vapor pressure of glyoxylic acid gem diol ensures that little glyoxylic acid will reappear in the gas-phase. This may account for the discrepancy between the modeled amounts of ketones and aldehydes in the atmosphere and the much lower observed concentrations of these species. In addition to the removal of the aldehyde from the gas-phase, the diol functional group also drastically changes the electronic states. glyoxylic acid has a low lying electronic state that can undergo photochemistry in the troposphere. However, glyoxylic acid gem diol has a higher energy excited electronic state and will thus remain inert to the accessible UV light in the troposphere[29]. As the first reported gas-phase spectrum of a gem diol, this work also highlights the question of how water affects the organic aerosol mass[48]. In the atmosphere, hydration seems to be an additional pathway that shifts the partitioning equilibrium[49]. Additionally the chemistry and contribution to SOA of aldehydes and ketones requires reevaluation in light of these results.

8.5 References

1. Carlton, A. G., Turpin, B. J., Altieri, K. E., Seitzinger, S., Reff, A., Lim, H. J.,Ervens, B. Atmospheric oxalic acid and SOA production from glyoxal: Results of aqueous photooxidation experiments. *Atmos. Environ.,* (2007), **41**, 7588-7602.
2. Ervens, B., Carlton, A. G., Turpin, B. J., Altieri, K. E., Kreidenweis, S. M., Feingold, G. Secondary organic aerosol yields from cloud-processing of isoprene oxidation products. *Geophys. Res. Lett.,* (2008), **35**, 5.
3. Ervens, B., Feingold, G., Frost, G. J., Kreidenweis, S. M. A modeling study of aqueous production of dicarboxylic acids: 1. Chemical pathways and speciated organic mass production. *J. Geophys. Res.-Atmos.,* (2004), **109**, 20.
4. Ervens, B., Gligorovski, S., Herrmann, H. Temperature-dependent rate constants for hydroxyl radical reactions with organic compounds in aqueous solutions. *Phys. Chem. Chem. Phys.,* (2003), **5**, 1811-1824.
5. Ervens, B., Kreidenweis, S. M. SOA formation by biogenic and carbonyl compounds: Data evaluation and application. *Environ. Sci. Technol.,* (2007), **41**, 3904-3910.
6. Hallquist, M., Wenger, J. C., Baltensperger, U., Rudich, Y., Simpson, D., Claeys, M., Dommen, J., Donahue, N. M., George, C., Goldstein, A. H., Hamilton, J. F., Herrmann, H., Hoffmann, T., Iinuma, Y., Jang, M., Jenkin, M. E., Jimenez, J. L., Kiendler-Scharr, A., Maenhaut, W., McFiggans, G., Mentel, T. F., Monod, A., Prevot, A. S. H., Seinfeld, J. H., Surratt, J. D., Szmigielski, R.,Wildt, J. The formation, properties and impact of secondary organic aerosol: current and emerging issues. *Atmos. Chem. Phys.,* (2009), **9**, 5155-5236.
7. Kanakidou, M., Seinfeld, J. H., Pandis, S. N., Barnes, I., Dentener, F. J., Facchini, M. C., Van Dingenen, R., Ervens, B., Nenes, A., Nielsen, C. J., Swietlicki, E., Putaud, J. P., Balkanski, Y., Fuzzi, S., Horth, J., Moortgat, G. K., Winterhalter, R., Myhre, C. E. L., Tsigaridis, K., Vignati, E., Stephanou, E. G.,Wilson, J. Organic aerosol and global climate modeling: a review. *Atmos. Chem. Phys.,* (2005), **5**, 1053-1123
8. Rosado-Reyes, C. M., Francisco, J. S. Atmospheric oxidation pathways of acetic acid. *J. Phys. Chem. A,* (2006), **110**, 4419-4433.
9. Warneck, P. Multi-phase chemistry of C-2 and C-3 organic compounds in the marine atmosphere. *J. Atmos. Chem.,* (2005), **51**, 119-159.
10. Kent, D. R., Widicus, S. L., Blake, G. A., Goddard, W. A. A theoretical study of the conversion of gas phase methanediol to formaldehyde. *J. Chem. Phys.,* (2003), **119**, 5117-5120.
11. Mugnai, M., Cardini, G., Schettino, V., Nielsen, C. J. Ab initio molecular dynamics study of aqueous formaldehyde and methanediol. *Mol. Phys.,* (2007), **105**, 2203-2210.
12. Chen, C., Shyu, S. F. Theoretical study of glyoxylic and pyruvic acids: rotamers and intramolecular hydrogen bonding. *Journal of Molecular Structure-Theochem,* (2000), **503**, 201-211.
13. Marstokk, K. M. and Mollenda, H. Microwave spectrum, conformation, dipole moment and centrifugal distortion of glyoxylic acid. *J. Mol. Struct.,* (1973), **15**, 137-150.
14. Vaneijck, B. P., Vanduijneveldt, F. B. Molecular structure and rotational isomerism in glyoxylic acid from microwave spectroscopy and ab inito calculations. *J. Mol. Struct.,* (1977), **39**, 157-163

15. Vaida, V. Spectroscopy of photoreactive systems: Implications for atmospheric chemistry. *J. Phys. Chem. A,* (2009), **113**, 5-18.
16. Vaida, V., Feierabend, K. J., Rontu, N.,Takahashi, K. Sunlight-initiated photochemistry: Excited vibrational states of atmospheric chromophores. *Int. J. Photoenergy,* (2008), 1-13.
17. Rodler, M. Ab inito studies of the structures and energies of methanediol and 1,1-ethenediol. *Chem. Phys.,* (1986), **105**, 345-353.
18. Volkamer, R., Jimenez, J. L., San Martini, F., Dzepina, K., Zhang, Q., Salcedo, D., Molina, L. T., Worsnop, D. R., Molina, M. J. Secondary organic aerosol formation from anthropogenic air pollution: Rapid and higher than expected. *Geophys. Res. Lett.,* (2006), **33**, 4.
19. Fleury, G., Tabacik, V. Glyoxylic acid - Asymmetry of free molecule vibration spectra and attribution. *J. Mol. Struct.,* (1971), **10**, 359.
20. Hollenstein, H., Ha, T. K., Gunthard, H. H. IR induced conversion of rotamers, matrix spectra, ab initio calculations of conformers, assignment, and valent force-field of trans glycolic acid. *J. Mol. Struct.,* (1986), **146**, 289-307.
21. Redington, R. L., Liang, C. K. J. Vibrational spectra of glyoxylic acid monomers. *J. Mol. Spectrosc.,* (1984), **104**, 25-39.
22. Bock, C. W., Redington, R. L. Isomerization and unimolecular dissociation channels of the glyoxylic acid monomer. *J. Phys. Chem.,* (1988), **92**, 1178-1187.
23. Cooper, A. J. L., Redfield, A. G. Proton magnetic resonance studies of alpha-keto acids. *J. Biol. Chem.,* (1975), **250**, 527-532
24. George, P., Bock, C. W., Trachtman, M. An ab initio study of the geometry and energy of the 4 planar conformers of glyoxylic acid and the glyoxylate ion. *Theochem-J. Mol. Struct.,* (1982), **4**, 1-18.
25. Sorensen, P. E., Bruhn, K., Lindelov, F. Kinetics and equilibria for reversible hydration of aldehyde group in glyoxylic acid. *Acta Chemica Scandinavica Series a-Physical and Inorganic Chemistry,* (1974), **A 28**, 162-168.
26. Howard, D. L., Jorgensen, P., Kjaergaard, H. G. Weak intramolecular interactions in ethylene glycol identified by vapor phase OH-stretching overtone spectroscopy. *J. Am. Chem. Soc.,* (2005), **127**, 17096-17103.
27. Howard, D. L., Kjaergaard, H. G. Influence of intramolecular hydrogen bond strength on OH-stretching overtones. *J. Phys. Chem. A,* (2006), **110**, 10245-10250.
28. Scharge, T., Luckhaus, D., Suhm, M. A. Observation and quantification of the hydrogen bond effect on O-H overtone intensities in an alcohol dimer. *Chem. Phys.,* (2008), **346**, 167-175.
29. Back, R. A., Yamamoto, S. The gas-phase photochemistry and thermal-decomposition of glyoxylic acid. *Can. J. Chem.-Rev. Can. Chim.,* (1985), **63**, 542-548.
30. Bakri, B., Demaison, J., Margules, L.,Mollendal, H. The submillimeter-wave spectrum and quantum chemical calculations of glyoxylic acid. *J. Mol. Spectrosc.,* (2001), **208**, 92-100.
31. Dunn, M. E., Shields, G. C., Takahashi, K., Skodje, R. T., Vaida, V. Experimental and theoretical study of the OH vibrational spectra and overtone chemistry of gas-phase vinylacetic acid. *J. Phys. Chem. A,* (2008), **112**, 10226-10235.

32. Eliason, T. L., Havey, D. K.,Vaida, V. Gas phase infrared spectroscopic observation of the organic acid dimers ($CH_3(CH_2)(6)COOH)(2)$, ($CH_3(CH_2)(7)COOH)(2)$, and ($CH_3(CH_2)(8)COOH)(2)$. *Chem. Phys. Lett.*, (2005), **402**, 239-244.
33. Plath, K. L., Takahashi, K., Skodje, R. T., Vaida, V. Fundamental and overtone vibrational spectra of gas-phase pyruvic acid. *J. Phys. Chem. A*, (2009), **113**, 7294-7303N.
34. Rontu, N., Vaida, V. Vibrational spectroscopy of perfluoroproplonic acid in the region between 1000 and 11000 cm^{-1}. *J. Mol. Spectrosc.*, (2006), **237**, 19-26.
35. Rontu, N., Vaida, V. Vibrational spectroscopy of perfluorocarboxylic acids from the infrared to the visible regions. *J. Phys. Chem. B*, (2008), **112**, 276-282.
36. Becke, A. D. Density-functional thermochemistry. 3. The role of exact exchange *J. Chem. Phys.*, (1993), **98**, 5648-5652.
37. Lee, C. T., Yang, W. T.,Parr, R. G. Development of the Colle-Salvetti correlation-energy formula into a functional of the electron-density. *Phys. Rev. B*, (1988), **37**, 785-789.
38. Clark, T., Chandrasekhar, J., Spitznagel, G. W.,Schleyer, P. V. Efficient diffuse function-augmented basis-sets for anion calculations. 3. The 3-21+G basis set for 1st-row elements, LI-F. *J. Comput. Chem.*, (1983), **4**, 294-301
39. Frisch, M. J., Pople, J. A., Binkley, J. S. Self-consistent molecular-orbital methods. 25. Supplementary functions for gaussian-basis sets. *J. Chem. Phys.*, (1984), **80**, 3265-3269
40. Frisch, M. J., G.W. Trucks, H.B. Schlegel, G.E. Scuseria, M.A. Robb, J.R. Cheeseman, J.A. Montgomery, T. Vreven, K.N. Kudin, J.C. Burant, J.M. Millam, S.S. Iyengar, ,J.Tomasi, V. B., B. Mennucci, M. Cossi, G. Scalmani, N. Rega, G.A. Petersson, H. Nakatsuji, M. Hada, M. Ehara, K. Toyota, R. Fukuda, J. Hasegawa, M. Ishida, T. Nakajima, Y. Honda, O. Kitao, H. Nakai, M. Klene, X. Li, J.E. Knox, H.P. Hratchian, J.B. Cross, V. Bakken, C. Adamo, J. Jaramillo, R. Gomperts, R.E. Stratmann, O. Yazyev, A.J. Austin, R. Cammi, C. Pomelli, J.W. Ochterski, P.Y. Ayala, K. Morokuma, G.A. Voth, P. Salvador, J.J. Dannenberg, V.G. Zakrzewski, S. Dapprich, A.D. Daniels, M.C. Strain, O.Farkas, D.K. Malick, A.D. Rabuck, K. Raghavachari, J.B. Foresman, J.V. Ortiz, Q. Cui, A.G. Baboul, S. Clifford, J. Cioslowski, B.B. Stefanov, G. Liu, A. Liashenko, P. Piskorz, I. Komaromi, R.L. Martin, D.J. Fox, T. Keith, M.A. Al-Laham, C.Y. Peng, A. Nanayakkara, M. Challacombe, P.M.W. Gill, B. Johnson, W. Chen, M.W. Wong, C. Gonzalez, J.A. Pople, *Gaussian03*, C.02 ed.; Gaussian Inc.: Wallingford, CT, 2004.
41. Krishnan, R., Binkley, J. S., Seeger, R., Pople, J. A. Self-consistent molecular-orbital methods. 20. Basis set for correlated wave-functions. *J. Chem. Phys.*, (1980), **72**, 650-654.
42. McLean, A. D., Chandler, G. S. Contracted Gaussian-basis sets for molecular calculations.1. 2nd row atoms, Z=11-18. *J. Chem. Phys.*, (1980), **72**, 5639-5648.
43. Yoshida, H., Ehara, A., Matsuura, H. Density functional vibrational analysis using wavenumber-linear scale factors. *Chem. Phys. Lett.*, (2000), **325**, 477-483
44. Takahashi, K., Plath, K. L., Skodje, R. T., Vaida, V. Dynamics of vibrational overtone excited pyruvic acid in the gas phase: Line broadening through hydrogen-atom chattering. *J. Phys. Chem. A*, (2008), **112**, 7321-7331.
45. Takahashi, K., Plath, K. L., Axson, J. L., Nelson, G. C., Skodje, R. T., Vaida, V. Dynamics and spectroscopy of vibrational overtone excited glyoxylic acid and 2,2-dihydroxyacetic acid in the gas-phase. *J. Chem. Phys.*, (2010), **132**, 1-10.

46. Havey, D. K., Feierabend, K. J., Takahashi, K., Skodje, R. T.,Vaida, V. Experimental and theoretical investigation of vibrational overtones of glycolic acid and its hydrogen bonding interactions with water. *J. Phys. Chem. A,* (2006), **110**, 6439-6446
47. Limbeck, A., Puxbaum, H., Otter, L., Scholes, M. C. Semivolatile behavior of dicarboxylic acids and other polar organic species at a rural background site (Nylsvley, RSA). *Atmos. Environ.,* (2001), **35**, 1853-1862.
48. Hennigan, C. J., Bergin, M. H., Dibb, J. E.,Weber, R. J. Enhanced secondary organic aerosol formation due to water uptake by fine particles. *Geophys. Res. Lett.,* (2008), **35**.
49. Altieri, K. E., Seitzinger, S. P., Carlton, A. G., Turpin, B. J., Klein, G. C.,Marshall, A. G. Oligomers formed through in-cloud methylglyoxal reactions: Chemical composition, properties, and mechanisms investigated by ultra-high resolution FT-ICR mass spectrometry. *Atmos. Environ.,* (2008), **42**, 1476-1490.